AN ABSTRACT OF THE THESIS OF

Oded Gottlieb for the degree of Doctor of Philosophy in Civil Engineering

presented on December 3, 1991.

Title: Nonlinear Oscillations, Bifurcations and Chaos in Ocean Mooring Systems

Abstract approved: Redacted for Privacy

Solomon C.S. Yim

Complex nonlinear and chaotic responses have been recently observed in various compliant ocean systems. These systems are characterized by a nonlinear mooring restoring force and a coupled fluid-structure interaction exciting force. A general class of ocean mooring system models is formulated by incorporating a variable mooring configuration and the exact form of the hydrodynamic excitation. The multi-degree of freedom system, subjected to combined parametric and external excitation, is shown to be complex, coupled and strongly nonlinear.

Stability analysis by a Liapunov function approach reveals global system attraction which ensures that solutions remain bounded for small excitation. Construction of the system's Poincaré map and stability analysis of the map's fixed points correspond to system stability of near resonance periodic orbits. Investigation of nonresonant solutions is done by a local variational approach. Tangent and period doubling bifurcations are identified by both local stability analysis techniques and are further investigated to reveal global bifurcations. Application of Melnikov's method to

the perturbed averaged system provides an approximate criterion for the existence of transverse homoclinic orbits resulting in chaotic system dynamics. Further stability analysis of the subharmonic and ultraharmonic solutions reveals a cascade of period doubling which is shown to evolve to a strange attractor.

Investigation of the bifurcation criteria obtained reveals a steady state superstructure in the bifurcation set. This superstructure identifies a similar bifurcation pattern of coexisting solutions in the sub, ultra and ultrasubharmonic domains. Within this structure strange attractors appear when a period doubling sequence is infinite and when abrupt changes in the size of an attractor occur near tangent bifurcations. Parametric analysis of system instabilities reveals the influence of the convective inertial force which can not be neglected for large response and the bias induced by the quadratic viscous drag is found to be a controlling mechanism even for moderate sea states.

Thus, stability analyses of a nonlinear ocean mooring system by semi-analytical methods reveal the existence of bifurcations identifying complex periodic and aperiodic nonlinear phenomena. The results obtained apply to a variety of nonlinear ocean mooring and towing system configurations. Extensions and applications of this research are discussed.

[c] Copyright by Oded Gottlieb
December 3, 1991

All Rights Reserved

NONLINEAR OSCILLATIONS, BIFURCATIONS AND CHAOS IN OCEAN MOORING SYSTEMS

by

Oded Gottlieb

A THESIS

submitted to

Oregon State University

in partial fulfillment of
the requirements for the
degree of

Doctor of Philosophy

Completed December 3, 1991

Commencement June 1992

Approved:

Redacted for Privacy

Professor of Civil Engineering in charge of major

Redacted for Privacy

Head of Department of Civil Engineering

Redacted for Privacy

Dean of Graduate School

Date thesis is presented: December 3, 1991

Typed by: Oded Gottlieb

ACKNOWLEDGEMENT

I wish to express my gratitude to my thesis advisor Dr. Solomon C.S. Yim, for enabling my research in the domain of nonlinear dynamical ocean systems.

I am also greatful to the other members of my committee: Dr. Ron B. Guenther, Dr. Robert T. Hudspeth, Dr. John W. Leonard and Dr. George W. Brown, for their continued interest and assistance.

Thanks are also extended to my colleagues, staff and faculty of the Ocean Engineering Program at Oregon State University.

The financial support from the United States Office of Naval Research (Grant No. N00014-88-K-0729) is greatfully acknowledged.

I would like to express my deepest gratitude to my parents Haya and Eli for direction, to my sons Or and Omer, for bringing sunshine into my life and to my wife Naomi, for crossing an ocean and a continent and particularly for her perseverance throughout the duration of this stage in our lives.

TABLE OF CONTENTS

TABLE OF CONTENTS (continued)

LIST OF FIGURES

LIST OF FIGURES (continued)

LIST OF FIGURES (continued)

LIST OF FIGURES (continued)

NONLINEAR OSCILLATIONS, BIFURCATIONS AND CHAOS IN OCEAN MOORING SYSTEMS

1. INTRODUCTION

Complex nonlinear and chaotic responses have recently been observed in various numerical and approximate semi-analytical models of compliant offshore structures and mooring systems (e.g. Thompson, 1983; Papoulias and Bernitsas, 1988; Sharma et al., 1988; Bishop and Virgin, 1988; Bernitsas and Chung, 1990; Jiang, 1991). These systems are characterized by a nonlinear mooring restoring force and a coupled hydrodynamic exciting force. The restoring force, which includes material discontinuities and geometric nonlinearities, has a unique equilibrium position or single well potential. The exciting force includes a quadratic fluid-structure interaction viscous drag and harmonic wave induced inertial components. The drag component includes a bias, a quadratic nonlinearity and combined parametric and external excitation. The inertial component consists of biased external excitation which for certain structural configurations, is complemented by an additional coupled nonlinear convective parametric excitation. Coupling of degrees of freedom further complicates system behavior.

Numerical investigation of systems which exhibit similar nonlinear properties have revealed complex behavior including coexisting periodic (harmonic, subharmonic, ultraharmonic, ultrasubharmonic) and aperiodic (quasiperiodic, chaotic) solutions defined by different initial conditions. System stability is governed by complex near resonant phenomena and sensitivity to initial conditions. A fundamental example of such systems

is the harmonically excited hardening Duffing equation (Ueda, 1980a,b; Parlitz and Lauterborn, 1985).

The development of deep water compliant offshore structures requires a comprehensive understanding of strongly nonlinear ocean systems designed for relatively large displacements. Existing mooring systems analyses are portrayed by complex numerical models incorporating both structural and hydrodynamic nonlinearities or by idealized numerical or semi-analytical models where the nonlinearities are approximated and are in part described by their linearized or quasi-static representation. Identification and control of system instabilities are not always attainable in the complex numerical models and require extensive parametric analysis, whereas the linearized models are limited by their restrictive assumptions and do not always reveal true system behavior. Therefore, the lack of systematic nonlinear analysis on one hand, and the numerical evidence of complex system response and sensitivity to initial conditions on the other, enhance the need for consistent analytical research of nonlinear ocean mooring systems.

1.1 Problem Overview

Ocean mooring systems include single and multi-point configurations (Skop, 1988) and are used to restrain the motion of compliant offshore structures (Leonard & Young, 1985). Single-point moorings (ABS, 1975) are characterized by curvature, material and hydrodynamic load nonlinearities (Leonard, 1988), whereas multi-point or spread moorings (API, 1987) include an additional geometric nonlinearity associated

with mooring line angles. The mooring restoring force is formulated by incorporating these nonlinearities by exact or approximate formulation based on the mooring line characteristics and its orientation in the system. The hydrodynamic excitation includes coupled nonlinear fluid-structure interaction viscous drag and inertial components and requires separate treatment for small versus large bodies (Sarpkaya & Isaacson, 1981).

Small bodies (with respect to flow wavelength) or structures with slender elements, do not alter the incident flow (Chakrabarti, 1987), whereas large bodies do change the characteristics of the flow field in the vicinity of the body and require knowledge of the scattered and radiated potential in addition to the incident potential (Wehausen, 1971). Therefore, small body problems can be solved directly due to the explicit form of the hydrodynamic excitation and large body problems require approximation of the hydrodynamic forces or simultaneous solution of the field-body boundary value problem (Newman, 1977). Small body mooring systems (e.g. semi-submersibles, articulated towers) are generally solved by a relative motion Morison formulation (Patel, 1989). Large body systems (e.g. ships, floating production systems) are solved by approximate quasi-static maneuvering equations (Abkovitz, 1972) or by numerical simulation via strip theory (Lewis, 1988) or boundary element methods (Garrison, 1978).

Although the hydrodynamic exciting force of small and large body systems fundamentally differ in their complexity, the fluid-structure interaction force of both systems incorporates similar elements of coupled nonlinear damping and inertial mechanisms. Furthermore, both small and large body systems equivalently incorporate

the nonlinearities of mooring restoring force. Consequently, ocean mooring systems belong to a class of finite multi-degree-of-freedom nonlinear dissipative dynamical systems.

The behavior of nonlinear dissipative dynamical systems subject to deterministic excitation has been studied extensively by both classical and modern techniques. Classical techniques have concentrated on obtaining closed form periodic solutions of integrable or weakly nonlinear systems and analyzing their stability (Bogliubov & Mitropolsky, 1961; Nayfeh & Mook, 1979). Modern techniques concentrate on global bifurcations and address the existence of chaotic solutions and global system behavior (Guckenheimer and Holmes, 1986; Wiggins, 1990).

Chaotic behavior has been shown to be inherent in a general class of nonlinear systems (Thompson and Stewart, 1986; Moon, 1987) and its detection requires the application of modern quantitative measures. Example of such measures are Liapunov exponents (Wolf et al., 1985) and fractal (Farmer et al., 1983; Grassberger and Procaccia, 1983)) or multi-fractal (Feder, 1989) dimensions. The geometric nonlinearity of a multi-point mooring system is equivalent to that of single (Timoshenko, 1974) and double-well potential snap-through oscillators (Clemens & Wauer, 1981; Poddar et al., 1987). The global and chaotic behavior of multi-well potential softening type oscillators has been extensively analyzed for a variety of systems. Examples include the pendulum (Miles, 1988), Josephson junction (Salam & Sastry, 1985) and the softening Duffing equation (Morozov, 1976; Holmes, 1979).

The modified classical methods consist of local stability analysis of all coexisting

solutions (Ioos & Joseph, 1981) which can be obtained by approximate perturbation techniques such as averaging (Sanders and Verhulst, 1985), harmonic balance (Hayashi, 1964) and multiple-scales (Nayfeh, 1973). The modern techniques include global bifurcation analysis based on an asymptotic stability criterion derived by Melnikov (1963) which has been applied to identify sensitivity to initial conditions and transverse intersections (Smale horseshoe type chaos) in a variety of systems exhibiting homoclinicity (Guckenheimer & Holmes, 1986; Wiggins, 1988).

Although numerical evidence of complex and chaotic solutions has been found in nonlinear single well potential systems, analytical research has been limited to modified classical analysis as these systems do not obtain the explicit physical homoclinicity exhibited by multi-well potential systems. Examples of such systems are the weakly nonlinear hardening Duffing equation subjected to combined parametric and external excitation (Yagasaki et al., 1990) and the subharmonic motions of a wind loaded structure analyzed by the general method of averaging (Holmes, 1980). These systems belong to a class of degenerate bifurcation problems which are sensitive to the order of their approximate solution and a higher order approximation is needed to obtain a valid stability criteria (Sanders, 1982). Although homoclinicity can be shown by a variety of transformation techniques, only estimates for the separatrix splitting of the rapidly forced system can be obtained (Holmes et al., 1988). Furthermore, while weakly nonlinear systems have been studied extensively from both classical and modern approaches, complex single equilibrium point systems with a strong nonlinearity are limited in their scope of analysis.

Two possible classical analytical methods of treating strong nonlinearities where small perturbation solutions break down, are modified multiple scales (Burton and Rahman, 1986) and the method of harmonic balance (Szemplinska-Stupnika, 1987). Both methods, applied to the hardening type Duffing equation, show good agreement with numerical solutions, but are sensitive to the order of approximation for a symmetric elastic configuration without a linear static term (Rahman and Burton, 1986; Szemplinska-Stupnika, 1986). Stability analysis of system behavior results in a local bifurcation map defining the regions of existence of the various nonlinear phenomena in parameter space. This analysis consists of perturbing an approximate solution and analyzing the resulting variational equation numerically by Floquet analysis (Nayfeh and Mook, 1979) or by analytically evaluating the equivalent Hill's variational equation (Hayashi, 1964). Stability analysis by these methods has been successfully employed on both hardening and softening Duffing equations (Szemplinska-Stupnika, 1986; Nayfeh and Sanchez, 1989; Szemplinska-Stupnika, 1988).

Coupling of the degrees of freedom in the mooring system further complicates system analysis of finite multi-degree-of-freedom systems (Rosenberg, 1977). Classical techniques (Szemplinska-Stupnika, 1990) complemented by numerical analysis identify an enlarged bifurcation set and chaotic solutions induced by internal resonance mechanisms in quadratically and cubical coupled oscillators (Miles, 1984,a,b). An example of a homoclinic two-degree-of-freedom system analyzed by a modified Melnikov method is the whirling pendulum (Shaw & Wiggins, 1988).

Qualitative analysis can also be performed on autonomous systems in which the

excitation is not time dependent or is replaced by its quasi-static representation (Nayfeh and Mook, 1979). This consists of finding all of the system's fixed points (or equilibrium solutions) and investigating their local stability by perturbation. This technique is employed in the analysis of quasi-statically formulated systems or as an alternative approach to analysis of time averaged amplitude equations obtained by quantitative analysis (Wiggins, 1988). Systems with combined parametric and external excitation (Troger & Hsu, 1977) numerically exhibit enlarged regions of instabilities and chaotic solutions (HaQuang et al., 1987) and are also sensitive to the high frequency of the averaged forcing defined by a small parameter (Yagasaki et al., 1990).

Nonlinear systems have been shown to numerically portray the existence of a superstructure (Parlitz & Lauterborn, 1985) which includes crisis and intermittent phenomena (Grebogi et al., 1983) and which organizes the bifurcation set (Ueda et al., 1990). This superstructure is similar to that observed and analytically determined in codimension-two bifurcation problems such as the Henon map (Holmes & Whitley, 1984) and Circle map (Arnold, 1965).

1.2 Existing Ocean Systems Research

The problems addressed in the area of nonlinear dynamics of compliant offshore structures include a variety of single and multi-point mooring system models. A similar problem addressed is that of nonlinear ocean vehicle roll models. Both types of models incorporate equivalent hydrodynamic exciting forces but fundamentally differ in their

restoring force formulation. The mooring problem has a single-well potential describing a unique physical equilibrium position, whereas the roll problem has a two well potential defining an explicit homoclinic stability (capsize) mechanism (Falzarano, 1990). In a recent paper, Bernitsas and Chung (1991), present a review of the approaches developed for single and multi-point systems in the past four decades. The nonlinear elastic force of a single cable line has been formulated by various methods. Examples include a quasi-static formulation of semi-empirical relations for elastic rope (McKenna and Wong, 1979), catenary equations for chain (Leonard, 1988), and finite elements for steel cable (Papoulias, 1987).

An alternative formulation is to incorporate a measured restoring force or its approximation. Examples of approximations by elementary functions include a piece-wise linear formulation (de Kat and Wichers, 1991), an exponential function description (Virgin and Bishop, 1988) and a truncated power series described by a quartic polynomial (Fujino and Sagara, 1990). Another single-point configuration, modeling coupled tanker-mooring tower motion, consists of a bi-linear formulation (Thompson et al., 1984) and a least square approximation of a discontinuous restoring force resulting in a biased Duffing equation (Lou and Choi, 1990). The geometric nonlinearity of multi-point systems has either been approximated from data (Bishop and Virgin, 1988) or has been incorporated exactly in various numerical models (e.g. Ansari and Khan, 1986; Chen and Chou, 1986; Chiou, 1990) and in a two-point quasi-static model (Bernitsas and Chung, 1991).

Numerical time domain simulation has been the primary tool for solution of both

large (Wichers, 1988) and small body configurations (Bishop and Virgin, 1988; Virgin, 1987). The harmonic balance method complemented by local stability analysis was applied to a moored single-point system modeled by quartic (Fujino and Sagara, 1990) and cubic polynomials (Choi and Lou, 1991). Local autonomous system stability analysis was performed on quasi-static, three-degree-of-freedom, large body models of single (Bernitsas and Papoulias, 1986; Jiang et al., 1987) and two-point (Bernitsas and Chung, 1991) mooring systems. These models incorporate constant descriptions of current, wind (Papoulias and Bernitsas, 1986) and memory effects due to radiated waves (Sharma et al., 1988). Addition of the nonsteady first and second order wave excitation (Jiang and Schellin, 1990), was performed by numerical simulation of the time dependent system for a given input parameter set. Local stability analysis was performed on the reduced time averaged components of the wave excitation (Schellin et al., 1990). Another example of local stability analysis is the ship roll model. The roll restoring moment described by a quintic polynomial approximation was analyzed by multiple scales (Nayfeh and Khdeir, 1986a,b; Nayfeh and Sanchez, 1990) and by an equivalent harmonic balance method (Witz et al., 1989).

These models can be described by two categories. The first category consists of models in which the nonlinear hydrodynamic exciting force is simplified in order to enable analysis of the nonlinear restoring force. A characteristic example is a single-degree-of-freedom harmonically excited nonlinear mooring or ship roll oscillator. This oscillator includes a nonlinear function describing a restoring force, in which the nonlinear drag force is equivalently linearized thus restricting the validity of the models

to very small amplitude motions (Thompson et al., 1984; Virgin, 1987; Bishop & Virgin, 1988; Witz et al., 1989; Choi and Lou, 1991). The second category consists of models incorporating both structural and hydrodynamic nonlinearities. Examples of models in which the influence of the nonlinear drag was not neglected can be found in the numerical analysis of a harmonically excited linearized system (Liaw, 1988) and in the analytical analysis of a simple quadratic (Fujino & Sagara, 1990; Falzarano et al., 1990) or mixed linear-cubic (Nayfeh and Khdeir, 1986a,b; Nayfeh and Sanchez, 1990) approximations of the coupled drag force. Another characteristic example is a three-degree-of-freedom, single point mooring system formulated by approximate quasi-static maneuvering equations (Papoulias and Bernitsas, 1988; Sharma et al., 1988). Nonsteady effects of gusting wind and wave excitation have also been numerically incorporated (Jiang and Schellin, 1990).

Comparison of the complex phenomena obtained by the qualitative global analysis of the quasi-static analysis of single versus two-point moorings analysis (Bernitsas and Chung, 1990) reveals the existence of similar singularities and bifurcations, however detailed bifurcation analysis is required to isolate and identify the various mechanisms governing system stability. In a recent analysis of a single-point mooring system, Jiang (1991), found self-sustained oscillations which became chaotic when the system was subjected to an additional bias or periodic waves. Evidence of strong subharmonic response and a period multiplying route to chaotic motion appears in numerical models of both large and small body ocean mooring models that are subjected to combined steady and fast motions (Bishop and Virgin, 1988; Jiang, 1991). These nonlinear

solutions exist in a relatively narrow parameter space but their magnitude is greater than that of the coexisting harmonic response. As noted above, the multi-point mooring systems exhibits a variety of both structural and hydrodynamical nonlinearities. Consequently, simplification of environmental conditions via equivalent linearization methods or quasi-static representation and approximations of structural nonlinearities may reveal only partial qualitative results and will not determine mechanisms governing system instabilities and sensitivity to initial conditions.

1.3 Thesis Outline

The overall goal of the research presented in this thesis is the investigation of periodic and aperiodic responses of nonlinear mooring systems subjected to excitation induced by a deterministic ocean field. A general class of multi-point mooring system models is formulated to comprehensively study system behavior and address the limitations of existing ocean system research. The models formulated employ an exact analytical form of both structural and hydrodynamical nonlinearities. A semi-analytical methodology is developed to determine existence of complex nonlinear and chaotic phenomena and to identify mechanisms governing system instabilities and sensitivity to initial conditions. Investigation of system stability and control is performed for a range of environmental conditions resulting in conclusions, potential applications and recommendations for future research. The following is a description of thesis chapters incorporating objectives, methodology and analysis summary.

System Model And Global Attraction - A fundamental small body, symmetric multi-point mooring configuration is chosen (Fig.1) to formulate a general class of ocean mooring models and to address the need for consistent analytical research. This configuration consists of an exact geometric nonlinearity and avoids the need for restoring force approximation by truncated elementary functions. Furthermore, the restoring force incorporates a variable mooring assembly representative of both linearized single-point and strongly nonlinear four-point mooring systems. The choice of a small body enables the direct formulation of the exact hydrodynamic exciting force retaining both quadratic drag and convective inertial components. Consequently, the model formulated consists of a three-degree-of-freedom system (surge, heave, pitch) driven by a biased, periodic, two dimensional field. The excitation includes a small amplitude (linear) wave with a weak colinear current and other slowly varying motions that could be represented by the bias (e.g. constant wind, second order drift forces). The ocean mooring system is shown to be a coupled, strongly nonlinear system subjected to a combined biased, parametric and external excitation. Stability analysis of the system by a Liapunov function approach reveals global system attraction which ensures that solutions remain bounded for small excitation. However, this approach does not address coexisting nonlinear solutions, sensitivity to initial conditions or the influence of larger combined excitation.

Stability and the Poincaré Map - Evaluation of system stability in the context of the Poincaré map is obtained by analysis of the nearly integrable averaged system. The hyperbolic fixed (equilibrium) points and closed orbits (limit cycles) of the map

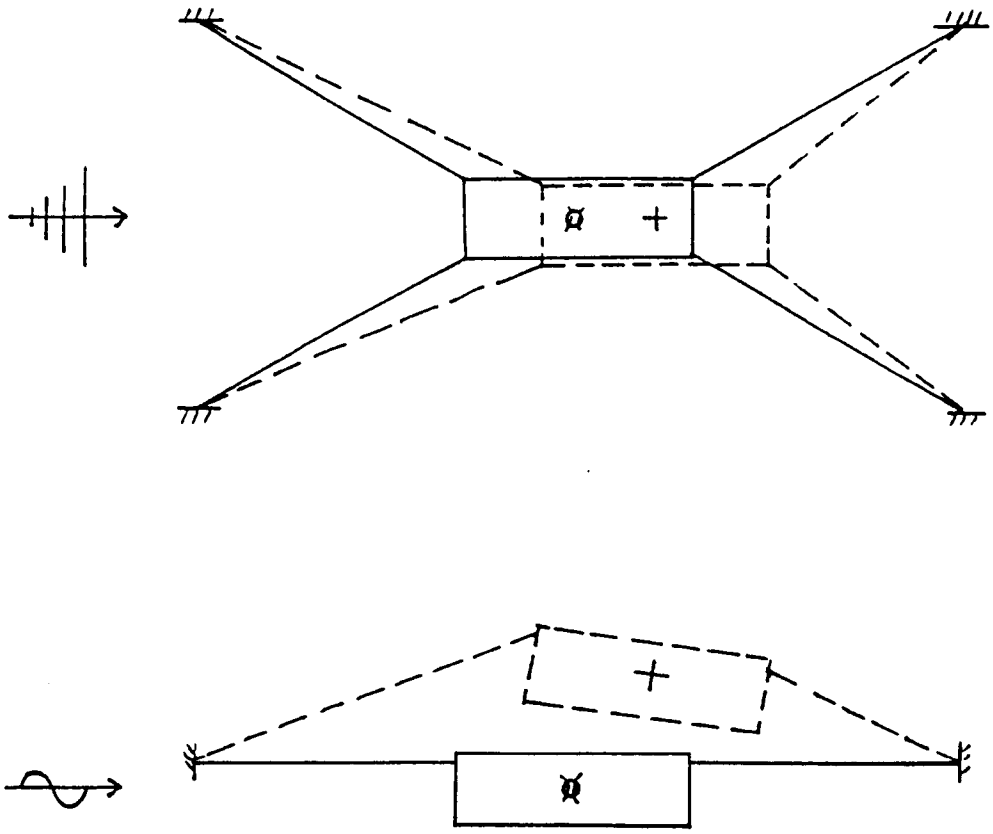

Fig. 1 Mooring assembly

correspond to periodic, steady state orbits of the system. Analysis of the map described by a perturbed Hamiltonian, determines existence and stability of near resonance, primary (harmonic) and secondary coexisting (sub, ultra, ultrasubharmonic) solutions. Furthermore, coexistence of periodic solutions is identified by saddle-node (tangent) bifurcations. Numerical simulations of system response verify the results obtained by stability analysis of the map.

Local Bifurcations - Investigation of nonresonant solutions is done by a local variational approach. This consists of perturbing of an approximate solution and evaluating its stability by analysis of the general Hill's system obtained after linearization of the corresponding variational. Due to the algebraic complexity of the geometric and quadratic drag nonlinearities, the approximate solution is obtained by the method of harmonic balance which is formulated to account for all periodic components. Stability regions are identified by Floquet theory. The first region corresponds to a primary resonant tangent bifurcation and the second region determines existence of secondary symmetry breaking and period doubling bifurcations. Numerical simulations of system response verify the harmonic balance approximation and validate results obtained by local bifurcation analysis.

Global Bifurcations - Existence of global bifurcations is demonstrated semi-analytically. Application of Melnikov's method to the perturbed averaged system provides a criterion for the existence of transverse homoclinic orbits resulting in chaotic system dynamics.

This criterion is sensitive to the high frequency of the averaged system and only estimates for the separatrix splitting of the rapidly forced system are obtained. The estimates, verified by numerical simulation of the system, show sensitivity to initial conditions. Further analysis of the period doubled solution obtained by local bifurcation, reveals possible existence of a cascade of period doubling which is shown by numerical simulation to evolve into a strange attractor. The abrupt transitions between periodic coexisting states are also shown to be sensitive to initial conditions.

Superstructure In The Bifurcation Set And Routes To Chaos - Analysis of the bifurcation criteria obtained reveals a steady state superstructure in the bifurcation set. This structure identifies a similar bifurcation pattern of coexisting solutions in the subharmonic, ultraharmonic and ultrasubharmonic domains. Within this structure strange attractors appear when a period doubling sequence is infinite and when an abrupt change in the size of an attractor occurs near the tangent bifurcation values. The superstructure enables identification of routes to chaos and their relationship with other instabilities for given environmental conditions.

Conclusions And Future Research - Summary of results and conclusions are presented in the final chapter. The applications of the study in the analysis and control of nonlinear ocean mooring, towing and equivalent single-well potential mechanical systems are discussed. Guidelines for further research of system behavior are formulated.

2. SYSTEM MODEL AND GLOBAL ATTRACTION

The multi-point mooring system considered (Fig.1) is formulated as a three-degree-of-freedom (surge, heave, pitch), rigid body, hydrodynamically damped and excited nonlinear oscillator. The equations of motion are derived in section 2.1 based on equilibrium of geometric restoring forces and small body motion under small amplitude monochromatic wave and current excitation. The equations of motion take the following classical form of three coupled nonlinear second order differential equations:

$$\ddot{\mathbf{X}} + \mathbf{D}(\dot{\mathbf{X}}) + \mathbf{R}(\mathbf{X}) = \mathbf{F}(\mathbf{X},\dot{\mathbf{X}},\ddot{\mathbf{X}},t) \tag{1}$$

where

$\mathbf{R}(\mathbf{X})$ and $\mathbf{D}(d\mathbf{X}/dt)$ are the system restoring force and structural damping vectors and $\mathbf{F}(\mathbf{X},d\mathbf{X}/dt,d^2\mathbf{X}/dt^2,t)$ is the time dependent exciting force vector. $\mathbf{X} = (X_1,X_3,X_5)^T$ is the system displacement vector representing surge (X_1), heave (X_3), and pitch (X_5) motions.

Note that $(\dot{\cdot})$ is differentiation with respect to time and that the position of the body centroid at its equilibrium position is the origin of the reference inertial frame. The exciting forces are formulated to account for convective properties caused by nonlinear structural motions and the restoring forces are formulated via a Lagrangian approach due to their complexity. Identification of system nonlinearites is performed in section 2.2 and global attraction of the fundamental nonlinear system is demonstrated in section 2.3.

2.1 Model Formulation

A symmetric multi-point mooring assembly yields an antisymmetric restoring force. Although the mooring lines may have linear elastic properties, the restoring force (stiffness) will include a strong geometric nonlinearity depending on the mooring angles. Two characteristic stiffness configurations which incorporate a material discontinuity are pretensioned (Fig.2a) and slack elastic cables (Fig.2c). The discontinuity in the former case is due to loss of pretension in two lines whereas the latter case is based on an initial slackness. Both configurations can be described by a ratio (l_c/l_0) of initial mooring line length (l_c) to the length of the gap to be bridged by that line (l_0). Therefore, slack or pretensioned lines can be described by $l_c/l_0 > 1$ and $l_c/l_0 < 1$ respectively. The case of taut mooring lines (Fig.2b) represents the limits of both slack and pretensioned cables ($l_c = l_0$). In order to avoid modeling of the discontinuity by an infinite set of describing functions and to isolate the geometric nonlinearity, a continuous mooring restoring force ($\mathbf{R_M}$) is chosen. This force consists of both taut and pretensioned configurations ($l_c \leq l_0$) of linear elastic mooring lines which restrict the motion to the region where all lines retain their initial pretension. The stiffness nonlinearity can vary from a strongly nonlinear two-point system (Fig.3: $b=0$) to an almost linear four-point system (Fig.3: $b >> d$). The total restoring force ($\mathbf{R}$) includes the influence of mooring ($\mathbf{R_M}$) and hydrostatic buoyancy ($\mathbf{R_B}$).

The exciting force ($\mathbf{F}$) is formulated to account for the influence of both nonlinear drag ($\mathbf{F_D}$) and inertial effects ($\mathbf{F_I}$). Both nonlinearities are incorporated

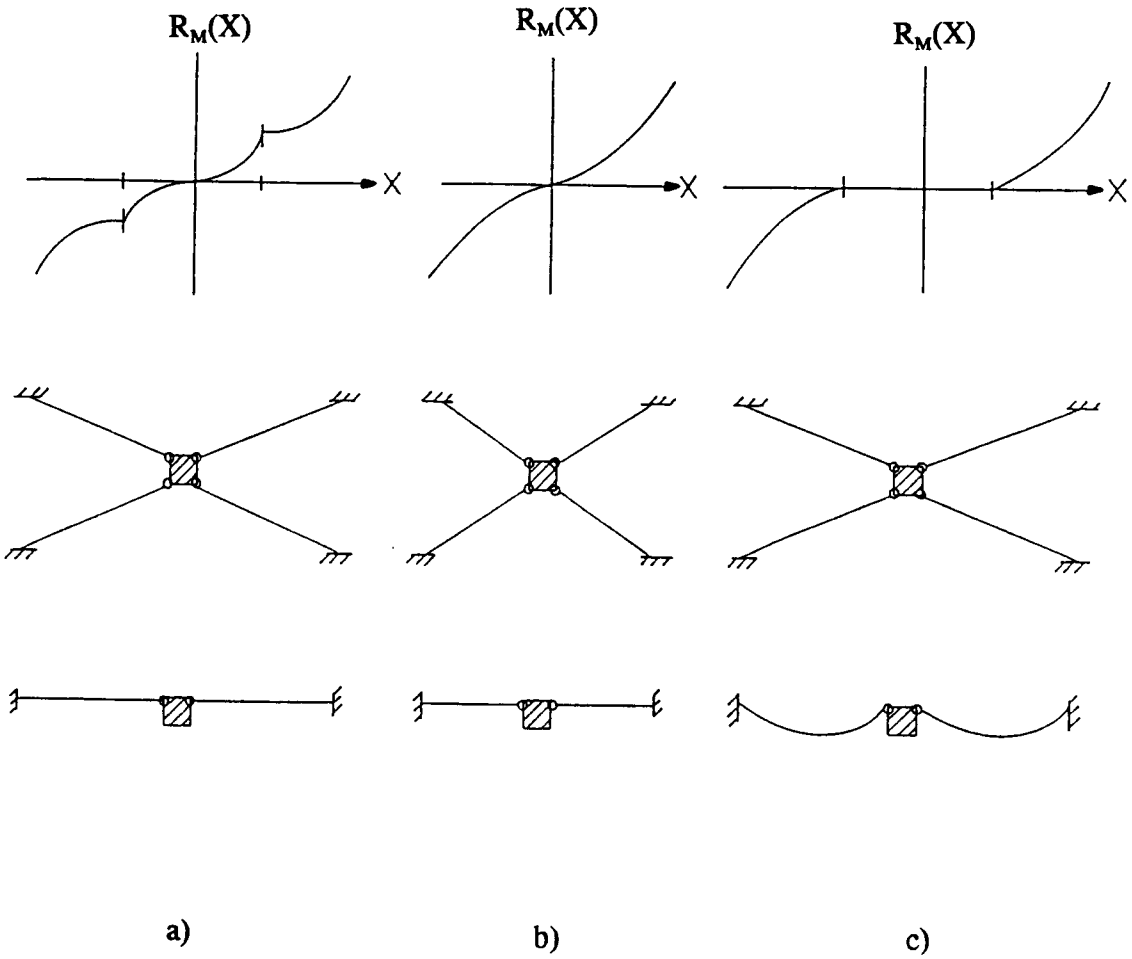

Fig. 2 Mooring restoring force configurations: a) pretension, b) taut, c) slack

exactly. The drag nonlinearity consists of a relative motion quadratic formulation whereas the inertial force consists of both temporal and a relative motion convective term representing body motion ($d\mathbf{X}/dt$) in an unsteady nonuniform flow field [$\mathbf{U}(\mathbf{X},t)$]. Isaacson (1979) demonstrated that the inertia forces calculated in the conventional manner (i.e. Morison equation) will generally overestimate the actual force on fixed bodies subjected to a nonlinear hydrodynamic wave field. The application of the Morison equation to a moving body incorporates a relative velocity ($\mathbf{U}$-$d\mathbf{X}/dt$) in which the second order quantities are typically neglected when linear wave theory is employed. This formulation is valid for linear structural response but the relative motion convective terms cannot be a-priori neglected for nonlinear motion.

Mooring restoring force:

The mooring restoring force [$\mathbf{R}_M(\mathbf{X})$] is conveniently derived from the potential function [$V_M(\mathbf{X})$] describing the pretensioned geometrical configuration of an axis-symmetric small body (Fig.3):

$$V_M(X_1,X_3,X_5) = K\{[l_1(X_1,X_3,X_5)-l_c]^2 + [l_2(X_1,X_3,X_5)-l_c]^2\} \qquad (2)$$

where

$$l_{1,2} = \left[d^2 + \left(\frac{L}{2}\right)^2 + (b \pm X_1)^2 + X_3^2 \pm L X_3 \sin X_5 - L(b \pm X_1)\cos X_5\right]^{1/2} \qquad (3)$$

and K is the elastic force coefficient, l_i ($i=1,2$) is the in-situ mooring line length and l_c is the the initial pretensioned length of the mooring line.

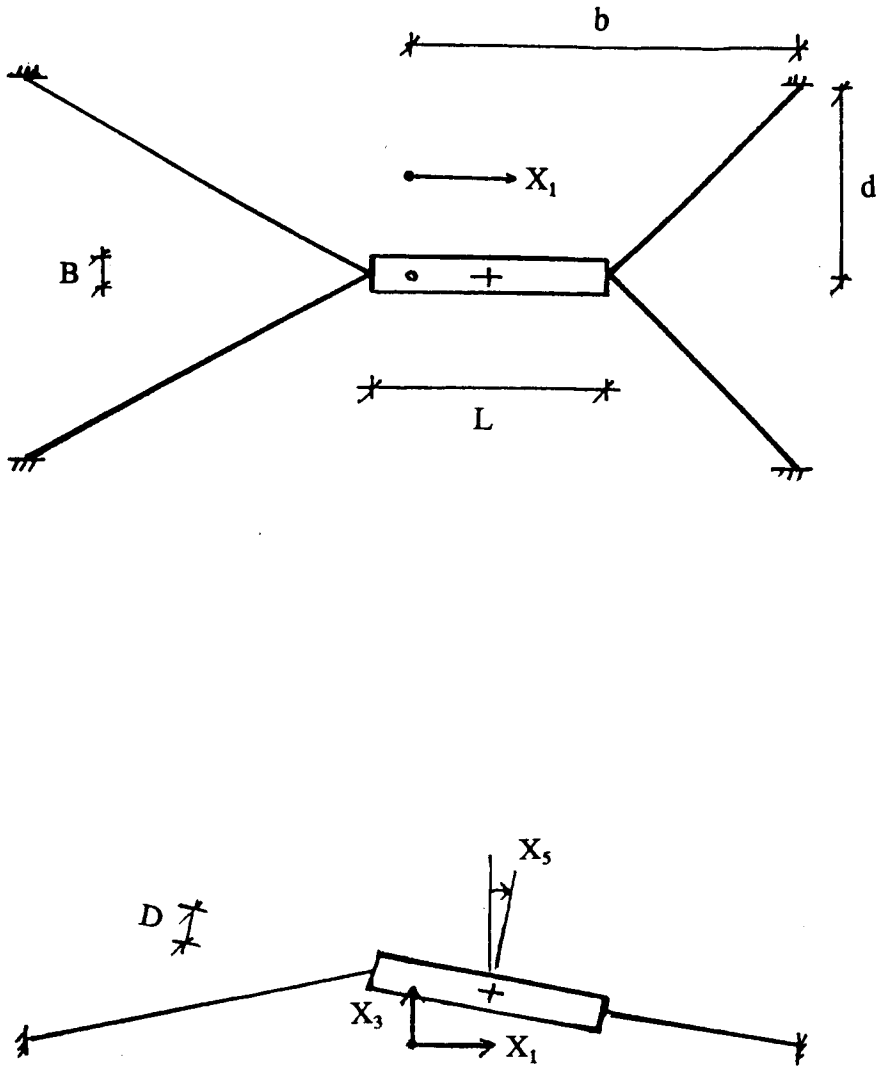

Fig. 3 Definition sketch

Note that the choice of the upper sign refers to l_1 and the lower sign to l_2.

Therefore, $\mathbf{R_M(X)}=dV_M(\mathbf{X})/d\mathbf{X}$ or:

$$\begin{aligned}
R_{M1} &= K\left\{4X_1 + l_c\left[(2b - L\cos X_5)\frac{l_1 - l_2}{l_1 l_2} - 2X_1\frac{l_1 + l_2}{l_1 l_2}\right]\right\} \\
R_{M3} &= K\left\{4X_3 + l_c\left[L\sin X_5\frac{l_1 - l_2}{l_1 l_2} - 2X_3\frac{l_1 + l_2}{l_1 l_2}\right]\right\} \\
R_{M5} &= K\left\{2bL\sin X_5 + l_c\left[L(X_1\sin X_5 + X_3\cos X_5)\frac{l_1 - l_2}{l_1 l_2} - bL\sin X_5\frac{l_1 + l_2}{l_1 l_2}\right]\right\}
\end{aligned} \tag{4}$$

Exciting force:

The exciting force (**F**) consists of drag ($\mathbf{F_D}$) and inertial ($\mathbf{F_I}$) components for an axis-symmetric small body in a biased harmonic two dimensional field:

$$\begin{aligned}
F_{D1} &= \frac{\rho}{2}C_{D1}A_{P1}\left(U_1 - \dot{X}_1\right)\left|U_1 - \dot{X}_1\right| \\
F_{D3} &= \frac{\rho}{2}C_{D3}A_{P3}\left(U_3 - \dot{X}_3\right)\left|U_3 - \dot{X}_3\right|
\end{aligned} \tag{5}$$

$$\begin{aligned}
F_{I1} &= \rho\forall\left(1 + C_{A1}\right)\left[\frac{\partial U_1}{\partial t} + \left(U_1 - \dot{X}_1\right)\frac{\partial U_1}{\partial X_1}\right] \\
&\quad + \rho\forall\left(1 + C_{A3}\right)\left(U_3 - \dot{X}_3\right)\frac{\partial U_3}{\partial X_1} - \rho\forall C_{A1}\ddot{X}_1 \\
F_{I3} &= \rho\forall\left(1 + C_{A3}\right)\left[\frac{\partial U_3}{\partial t} + \left(U_3 - \dot{X}_3\right)\frac{\partial U_3}{\partial X_3}\right] \\
&\quad + \rho\forall\left(1 + C_{A1}\right)\left(U_1 - \dot{X}_1\right)\frac{\partial U_1}{\partial X_3} - \rho\forall C_{A3}\ddot{X}_3
\end{aligned} \tag{6}$$

where

$$U_1 = U_0 + \omega a \frac{\cosh[k(X_3+h)]}{\sinh(kh)} \cos(kX_1 - \omega t)$$
$$U_3 = \omega a \frac{\sinh[k(X_3+h)]}{\sinh(kh)} \sin(kX_1 - \omega t) \quad (7)$$

and

$C_{D1,3}$, $C_{A1,3}$ are hydrodynamic viscous drag and added mass coefficients.

$A_{P1,3}$, $\forall$ are projected drag areas and displaced volume.

U_0 is a colinear current magnitude.

a, ω, k are wave amplitude, frequency and number.

ρ, g, h are water mass density, gravitational acceleration and water depth.

Note that both projected drag areas ($A_{p1,3}$) and displaced volume ($\forall$) are frequency dependent functions when the body is surface piercing and that the projected areas are sensitive to the magnitude of body orientation (or pitch angle): $A_{P1}=B(D\cos X_5+L\sin X_5)$ and $A_{P3}=B(D\sin X_5+L\cos X_5)$. Furthermore, the relationship between wave frequency and number is determined by the linear dispersion equation: $\omega^2=gk\tanh(kh)$.

The drag and inertial components for pitch (F_{D5}, F_{M5}) can be formulated by integrating the differential moments ($dM_{D,I}$) along the length (z': -L/2 to +L/2) of the body: $F_{D5}=\int dM_D(z')$ and $F_{I5}=\int dM_I(z')$ where:

$$dM_{D5} = \frac{\rho}{2} B C_{D5} z' \left(U^* - z'\dot{X}_5\right) \left| U^* - z'\dot{X}_5 \right| dz'$$
$$dM_{I5} = \rho \forall \left\{ (1+C_{A5}) \left[\frac{\partial U^*}{\partial t} + \left(U^* - z'\dot{X}_5\right) \frac{\partial U^*}{\partial X_5} \right] - C_{A5} z' \ddot{X}_5 \right\} dz' \quad (8)$$

and $U^* = U_1 \sin X_5 + U_3 \cos X_5$.

Structural damping force:

The structural damping force (D) consists of independent linearized friction components: $D_i = C_i\, dX_i/dt$ (i=1,3,5), where the damping coefficients are $C_{1,3,5}$.

Equations of motion:

The equations of motion are derived by the Lagrange approach:

$$\frac{d}{dt}\left[\frac{\partial \mathcal{L}}{\partial \dot{q}_i}\right] - \frac{\partial \mathcal{L}}{\partial q_i} = Q_i' \tag{9}$$

where $\mathcal{L}=T-V$ is the Lagrangian function and T, V are the kinetic and potential energies. q_i are generalized coordinates and Q'_i are generalized forces not derivable from the total potential.

The displacement vector components are generalized coordinates and exciting force vector components are generalized forces as they are time dependent. The Lagrangian function is obtained from the kinetic and total potential energies. The potential consists of a mooring component (V_M in Eqn.2) and a body force due to hydrostatic buoyancy and gravity [$V_B=(\rho g \forall - Mg)X_3$)].

$$\begin{aligned} T &= \frac{M}{2}\left(\dot{X}_1^2+\dot{X}_3^2\right) + \frac{I}{2}\dot{X}_5^2 \\ V &= K \sum_i \left[l_i\left(X_1,X_3,X_5\right)-l_c\right]^2 + \left(\rho g \forall - Mg\right)X_3 \end{aligned} \tag{10}$$

where M, I are the body mass and moment of inertia and l_i (i=1,2), the mooring line lengths are given in (Eqn.3).

Rearranging and scaling ($x=X/d$, $\theta=\omega t$) the equations of motion yields the following autonomous system which consists of seven coupled nonlinear first order ordinary differential equations:

$$\begin{aligned} \dot{\mathbf{x}} &= \mathbf{y} \\ \dot{\mathbf{y}} &= -\mathbf{R}(\mathbf{x}) - \mathbf{D}(\mathbf{y}) + \mathbf{F}_{\mathbf{D}}(\mathbf{x},\mathbf{y},\theta) + \mathbf{F}_{\mathbf{I}}(\mathbf{x},\mathbf{y},\theta) \\ \dot{\theta} &= \omega \end{aligned} \tag{11}$$

where

$\mathbf{x}=(x_1,x_3,x_5)^T$, $\mathbf{y}=(y_1,y_3,y_5)^T$ are the length scaled system displacement and velocity vectors. Note that the velocity vector retains the time dimension.

For negligible pitch angles the system simplifies to the following:

$$\begin{aligned} \dot{x}_1 &= y_1 \\ \dot{y}_1 &= -R_1(x_1,x_3) - \gamma_1 y_1 + F_{D1}(x_1,x_3,y_1,\theta) + F_{I1}(x_1,x_3,y_1,y_3,\theta) \\ \dot{x}_3 &= y_3 \\ \dot{y}_3 &= -R_3(x_1,x_3) - \gamma_3 y_3 + F_{D3}(x_1,x_3,y_3,\theta) + F_{I3}(x_1,x_3,y_1,y_3,\theta) \\ \dot{\theta} &= \omega \end{aligned} \tag{12}$$

where

$$\begin{aligned} R_1 &= \alpha \left[x_1 - \tau \left[\frac{l_1+l_2}{l_1 l_2}\, x_1 - \beta\, \frac{l_1-l_2}{l_1 l_2} \right] \right] \\ R_3 &= \alpha \left[(1+\sigma)\, x_3 - \tau \left[\frac{l_1+l_2}{l_1 l_2}\, x_3 \right] \right] \end{aligned} \tag{13}$$

$$l_{1,2} = \left[1 + (\beta \pm x_1)^2 + x_3^2 \right]^{1/2} \tag{14}$$

$$F_{D1} = \mu_1 \delta_1 \left[u_1 - \frac{y_1}{\omega} \right] \left| u_1 - \frac{y_1}{\omega} \right| \qquad (15)$$

$$F_{D3} = \mu_3 \delta_3 \left[u_3 - \frac{y_3}{\omega} \right] \left| u_3 - \frac{y_3}{\omega} \right|$$

$$F_{I1} = \mu_1 \omega^2 \left[\frac{\partial u_1}{\partial \theta} + \left(u_1 - \frac{y_1}{\omega} \right) \frac{\partial u_1}{\partial x_1} \right] + \mu_3 \omega^2 \left(u_3 - \frac{y_3}{\omega} \right) \frac{\partial u_3}{\partial x_1} \qquad (16)$$

$$F_{I3} = \mu_3 \omega^2 \left[\frac{\partial u_3}{\partial \theta} + \left(u_3 - \frac{y_3}{\omega} \right) \frac{\partial u_3}{\partial x_3} \right] + \mu_1 \omega^2 \left(u_1 - \frac{y_1}{\omega} \right) \frac{\partial u_1}{\partial x_3}$$

$$u_1 = f_0 + \frac{\chi}{\kappa} \frac{\cosh[\kappa(x_3 + h')]}{\sinh(\kappa h')} \cos(\kappa x_1 - \theta) \qquad (17)$$

$$u_3 = \frac{\chi}{\kappa} \frac{\sinh[\kappa(x_3 + h')]}{\sinh(\kappa h')} \sin(\kappa x_1 - \theta)$$

and

$$\alpha = \frac{4K}{M + \rho \forall C_{A1}}$$

$$\beta = \frac{2b - L}{2d} \quad ; \quad \tau = \frac{l_c}{2d}$$

$$\sigma = \frac{g}{4K}(\rho \forall - M)$$

$$\gamma_{1,3} = \frac{C_{1,3}}{M + \rho \forall C_{A1}} \qquad (18)$$

$$\delta_{1,3} = \frac{1}{2} \frac{C_{D1,3}}{1 + C_{A1}} \frac{A_{P1,3}}{\forall} g \kappa \tanh(\kappa h')$$

$$\mu_{1,3} = \frac{\rho \forall (1 + C_{A1,3})}{M + \rho \forall C_{A1}}$$

$$f_0 = \frac{U_0}{\omega d} \quad ; \quad \chi = ka \quad ; \quad \kappa = kd \quad ; \quad h' = \frac{h}{d}$$

Note that $\beta,\tau,\sigma,\mu,\kappa,\chi$ are nondimensional parameters whereas α,γ,δ and ω incorporate a time dimension. The restoring force is characterized by four parameters: α is a scaling amplitude, β describes the geometric nonlinearity in the horizontal plane, τ is a measure of the pretension in the mooring lines and $\sigma \geq 1$ characterizes non-negative buoyancy. The inertial exciting force is characterized by the wave frequency ω, a limiting wave steepness parameter $\chi < \pi/7$ and $\mu_1 > 1$ defines positive buoyancy. The damping force includes hydrodynamic drag δ and structural damping γ.

2.2 Identification of Nonlinearites

The system nonlinearities appear in each of the principal equations (dy/dt) which are further complicated by coupling. System reduction to surge and heave for small pitch angles (Eqn.12) reveals that the coupling appears in the symmetric restoring force (Eqns.13,14) and in both drag and inertia components of the exciting force (Eqns.15,16) due to the coupled hydrodynamic velocity potential (Eqn.17). Note that for a neutrally buoyant ($\sigma=0$), strongly nonlinear ($\beta=0$) configuration the restoring force components ($R_{1,3}$: Eqn.13) are identical for surge and heave. Consequently, the fundamental nonlinearities can be identified in the following limiting single-degree-of-freedom equation for surge [$(x,y) \equiv (x_1,y_1)$]:

$$\begin{aligned} \dot{x} &= y \\ \dot{y} &= -R(x) - \gamma y + F_D(x,y,\theta) + F_I(x,y,\theta) \\ \dot{\theta} &= \omega \end{aligned} \tag{19}$$

where

$$R = \alpha \left[x - \tau \left[\frac{\beta + x}{\sqrt{1+(\beta+x)^2}} - \frac{\beta - x}{\sqrt{1+(\beta-x)^2}} \right] \right] \tag{20}$$

$$F_D = \mu\delta \left[u - \frac{y}{\omega} \right] \left| u - \frac{y}{\omega} \right| \tag{21}$$

$$F_I = \mu\omega^2 \left[\frac{\partial u}{\partial \theta} + \left[u - \frac{y}{\omega} \right] \frac{\partial u}{\partial x} \right] \tag{22}$$

$$u = f_0 + f_1 \cos(\kappa x - \theta) \tag{23}$$

and

$$\alpha = \frac{4K}{M + \rho \forall C_{A1}}$$

$$\beta = \frac{2b - L}{2d} \quad ; \quad \tau = \frac{l_c}{2d}$$

$$\gamma = \frac{C_1}{M + \rho \forall C_{A1}}$$

$$\delta = \frac{1}{2} \frac{C_{D1}}{1 + C_{A1}} \frac{A_{P1}}{\forall} g\kappa \tanh(\kappa h') \tag{24}$$

$$\mu = \frac{\rho \forall (1 + C_{A1})}{M + \rho \forall C_{A1}}$$

$$f_0 = \frac{U_0}{\omega d} \quad ; \quad \chi = ka \quad ; \quad \kappa = kd \quad ; \quad h' = \frac{h}{d}$$

$$f_1 = \frac{\chi}{\kappa} \frac{\cosh[\kappa(x_3 + h')]}{\sinh(\kappa h')}$$

The fundamental O(1) geometric nonlinearity of the system is identified by the frequency response of the associated Hamiltonian system (Eqn.19: $\gamma=0$, $F_D=F_I=0$). The response (natural) period of the Hamiltonian system T_n, can be directly computed

by integrating the Hamiltonian phase plane $(x,y)_H$: $T_n=4 \int y(x)^{-1}dx$, resulting in an integral form of the frequency response ($\omega_n=2\pi/T_n$):

$$\omega_n = \frac{\pi}{2} \left[\int_0^{x_{max}} \frac{dx}{y(x)} \right]^{-1} \tag{25}$$

where

$$y(x) = \sqrt{2 \left[V(x_0) - V(x) \right]} \qquad \equiv \dot{x} \tag{26}$$

$$V(x) = \alpha \left\{ \frac{x^2}{2} - \tau \left[\sqrt{1+(\beta+x)^2} + \sqrt{1+(\beta-x)^2} \right] \right\} \tag{27}$$

and $V(x_0)$ is a function of initial conditions calculable from the invariant Hamiltonian energy $H(x,y)= \frac{1}{2}y^2+V(x)$.

The integral form (Eqn.25) of the frequency response ("backbone") characterizes the systems degree of geometric nonlinearity as is depicted in Fig.4 by the curvature of the backbone curves. The strongest nonlinearity is obtained for right angle mooring ($\beta=0$) whereas the weakest nonlinearity is found for small angles ($\beta>>1$).

Identification of the exciting force nonlinearities is conveniently described by scaling system displacement by the wave number k ($x=kX$). The restoring force is approximated by a least square representation: $R(x)=\Sigma\alpha_n x^n$, $n=1,3,\ldots,N$ where the coefficients α_n, are functions of exciting frequency (ω) in addition to the structural coefficients (α, β, τ). Note that the strongly nonlinear mooring system ($\beta=0$) does not have a linear term ($\alpha_1=0$). The weakly nonlinear system is described with decreasing

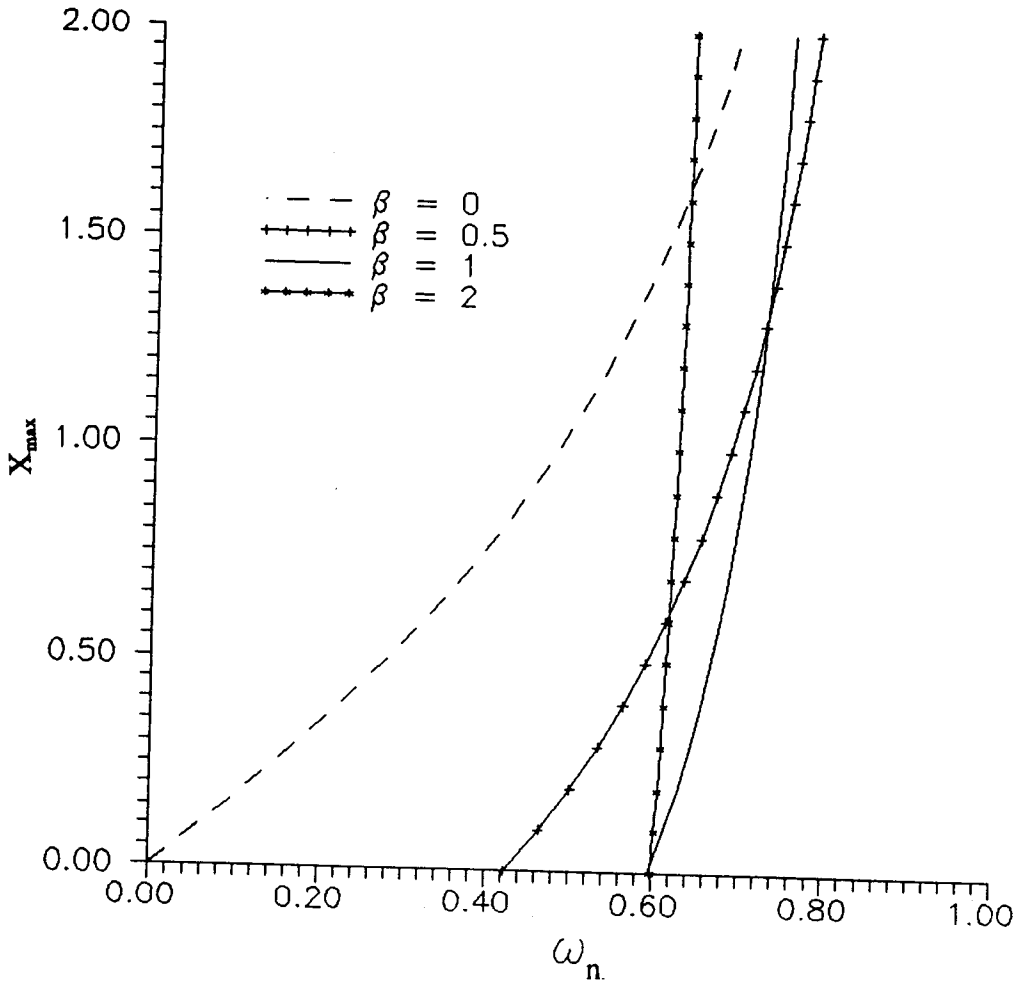

Fig. 4 Degree of geometric nonlinearity

coefficients and is limited by a linearized mooring configuration ($\alpha_1=1$, $\alpha_{n>1}=0$) corresponding to very small mooring line angles ($\beta >> 1$). As the scaled displacement is not large, wave kinematics can be represented by the following finite trigonometric series expansion obtained by expanding $\sin(\kappa x)$ and $\cos(\kappa x)$ in Eqn.23:

$$u(x,\theta) = f_0 + f_1 \sum_n \left[\frac{x^{n-1}}{(n-1)!}\cos\theta + \frac{x^n}{n!}\sin\theta \right]$$
$$\dot{u}(x,\theta) = f_1 \sum_n \left[\frac{x^n}{n!}\cos\theta - \frac{x^{n-1}}{(n-1)!}\sin\theta \right] \qquad (28)$$

where $n=1,3,5,\ldots,N.$

Substitution of the trigonometric series, enables the isolation of nonlinear terms and identification of the controlling parameters governing the response in the following system representation:

$$\begin{aligned} \dot{x} &= y \\ \dot{y} &= F_1(x,\theta) + F_2(x,y,\theta) \\ \dot{\theta} &= \omega \end{aligned} \qquad (29)$$

where

$$F_1(x,\theta) = \sum_l \left[B_l + K_l(\theta) \right] x^l \qquad (30)$$

$$F_2(x,y,\theta) = \sum_l \Gamma_l\, y^l + \left[\sum_l \Lambda_l(\theta)\, x^l \right] y \qquad (31)$$

and $l=0,1,2,3,\ldots,L$

[see Appendix (A.1) for parameter detail (L=3)].

Note that $F_1(l=0)$ contributes a bias ($B_0 \propto f_0^2, f_1^2$) and an external excitation [$\kappa_0(\theta) \propto \cos(j\theta+\phi_j)$;$j=1,2$] whereas both $F_1(l\geq 1)$ and $F_2(l\geq 0)$ include parametric excitation [$\Sigma\kappa_l(\theta)x^l$ and $\Sigma\Lambda_l(\theta)yx^l$ where $\kappa(\theta)$ and $\Lambda(\theta) \propto \cos(j\theta+\phi_j)$;$j=1,2$]. The bias and parametric excitation are functions of both current ($f_0 \propto U_0$) and waves ($f_1 \propto ka$) and their governing mechanisms can be identified in both drag (F_D: $u|u|$ in Eqn.21) and inertial (F_I: $u\, du/dx$ in Eqn.22) components of the exciting force.

The governing system nonlinearities ($L=3$) are quadratic (x^2, xy, y^2) and cubic (x^3). Furthermore, even the linearized mooring system ($\alpha_1=1$, $\alpha_{n>1}=0$) when subjected to small excitation ($\cos x \to 1$, $\sin x \to x$) retains the quadratic nonlinearities (y^2, xy) and the biased combined external and parametric excitation. The biased combined parametric and external excitation include leading order terms from both drag [$\mu\delta(f_0^2+f_1^2/2)$, $\mu\delta f_1$, $\mu\delta\sqrt{(f_0^2+f_1^2)}$] and inertial [$\mu\omega^2\kappa f_1^2$, $\mu\omega^2\kappa f_1(f_0+1)$, $\mu\omega^2 f_1\sqrt{(\kappa^2+1)}$] exciting forces. Comparison of weakly nonlinear quadratic and equivalently linearized damping functions (e.g. Nayfeh and Mook, 1979) reveals that their rates of decay are proportional to the square of the amplitude of the initial disturbance and to the amplitude itself respectively. Consequently, the bias and parametric excitation can only be neglected (e.g. by equivalent linearization) for very small hydrodynamic excitation. A bias and parametric excitation have been found to be a precursor of symmetry breaking leading to period doubling and a generating mechanism for system instabilities even for small amplitude response (Salam and Sastry, 1985; Miles, 1988). Thus, the mooring system is shown to be a coupled nonlinear parametrically excited system and is expected to exhibit complex dynamics (Troger and Hsu, 1977) and chaotic motions (HaQuang et al., 1987).

2.3 Integrability and Global Attraction

The system (Eqn.11) does not have any fixed points in seven-dimensional space $(\mathbf{x},\mathbf{y},\theta)$ because $d\theta/dt=\omega$. However, a unique equilibrium position $[(\mathbf{x},\mathbf{y})_e=\mathbf{0}]$ in six-dimensional space $(\mathbf{x},\mathbf{y})$ can be determined via the associated integrable Hamiltonian system which yields an elliptic phase space described by the invariant Hamiltonian energy depicted (in any choice of two dimensions) by stable centers (Fig.5c).

$$H(x_1,x_3,x_5,y_1,y_3,y_5) = \frac{1}{2}\left(y_1^2+y_3^2+y_5^2\right) + V(x_1,x_3,x_5) \tag{32}$$

Investigation of the structurally damped [Eqn.12: $\boldsymbol{\gamma}\neq\mathbf{0}$, $\boldsymbol{\gamma}=(\gamma_1,\gamma_3)^T$] unforced system (Eqn.12: $F_{D1,3}=F_{I1,3}=0$) by local stability analysis is performed by linearizing the system about the unique equilibrium position (fixed point) at the origin $[(\mathbf{x},\mathbf{y})_e=\mathbf{0}]$. The associated linearized system [or vector field: $d\mathbf{z}/dt=\mathbf{A}\,\mathbf{z}$ where $\mathbf{z}=(\mathbf{x}-\mathbf{x}_e,\mathbf{y}-\mathbf{y}_e)$ and $\mathbf{A}$ is the derivative matrix of $-\mathbf{R}(\mathbf{x})-\boldsymbol{\gamma}\mathbf{y}$ from Eqn.12 evaluated at $(\mathbf{x},\mathbf{y})_e$] is structurally (asymptotically) stable if all the eigenvalues of the describing matrix ($\mathbf{A}$) have negative real parts. Consequently, the equilibrium solution $(\mathbf{x},\mathbf{y})=(\mathbf{x},\mathbf{y})_e$ of the nonlinear vector field is asymptotically stable. The following characteristic equation describes linearized vector field of the system (Eqn.12: $\boldsymbol{\gamma}\neq\mathbf{0}$, $F_{D1,3}=F_{I1,3}=0$) about the fixed point $[(x_1,x_3,y_1,y_3)_e=(0,0,0,0)]$:

$$a_4\lambda^4+a_3\lambda^3+a_2\lambda^2+a_1\lambda+a_0 = 0 \tag{33}$$

where

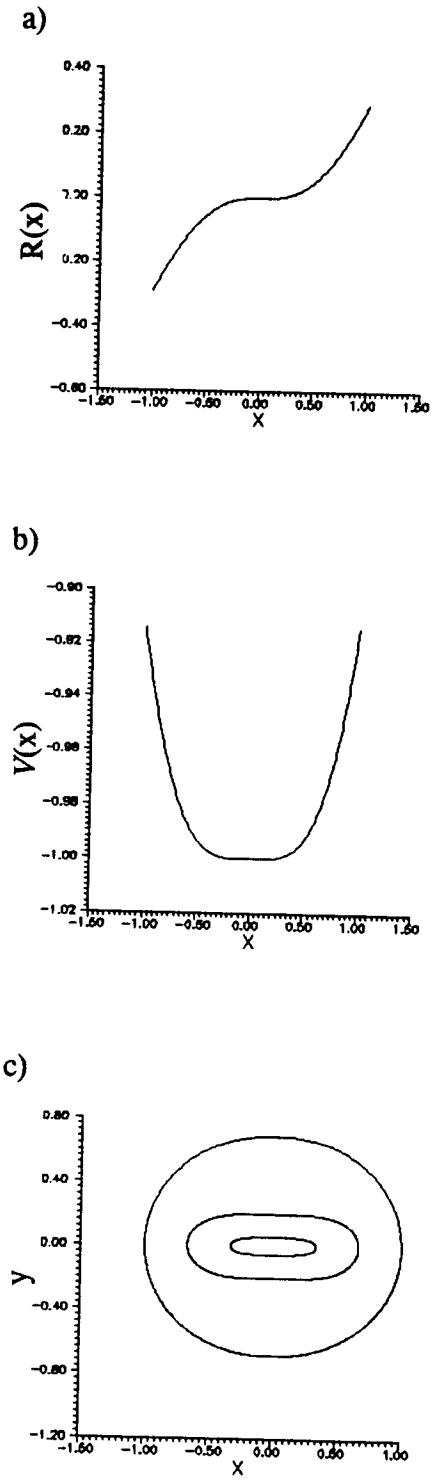

Fig.5 Hamiltonian system: a) restoring force, b) potential, c) phase plane

$$
\begin{aligned}
a_4 &= 1 \\
a_3 &= \gamma_1 + \gamma_3 \\
a_2 &= \gamma_1\gamma_3 + \alpha\left[2 + \sigma - 2\tau\frac{2+\beta^2}{(1+\beta^2)^{3/2}}\right] \\
a_1 &= \alpha\left[(1+\sigma)\gamma_1 + \gamma_3 - 2\tau\frac{(1+\beta^2)\gamma_1+\gamma_3}{(1+\beta^2)^{3/2}}\right] \\
a_0 &= \alpha^2\left[1 + \sigma - \frac{2\tau(2+\beta^2)}{(1+\beta^2)^{3/2}} + \left[\frac{2\tau}{1+\beta^2}\right]^2\right]
\end{aligned}
\tag{34}
$$

According to the Hurwitz criterion (e.g. Schmidt and Tondl, 1986), the linear vector field near the origin is structurally stable [λ_i (i=1,..,4) have negative real parts] if and only if the coefficients a_i (i=0,..,4) and the following determinants ($D_{1,2}$) are always positive.

$$
D_1 = \begin{vmatrix} a_3 & 1 \\ a_1 & a_2 \end{vmatrix} \quad ; \quad D_2 = \begin{vmatrix} a_3 & 1 & 0 \\ a_1 & a_2 & a_3 \\ 0 & a_0 & a_1 \end{vmatrix} \tag{35}
$$

Evaluation of the determinants results in the following:

$$
\begin{aligned}
D_1 &= (\gamma_1+\gamma_3)\gamma_1\gamma_3 + \alpha[\gamma_1 + (1+\sigma)\gamma_3] - 2\alpha\tau\frac{\gamma_1 + (1+\beta^2)\gamma_3}{(1+\beta^2)^{3/2}} \\
D_2 &= \alpha(\gamma_1+\gamma_3)\gamma_1\gamma_3\left\{[(1+\sigma)\gamma_1+\gamma_3] - 2\tau\frac{(1+\beta^2)^2\gamma_1+\gamma_3}{(1+\beta^2)^{3/2}}\right\} \\
&\quad + \alpha^2(\gamma_1^2+\gamma_3^2)\left\{1+\sigma-2\tau\frac{2+\sigma+\beta^2}{(1+\beta^2)^{3/2}} + \left(\frac{2\tau}{1+\beta^2}\right)^2\right\} \\
&\quad + \alpha^2\gamma_1\gamma_3\left\{[1+(1+\sigma)^2] - 2\tau\frac{1+\sigma+\sigma\beta^2+\beta^2}{(1+\beta^2)^{3/2}} + (2\tau)^2\frac{1+(1+\beta^2)^2}{(1+\beta^2)^3}\right\}
\end{aligned}
\tag{36}
$$

Investigation of the coefficients and determinants is done by introducing the pretension constraint $2\tau \leq \sqrt{(1+\beta^2)}$ (i.e. $l_c \leq l_0$). The resulting inequalities show that the vector field is structurally stable throughout parameter space $(\alpha,\beta,\tau,\sigma,\gamma_{1,3})$ with the exception of a neutrally buoyant ($\sigma=0$), taut ($\tau=1/2$) right angle mooring configuration ($\beta=0$) which reveals a higher order degeneracy.

Excitation of the system by a weak horizontal current alone (Eqns.19-23: $f_0 \neq 0$, $f_1=0$) creates a bias or shift in the location of the unique equilibrium position $[(x,y)_e=(x_c,0)$ where $R(x_c)=\delta' f'_0$ and $\delta'=\frac{1}{2}\rho C_D A_P/Md$, $f'_0=U_0/d]$ but does not change system stability. An increase in current magnitude reveals the existence of two additional fixed points $[(x,y)_e = (x_{ci},0)$, $i=1,2,3$ where $x_{c1} > x_{c2} > x_{c3}]$. Stability of these fixed points ($i=1,2,3$) is characterized by the eigenvalues $(\lambda_{1,2})_i$ of the characteristic equation derived from the associated linearized system: $\lambda^2 - p_i\lambda + q_i = 0$, where p_i and q_i are the trace and determinant of the derivative matrix (evaluated for each fixed point i) respectively (e.g. Jordan & Smith, 1987):

$$(\lambda_{1,2})_i = \frac{1}{2}\left(p_i \pm \sqrt{p_i^2 - 4q_i}\right) \tag{37}$$

where

$$\begin{aligned} p_i &= -\gamma - 2\delta' f'^2_0 \qquad < 0 \\ q_i &= \alpha\left[1 - \tau\left\{\left[1+(\beta+x_{ci})^2\right]^{-3/2} + \left[1+(\beta-x_{ci})^2\right]^{-3/2}\right\}\right] \end{aligned} \tag{38}$$

Substitution of x_{ci} into q_i reveals three coexisting hyperbolic fixed points: two sinks ($p_{1,3}<0$, $q_{1,3}>0$) separated by a saddle ($q_2<0$).

Application of Bendixson's criterion [Guckenheimer and Holmes, 1986: $B=\partial f_1/\partial x+\partial f_2/\partial y$ where $dx/dt=f_1(x,y,t)$, $dy/dt=f_2(x,y,t)$] reveals that the phase plane (x,y) of the biased system cannot contain limit cycles ($B\neq 0$ and does not change sign):

$$B(x,y) = -\left(\gamma + 2\delta\,|f_0 - y|\right) \qquad < 0 \tag{39}$$

Furthermore, no homoclinic loops can occur as there is only one possible saddle point $(x_{c2},0)$ in the plane and the stable and unstable manifolds of this saddle cannot intersect.

However, with the addition of harmonic wave excitation the hyperbolic fixed points (sinks, saddle) become hyperbolic closed orbits (stable and unstable limit cycles). Although the stable limit cycle loses the circularity of the sink, it is anticipated by the invariant manifold theorem to retain its stable characteristics for small excitation (Guckenheimer and Holmes, 1986). In order to validate and quantify the qualitative results of local analysis, global stability of the system is performed by a Liapunov function approach (e.g. Hagedorn, 1978).

For the undamped (Hamiltonian) system, a weak Liapunov function $L(x,y)$ with $L(0,0)=0$ at $(x,y)_e=(0,0)$, and $dL/dt\equiv 0$, can be found by adding a constant term $[2\alpha\tau\sqrt{(1+\beta^2)}]$ to the Hamiltonian energy [$H(x,y)=\frac{1}{2}y_2+V(x)$ where $V(x)$ is in Eqn.27]. Thus, the origin is neutrally stable.

Modification of $L(x,y)$ to account for damping defines the following:

$$L(x,y) = \frac{y^2}{2} + V(x) + 2\alpha\tau\sqrt{1+\beta^2} + \nu\left[xy + \frac{1}{2}\gamma x^2\right] \tag{40}$$

and

$$\begin{aligned} \dot{L}(x,y) &= y\dot{y} + \frac{dV(x)}{dx}\dot{x} + \nu(y\dot{x} + x\dot{y} + \delta x\dot{x}) \\ &= -\nu[\alpha \text{ x } R(x)] - (\delta - \nu)\, y^2 \end{aligned} \tag{41}$$

Choosing ν in Eqns.40,41 sufficiently small ($0<\nu<\gamma$) results in a globally stable unforced system where $L(x,y)$ positive definite and $dL/dt \leq 0$.

The characteristics of the biased system with current alone remain unchanged. The biased system describes a quasi-statically formulated single-degree-of-freedom mooring system. Consequently, this result implies the existence of an attractive set for multi-point mooring systems driven by steady excitation representative of superimposed constant forcing.

In order to confirm global stability of the harmonically excited system, differentiation of the Liapunov function is performed along solution curves of the forced system (Holmes, 1979):

$$\begin{aligned} \dot{L} &= -\nu x R(x) - (\delta - \nu) y^2 + (f_0 - f_1 \sin\theta)(\nu x + y) \\ &\leq -\nu x R(x) - (\delta - \nu) y^2 + |\nu f_0 x| + |f_0 y| + |\nu f_1 x| + |f_1 y| \end{aligned} \tag{42}$$

Thus, for small f_0 and f_1, and in the neighborhood of $(x,y)=(0,0)$, solutions of the system remain bounded ($dL/dt \leq 0$), and the limit cycles are globally stable for small excitation. Strong excitation and coexistence of solutions will be addressed by local stability analysis in the following chapters.

3. STABILITY AND THE POINCARÉ MAP

In order to evaluate the stability of system response under larger excitation, it is convenient to consider system response in the context of the Poincaré map where the solution is stroboscopically sampled at each forcing period ($T=2\pi/\omega$). By employing the averaging theorem (Sanders and Verhulst, 1985), hyperbolic fixed points of the resulting system will correspond to periodic orbits of the forcing period. Following Wiggins (1990), consider the following vector field which posses an unperturbed ($\epsilon=0$) solution that is periodic in t with frequency ω_0:

$$\begin{aligned} \dot{x} &= y \\ \dot{y} &= -\omega_0^2 x + \epsilon G(x,y,t;\epsilon) \end{aligned} \tag{43}$$

By assuming a near resonance relationship ($n\omega \approx m\omega_0$) and time dependent initial conditions $[x_0(t),y_0(t)]$, the approximate solution to Eqn.43 can be formulated:

$$\begin{aligned} x(t) &= x_0(t)\cos\frac{n}{m}\omega t + y_0(t)\frac{m}{n\omega}\sin\frac{n}{m}\omega t \\ y(t) &= -x_0(t)\frac{n}{m}\omega \sin\frac{n}{m}\omega t + y_0(t)\cos\frac{n}{m}\omega t \end{aligned} \tag{44}$$

where $x_0(t)$ and $y_0(t)$ are periodic with period $2\pi/\omega$.

Let r be a resonance ratio $r \equiv n/m$ where n,m are relatively prime integers (i.e. all common factors have been divided out). In the case of near primary resonance: $r=1$ ($m=n=1$), the solution returns to its starting point on the Poincaré map whereas in the case of near secondary resonance: $r \neq 1$ ($m,n>1$), three subcases are identified:

i) subharmonic of order m ($r=1/m$: $n=1, m>1$) - the solution pierces the Poincaré cross section m times before returning to its starting point and the fixed point of the averaged system corresponds to a period m point of the Poincaré map.

ii) ultraharmonic of order n ($r=n$: $n>1, m=1$) - the solution returns to its starting point and a fixed point of the averaged system corresponds to a point of the Poincaré map.

iii) ultrasubharmonic of order m,n ($r=n/m$: $n>1$, $m>1$) - hyperbolic fixed points of the averaged equation correspond to period m points of the Poincaré map.

Section 3.1 describes the formulation of the averaged system and its transformation to a perturbed Hamiltonian system. The transformed system includes an unperturbed potential function consisting of the averaged restoring force and the inertial exciting force whereas the perturbation consists of the hydrodynamic drag force complemented by structural damping. Sections 3.2 and 3.3 describe stability analysis of the primary and secondary resonances and section 3.4 includes some geometric properties of resonant and nonresonant nonlinear solutions. Numerical simulations of the system (see details in Appendix B) verify the results obtained by stability analysis of the map and depict solutions in phase space (x,y), Poincaré map (X_P, Y_P) and power spectrum [$S_x(\omega)$]. The subharmonic and ultrasubharmonic solutions are portrayed by a finite set of m points in the Poincaré map whereas the order of the solution is that of the peak with the largest energy content in the power spectra. Note that the map does not identify an ultraharmonic and the spectra does not always discern between close ultrasubharmonics. Consequently, both the Poincaré map and the power spectra are needed to resolve the question of solution identity.

3.1 The Averaged System

We prepare our system (Eqn.19) for averaging by rewriting the restoring force as an odd polynomial by a least square approximation: $R(x)=\Sigma\alpha_l x^l$, $l=1,3,..,L$. This representation enables the formulation of a detuning parameter:

$$\epsilon\Omega' = \omega^2 - \left[\frac{m}{n}\right]^2 \alpha_1 \tag{45}$$

denoting the nearness to primary ($r=1$: $m=n=1$) and secondary ($r\neq 1$: $m>1$, $n>1$) resonances by identification of a fundamental linear natural frequency $\sqrt{\alpha_1}$. Furthermore, as first order averaging precludes a bias, the hydrodynamic excitation is simplified to harmonic wave representation ($f_0=0$: $u=f_1\cos\theta$, $F_I=\mu\omega^2 u$). Thus, the system can be put in standard form for averaging (Sanders & Verhulst, 1985): $dq/d\theta=\mathbf{F}(q)+\epsilon\mathbf{G}(q)$ where $\epsilon<<1$ $[\mathbf{F}=(F_1(q),F_2(q))^T$, $\mathbf{G}=(G_1(q,\theta),G_2(q,\theta))^T]$.

The following invertible van der Pol transformation is applied to the system

$$\begin{bmatrix} u \\ v \end{bmatrix} = \mathbf{A} \begin{bmatrix} x \\ y \end{bmatrix}$$

$$\mathbf{A} = \begin{bmatrix} \cos\frac{n}{m}\theta & -\frac{m}{n\omega}\sin\frac{n}{m}\theta \\ -\sin\frac{n}{m}\theta & -\frac{m}{n\omega}\cos\frac{n}{m}\theta \end{bmatrix} \tag{46}$$

$$\mathbf{A}^{-1} = \begin{bmatrix} \cos\frac{n}{m}\theta & -\sin\frac{n}{m}\theta \\ -\omega\frac{n}{m}\sin\frac{n}{m}\theta & -\omega\frac{n}{m}\cos\frac{n}{m}\theta \end{bmatrix}$$

resulting in the following transformed system:

$$\begin{bmatrix} \dot{u} \\ \dot{v} \end{bmatrix} = -\frac{\epsilon}{\omega}\frac{n}{m}\left[R(u,v,\theta)+C(u,v,\theta)+F_D(u,v,\theta)+F_I(\theta)\right]\begin{bmatrix} \sin\frac{n}{m}\theta \\ \cos\frac{n}{m}\theta \end{bmatrix} \tag{47}$$

where

$$R(u,v,\theta)=\Omega'\left[u\cos\frac{n}{m}\theta - v\sin\frac{n}{m}\theta\right] - \left[\frac{m}{n}\right]^2 \sum_{l+2}^{L}\alpha_n'\left[u\cos\frac{n}{m}\theta - v\sin\frac{n}{m}\theta\right]^{l+2} \tag{48}$$

$$C(u,v,\theta) = \frac{m}{n}\omega\,\gamma'\left[u\sin\frac{n}{m}\theta + v\cos\frac{n}{m}\theta\right] \tag{49}$$

$$F_D(u,v,\theta)=\mu\delta'\left[\frac{m}{n}f_1\cos\theta + u\sin\frac{n}{m}\theta + v\cos\frac{n}{m}\theta\right] \left|\frac{m}{n}f_1\cos\theta + u\sin\frac{n}{m}\theta + v\cos\frac{n}{m}\theta\right| \tag{50}$$

$$F_I(\theta) = -\left[\frac{m}{n}\right]^2\omega^2\mu\, f_1'\sin\theta \tag{51}$$

and $\alpha_{n+2} = \epsilon\alpha'_{n+2}$, $\gamma = \epsilon\gamma'$, $\delta = \epsilon\delta'$, $f_1 = \epsilon f_1'$.

Averaging of the transformed system (Eqn.47 with L=3 in Eqn.48) over $2m\pi/n$ ($T=2\pi/\omega$) results in the following autonomous system:

$$\begin{bmatrix} \dot{u} \\ \dot{v} \end{bmatrix} = -\frac{\epsilon}{2\omega}\frac{n}{m}\left[S(u,v)\begin{bmatrix} u \\ v \end{bmatrix} + \frac{n}{m\pi}\begin{bmatrix} I_S(u,v) \\ I_C(u,v) \end{bmatrix} + \delta_{r,1}\begin{bmatrix} -\omega^2\mu f_1' \\ 0 \end{bmatrix}\right] \tag{52}$$

where

$$S(u,v) = \begin{bmatrix} \frac{m}{n}\omega\ \gamma' & -\Omega' + \frac{3}{4}\left[\frac{m}{n}\right]^2 \alpha_3'(u^2+v^2) \\ \Omega' - \frac{3}{4}\left[\frac{m}{n}\right]^2 \alpha_3'(u^2+v^2) & \frac{m}{n}\omega\ \gamma' \end{bmatrix} \tag{53}$$

$$\begin{bmatrix} I_S(u,v) \\ I_C(u,v) \end{bmatrix} = \int_0^{2\frac{n}{m}\pi} F_D(u,v,\theta) \begin{bmatrix} \sin\frac{n}{m}\theta \\ \cos\frac{n}{m}\theta \end{bmatrix} d\theta \tag{54}$$

and $\delta_{r,1}$ is the Kronecker delta function: $\delta_{r,1}=1$ for $r=1$ and $\delta_{r,1}=0$ for $r\neq 1$.

Note that the Kronecker delta function determines the existence of an averaged forcing term near primary resonance ($r=1$: $n=m=1$). Consequently, secondary resonances ($r\neq 1$: $n,m>1$) are not excited by the averaged inertial forcing.

By employing the following nonlinear polar transformation (e.g. Meirovitch, 1970):

$$J = \tfrac{1}{2}(u^2+v^2) \quad \text{and} \quad \Phi = \tan^{-1}(v/u),$$

the averaged system (Eqn.52) can be written as a perturbed ($\delta^* < 1$) Hamiltonian system: $d\mathbf{q}/d\theta = \mathbf{F}(\mathbf{q}) + \delta^*\mathbf{G}(\mathbf{q},\theta)$ where $\mathbf{q}=(J,\Phi)^T$. The potential function ($\mathbf{F}$) consists of the averaged mooring restoring force excited near primary resonance by an averaged inertial force, whereas the damping perturbation ($\mathbf{G}$) includes the averaged drag force complemented by structural damping. This transformation is invertible and can be made in any region containing an elliptic center that is filled with a continuous family of periodic orbits (Arnold, 1978). Note that (J,Φ) are equivalent action angle coordinates of the integrable averaged system. Thus, Eqns.52-54 are transformed to the following:

$$\begin{bmatrix} \dot{J} \\ \dot{\Phi} \end{bmatrix} = \begin{bmatrix} F_1(J,\Phi) \\ F_2(J,\Phi) \end{bmatrix} + \delta^* \begin{bmatrix} G_1(J,\Phi) \\ G_2(J,\Phi) \end{bmatrix} \tag{55}$$

where

$$\begin{aligned} F_1(J,\Phi) &= \delta_{r,1} f_1^* \sqrt{2J} \cos\Phi \\ F_2(J,\Phi) &= -\Omega^* + \alpha_3^* (2J) - \delta_{r,1} \frac{f_1^* \sin\Phi}{\sqrt{2J}} \end{aligned} \tag{56}$$

$$\begin{aligned} G_1(J,\Phi) &= -\gamma^* (2J) - \sqrt{2J} \; [I_S(J,\Phi)\cos\Phi + I_C(J,\Phi)\sin\Phi] \\ G_2(J,\Phi) &= \frac{I_S(J,\Phi)\cos\Phi - I_C(J,\Phi)\sin\Phi}{\sqrt{2J}} \end{aligned} \tag{57}$$

$$\begin{bmatrix} I_S(J,\Phi) \\ I_C(J,\Phi) \end{bmatrix} = \begin{bmatrix} \int_0^{2\frac{m}{n}\pi} D(J,\Phi,\theta) \mid D(J,\Phi,\theta) \mid \sin\frac{n}{m}\theta \, d\theta \\ \int_0^{2\frac{m}{n}\pi} D(J,\Phi,\theta) \mid D(J,\Phi,\theta) \mid \cos\frac{n}{m}\theta \, d\theta \end{bmatrix} \tag{58}$$

$$D(J,\Phi,\theta) = f_1 \cos\theta - \sqrt{2J} \sin\left[\frac{n}{m}\theta + \Phi\right] \tag{59}$$

and

$$\begin{aligned} \delta^* &= \frac{\mu\delta}{\pi\omega} \\ \Omega^* &= \frac{\omega^2 - \left[\frac{m}{n}\right]^2 \alpha_1}{2\frac{m}{n}\omega} \quad ; \quad \alpha_3^* = \frac{m}{n}\frac{\alpha_3}{\omega} \\ \gamma^* &= \frac{\pi\omega\gamma}{2\mu\delta} \quad ; \quad f_1^* = \frac{1}{2}\mu\omega f_1 \end{aligned} \tag{60}$$

This system (Eqn.55) consists of an integrable potential function [$\mathbf{F}=(F_1(\mathbf{q}),F_2(\mathbf{q}))^T$] perturbed by a damping mechanism [$\mathbf{G}=(G_1(\mathbf{q},\theta),G_2(\mathbf{q},\theta))^T$], where there exists an invariant quantity (Hamiltonian energy) $H(\mathbf{q})$ such that $F_1(\mathbf{q})=\partial H(\mathbf{q})/\partial\Phi$ and $F_2(\mathbf{q})=-\partial H/\partial J$. The Hamiltonian energy of the averaged system (Eqn.55, $\delta^*=0$) can be found by integrating Eqn.56:

$$H(J,\Phi) = \Omega^* J - \alpha_3^* J^2 + \delta_{r,1} f_1^* \sqrt{2J} \sin\Phi \tag{61}$$

Note that orbits with $H=0$ have discontinuites at $(J,\Phi)=(0,0)$ and $(J,\Phi)=(0,\pi)$.

The structure of the averaged Hamiltonian system (Fig.6) is described by the stability characteristics (e.g. Wiggins, 1990) of its fixed points [$(J_i,\Phi_i)_e=(j_i,\phi_i)$; i=1,2,3] which are found from $d\mathbf{q}/dt=\mathbf{0}$ (Eqn.55, $\delta_*=0$). The fixed points are the roots [$\mathbf{F}(j_i,\phi_i)=\mathbf{0}$: Eqn.56] of the following equations:

$$\begin{gathered} (2j_i)^3 - 2\left[\frac{\Omega^*}{\alpha_3^*}\right](2j_i)^2 + \left[\frac{\Omega^*}{\alpha_3^*}\right]^2(2j_i) - \delta_{r,1}\left[\frac{f_1^*}{\alpha_3^*}\right]^2 = 0 \\ \cos\phi_i = 0 \end{gathered} \tag{62}$$

The structure of near secondary resonance response ($r\neq 1$) is always characterized by a unique center [$(J_1,\Phi_1)_e=(\tfrac{1}{2}\Omega^*/\alpha_3^*,\phi_1)$] whereas the structure of the solution near primary resonance (r=1) consists of either unique centers [$(J_1,\Phi_1)_e=(j_1,\phi_1)$] or of two coexisting centers [$(J_{1,3},\Phi 1,3_{1,3})_e=(j_1,\pi/2)$ and $(j_3,3\pi/2)$] separated by a hyperbolic saddle [$(J_2,\Phi_2)_e=(j_2,3\pi/2)$]. The primary resonance structure defines a classical jump bifurcation set where existence of unique ($f_1>\beta_c^H$) or coexisting centers ($f_1<\beta_c^H$) is defined in parameter space by the following bifurcation value:

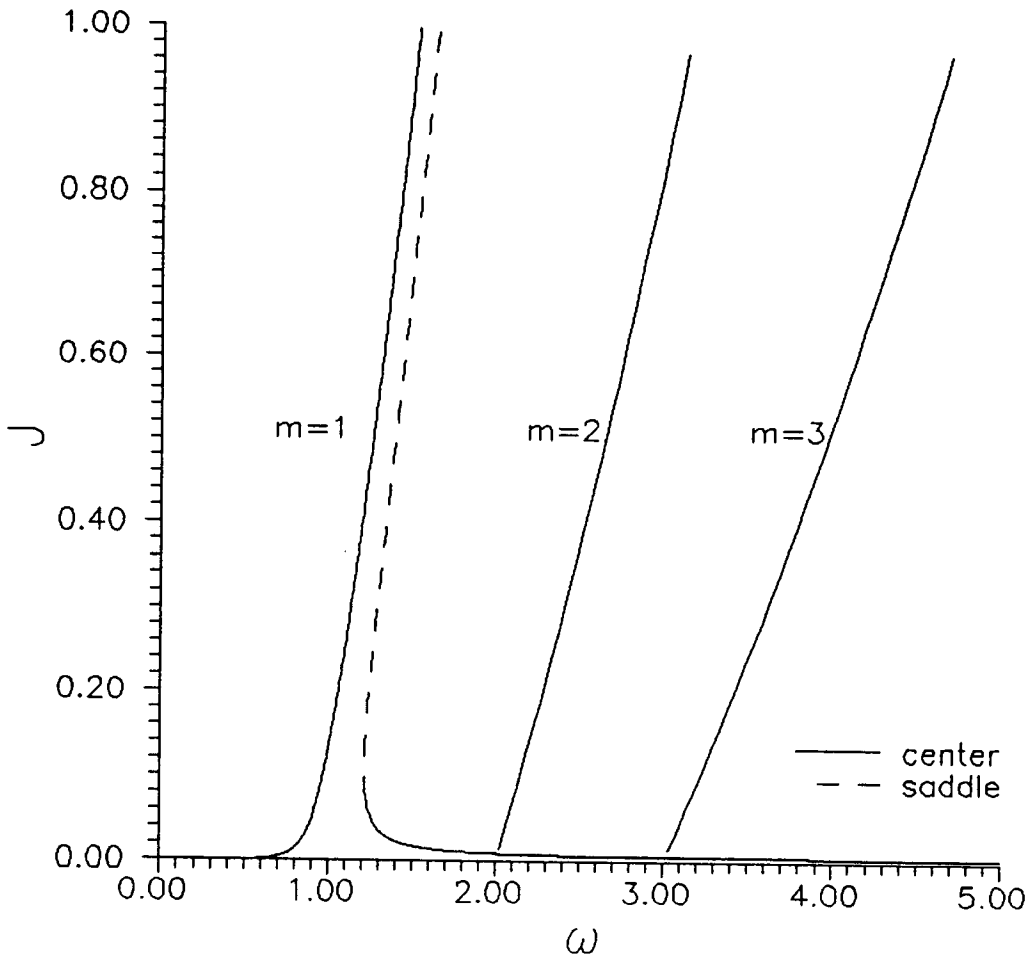

Fig.6 Structure of the Hamiltonian Poincaré map

$$\beta_c^H = \left[\frac{2}{3}\right]^2 \frac{(\omega^2-\alpha_1)^{3/2}}{\mu\ \omega^2\ \sqrt{\alpha_3}} \tag{63}$$

Note that for the linearized mooring system ($\alpha_3=0$) there exists a unique center $[(J_1,\Phi_1)_e=(\frac{1}{2}(f_1^*/\Omega^*)^2,\pi/2)]$, which is identical to the anticipated response of a linear harmonically excited, undamped oscillator.

3.2 Primary Resonance

Stability of the averaged system near primary resonance (r=1) is performed analytically by characterization of the system's fixed points where the damping perturbation [$\mathbf{G}(J,\Phi)$: Eqn.57] can be integrated in closed form. Therefore, the system (Eqns.55-60) near primary resonance reduces to the following:

$$\begin{bmatrix}\dot{J}\\ \dot{\Phi}\end{bmatrix} = \begin{bmatrix}F_1(J,\Phi)\\ F_2(J,\Phi)\end{bmatrix} + \delta^* \begin{bmatrix}G_1(J,\Phi)\\ G_2(J,\Phi)\end{bmatrix} \tag{64}$$

where

$$\begin{aligned} F_1(J,\Phi) &= f_1^*\ \sqrt{2J}\ \cos\Phi \\ F_2(J,\Phi) &= -\Omega^* + \alpha_3^*\ (2J) - \frac{f_1^*\sin\Phi}{\sqrt{2J}} \end{aligned} \tag{65}$$

$$\begin{aligned} G_1(J,\Phi) &= -\gamma^*(2J) - \frac{4}{3}\sqrt{f_1^2+2f_1\sqrt{2J}\sin\Phi+(2J)}\ \left[(2J)+f_1\sqrt{2J}\sin\Phi\right] \\ G_2(J,\Phi) &= -\frac{4}{3}\sqrt{f_1^2+2f_1\sqrt{2J}\sin\Phi+(2J)}\ \left[\frac{f_1\cos\Phi}{\sqrt{2J}}\right] \end{aligned} \tag{66}$$

The fixed points $[(J_i,\Phi_i)_e=(j'_i,\phi'_i)]$ of the averaged system (Eqn.64: $dq/dt=0$) are the roots of $\mathbf{F}(j'_i,\phi'_i)+\delta^*\mathbf{G}(j'_i,\phi'_i)=0$. Stability of the fixed points is characterized by solution of a standard eigenfunction: $\lambda^2-p_i\lambda+q_i=0$, where p_i and q_i are the trace and determinant of the derivative matrix (evaluated for each fixed point i), respectively. Asymptotic stability is defined by negative real parts of the derivative matrix (e.g. Jordan & Smith, 1987). For small values of δ^* we assume a perturbed solution form to the averaged near resonance system (Eqn.64):

$$\begin{aligned} j_i' &= j_i + \epsilon_i \\ \phi_i' &= \phi_i + \eta_i \end{aligned} \tag{67}$$

where (j_i,ϕ_i) are solutions (i=1,2,3) to the Hamiltonian system (Eqn.64: $\delta^*=0$) and (ϵ_i, η_i) are $O(\delta^*)$.

Stability of the perturbed fixed points (j'_i,ϕ'_i) is then obtained by evaluation of the eigenfunction coefficients to $O(\delta^*)$:

$$\begin{aligned} p_i &= -\gamma - 4\delta^* \sqrt{\Gamma_i(j_i',\phi_i')} \\ q_i &= \left[\Omega^* - \alpha_3^*(2j_i')\right]\left[\Omega^* - 3\alpha_3^*(2j_i')\right] \\ &\quad + \frac{8}{3}\delta^* f_1 \sqrt{\frac{\Gamma_i(j_i',\phi_i')}{2j_i'}} \left\{ \Omega^* - \alpha_3^* f_1 (2j_i') \frac{f_1+\sqrt{2j_i'}\sin\phi_i'}{\Gamma_i(j_i',\phi_i')} \right\} \cos\phi_i' \end{aligned} \tag{68}$$

where

$$\Gamma_i(j_i',\phi_i') = f_1^2 + 2f_1\sqrt{2j_i'}\sin\phi_i' + (2j_i') \tag{69}$$

Substitution of (Eqn.67) into $F(j'_i,\phi'_i)+\delta^* G(j'_i,\phi'_i)$ (Eqns.65,66) and their expansion in a Taylor series for functions of two variables results in the following values of (ϵ_i,η_i) to $O(\delta^*)$:

$$\epsilon_i = 0$$
$$\eta_i = \left[\frac{4}{3}\frac{\delta^*}{f_1^*}\right]\left[\left(f_1 \pm \sqrt{2j_i}\right)^2 \pm \left[\frac{3}{4}\right]\gamma^* \sqrt{2j_i}\right] \qquad (70)$$

where the upper choice of sign (+ in $\pm$) refers to i=1 and the lower choice of sign (- in $\pm$) refers to i=2 and i=3.

But as $\sin\phi'_i \to \pm 1$, $-\cos\phi'_i \to \pm\eta_i$ and as η_i is of $O(\delta^*)$, stability of the system fixed points is found to be governed by the following coefficients:

$$p_i = -\gamma - 4\delta^* \left(f_1 \pm \sqrt{2j_i}\right)$$
$$q_i = \left[\Omega^* - \alpha_3^* (2j_i)\right]\left[\Omega^* - 3\alpha_3^* (2j_i)\right] \qquad (71)$$

Consequently, (j'_1,ϕ'_1) and (j'_3,ϕ'_3) are hyperbolic sinks $(q_{1,3}>0)$ and (j'_2,ϕ'_2) remains a hyperbolic saddle $(q_2<0)$. While (j'_1,ϕ'_1) is always an attractor $(p_1<0)$, (j'_3,ϕ'_3) exists only in limited parameter space $(f_1<\beta_c^P)$ defined by the following bifurcation value:

$$\beta_c^P = \frac{2}{3}\sqrt{\frac{\omega^2-\alpha_1}{\alpha_3}} - \frac{\pi}{4}\frac{\omega}{\mu}\frac{\gamma}{\delta} \qquad (72)$$

Furthermore, coexistence of attractors ($j'_{1,3}, \phi'_{1,3}$) will only occur for stable values of (j'_3, ϕ'_3) [$p_3 < 0$: $(f_1 + \frac{1}{2}\gamma^*)^2 < (2j_3) < (\Omega^*/3\alpha_3^*)$] and is controllable by the magnitude of the relative damping, γ^* (Fig.7). This result is verified by numerical simulation of the system (Eqn.19) resulting in two coexisting attractors (Fig.8) for two sets of initial conditions. Note the symmetric shape of the phase plane and lack of significant bias for the parameter set chosen for this figure from Eqn.71. The power spectra depicts the nonlinear harmonic content of the solution and the lack of bias can be seen by the value of $S_x(0)$. Thus, stability analysis of the Poincaré map, portrayed by the perturbed averaged system near primary resonance, ensures global attraction for larger excitation values and describes conditions for coexistence of solutions in the system.

3.3 Secondary Resonances

Stability of the averaged system near secondary resonances $r = \neq 1$ [$r = n/m$: subharmonic ($r = 1/m$: $n = 1$, $m > 1$), ultraharmonic ($r = n$: $n > 1$, $m = 1$), ultrasubharmonic ($r = n/m$: $n, m > 1$)], can be performed by numerically evaluating the system's fixed points. In order to obtain approximate analytical stability criteria, limiting upper and lower bounds of the nonlinear viscous drag component are calculated. Substituting the averaged relative motion term [$D(J, \Phi, \theta)$ Eqn.59 obtained from the drag force in Eqn.50] with its upper ($|\sqrt{(2J)}\sin(n\theta/m + \Phi)|$) and lower ($|m/n\cos\theta|$) values enables a closed form evaluation of the damping perturbation [$G(J, \Phi)$: Eqn.57] for limiting values of the drag integral [$I_{s,c}(J, \Phi)$: Eqn.58]. The upper (G^U) and lower bounds (G^L) of the

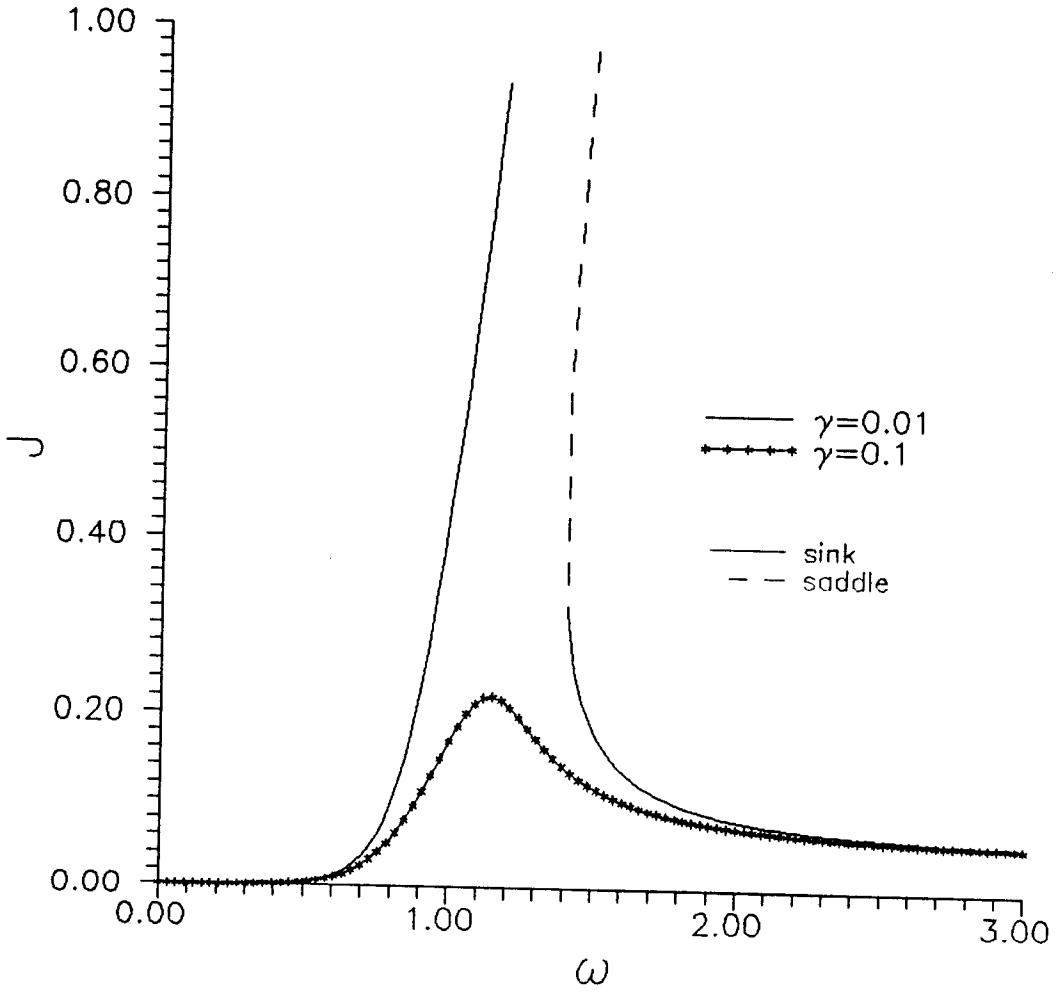

Fig.7 Primary resonant structure of the forced Poincaré map (n=m=1)

a)

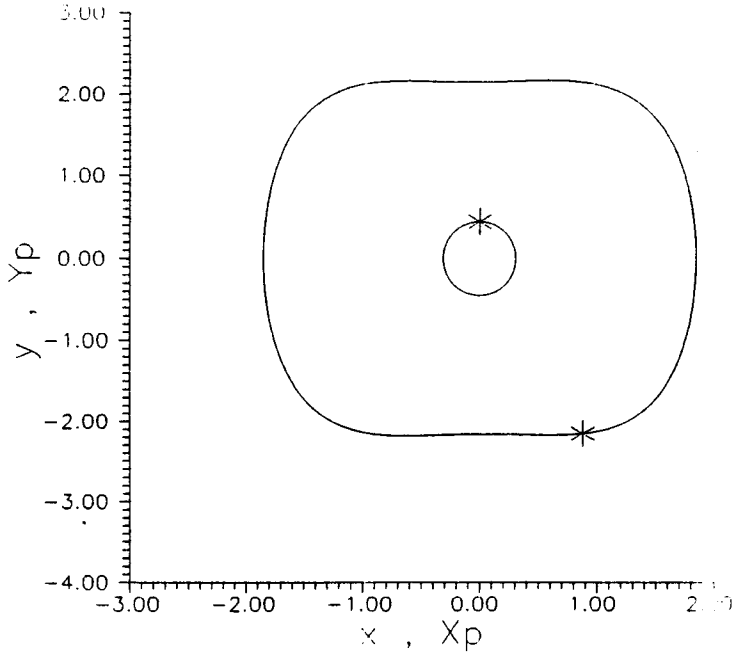

b)

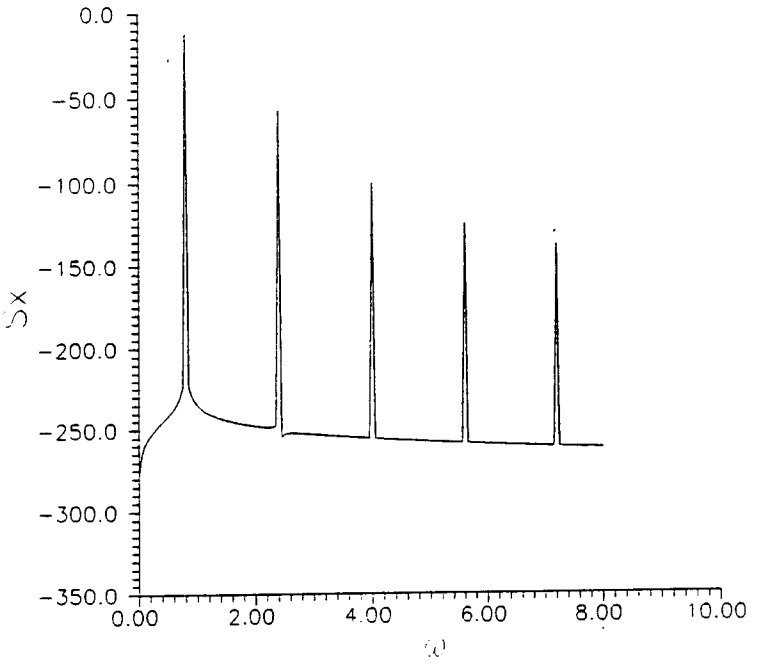

Fig.8 Coexisting attractors (m=n=1): a) phase plane [(x(0),y(0))=(0,0); (2,2)], b) power spectra [(x(0),y(0))=(0,0)]

damping perturbation correspond to assumptions on the magnitude of system response ($\sqrt{2J}$) with respect to the magnitude of the exciting hydrodynamic motion ($|u| \propto f_1$). The lower bound (G^L) is valid for small amplitude motions ($\sqrt{2J} << mf_1/n$) and is representative of drag equivalent linearization techniques [$F_D \propto (U-dX/dt)|U|$ in Eqn.5], whereas the upper bound (G^U) is valid for large motions ($\sqrt{2J} >> mf_1/n$) corresponding to near resonant responses [$F_D \propto (U-dX/dt)|dX/dt|$]. The choice of the upper bound is consistent with the averaging theorem as near resonance conditions were defined previously by the detuning parameter (Eqn.45). Therefore, the system (Eqns. 55-60) near secondary resonances is the following:

$$\begin{bmatrix} \dot{J} \\ \dot{\Phi} \end{bmatrix} = \begin{bmatrix} F_1(J,\Phi) \\ F_2(J,\Phi) \end{bmatrix} + \delta^* \begin{bmatrix} G_1(J,\Phi) \\ G_2(J,\Phi) \end{bmatrix} \tag{73}$$

where

$$\begin{aligned} F_1(J,\Phi) &= 0 \\ F_2(J,\Phi) &= -\Omega^* + \alpha_3^* (2J) \end{aligned} \tag{74}$$

$$\begin{aligned} G_1^L(J,\Phi) &= -(\gamma^* + f_1)(2J) \\ G_2^L(J,\Phi) &= 0 \end{aligned} \tag{75}$$

$$\begin{aligned} G_1^U(J,\Phi) &= -\gamma^*(2J) - \left[\frac{4n}{3m}\right](2J)^{3/2} \\ &\quad + \delta_{m,(2j+1)} \left[\frac{4n^2}{m^2-4n^2}\right] f_1 (2J) \sin\frac{m}{n}\Phi \\ G_2^U(J,\Phi) &= \delta_{m,(2j+1)} \left[\frac{2n^2}{m^2-4n^2}\right] f_1 \cos\frac{m}{n}\Phi \end{aligned} \tag{76}$$

and $\delta_{m,(2j+1)}$ is the Kronecker delta function: $\delta_{m,(2j+1)}=1$ for $m=2j+1$ and $\delta_{m,(2j+1)}=0$ for $m \neq 2j+1$, where m is the order of subharmonic and $j=1,2,3,\ldots,J$

Note that the Kronecker delta function determines the existence of additional damping components for odd subharmonics and ultrasubharmonics in $\mathbf{G^U}$ (Eqn.76).

The fixed points $[(J_i,\Phi_i)_e=(j'_i,\phi'_i)\ ;\ i=1,2,3,4]$ of the averaged near secondary resonance system (Eqns.73) with the upper bound damping perturbation ($\mathbf{G^U}$) for odd values of ultrasubharmonics ($m=2j+1$: $\delta_{mj+1}=1$ in Eqn.76) are the roots $[\mathbf{F}(j'_i,\phi'_i)+\delta^*\mathbf{G^U}(j'_i,\phi'_i)=\mathbf{0}]$ of the following equations:

$$\left(2j_i'\right)^2 + \left[\left[\frac{2}{3}\frac{\delta^*}{\alpha_3^*}\right]^2 - 2\left[\frac{\Omega^*}{\alpha_3^*}\right]\right]\left(2j_i'\right) + \left[\frac{m}{3n}\frac{\gamma\delta^*}{(\alpha_3^*)^2}\right]\sqrt{2j_i'} + \left[\left[\frac{\Omega^*}{\alpha_3^*}\right]^2 + \left[\frac{m}{4n}\right]^2\left[\frac{\gamma}{\alpha_3^*}\right]^2 - \left[\frac{2n^2 f_1\,\delta^*}{(m^2-4n^2)\alpha_3^*}\right]^2\right] = 0 \qquad (77)$$

$$\sin\frac{m}{n}\phi_i' = \left[\frac{m^2-4n^2}{3mn}\right]\left[\left[\frac{3m}{4n}\right]\gamma^* + \sqrt{2j_i'}\right] f_1$$

Note that the near secondary resonance system (Eqn.73) with the lower bound damping perturbation ($\mathbf{G^L}$: Eqn.75) and the upper bound damping perturbation ($\mathbf{G^U}$: Eqn.76) for even values of ultrasubharmonics ($m\neq 2j+1$: $\delta_{mj+1}=0$ in Eqn.76) does not reveal existence of fixed points to $O(\delta^*)$ $[\mathbf{F}(j'_i,\phi'_i)+\delta^*\mathbf{G^U}(j'_i,\phi'_i)\neq\mathbf{0}]$ and higher order averaging is required to determine existence of ultrasubharmonic solutions for these conditions.

Stability of the fixed points determined by Eqn.77 (j'_i,ϕ'_i) is characterized by the following coefficients evaluated for each fixed point i, respectively:

$$p_i = -\left[\frac{m}{2n}\right]^2 \gamma - \frac{2}{3}\frac{m^2+2n^2}{nm}\delta^* \sqrt{2j_i'}$$
$$q_i = (2\alpha_3^*)^2 (2j_i')^2 + \left[2\left[\frac{2}{3}\delta^*\right]^2 - 4\Omega^* \alpha_3^*\right] (2j_i') + \frac{m}{3n}\gamma\delta^* \sqrt{2j_i'} \qquad (78)$$

The structure of the averaged subharmonic system for very small values of structural damping ($\gamma << \delta < 1$) can be described (Fig.9: n/m=1/3) by a saddle-node bifurcation as there exist to $O(\delta^*)$ four possible roots to (Eqn.77) for the following bifurcation value ($f > \beta_c^S$):

$$\beta_c^S = \frac{m^2-4n^2}{3n^2} \sqrt{\frac{\Omega^*}{\alpha_3^*} - \left[\frac{\delta^*}{3\alpha_3^*}\right]^2} \qquad (79)$$

Therefore, the fixed points [(j'_i, ϕ'_i), i=1,..,4] are hyperbolic saddles ($q_{1,3} < 0$) and attractors ($p_{2,4} < 0$, $q_{2,4} > 0$). Furthermore, the linearized system ($\alpha_{1>1} = 0$) reveals existence of two roots [(j'_i, ϕ'_i); i=1,2 in Eqn.77 where $\alpha_3 = 0$] which are a stable attractor ($p_1 < 0$, $q_1 > 0$) and a saddle ($q_2 < 0$) for the following bifurcation value ($f > \beta_c^S$):

$$\beta_c^S = \frac{m^2-4n^2}{2n^2} \frac{\Omega^*}{\delta^*} \qquad (80)$$

Note in Fig.9 the narrow domain of existence for the subharmonic solution (n/m=1/3) of the linearized system versus that with the nonlinear restoring force.

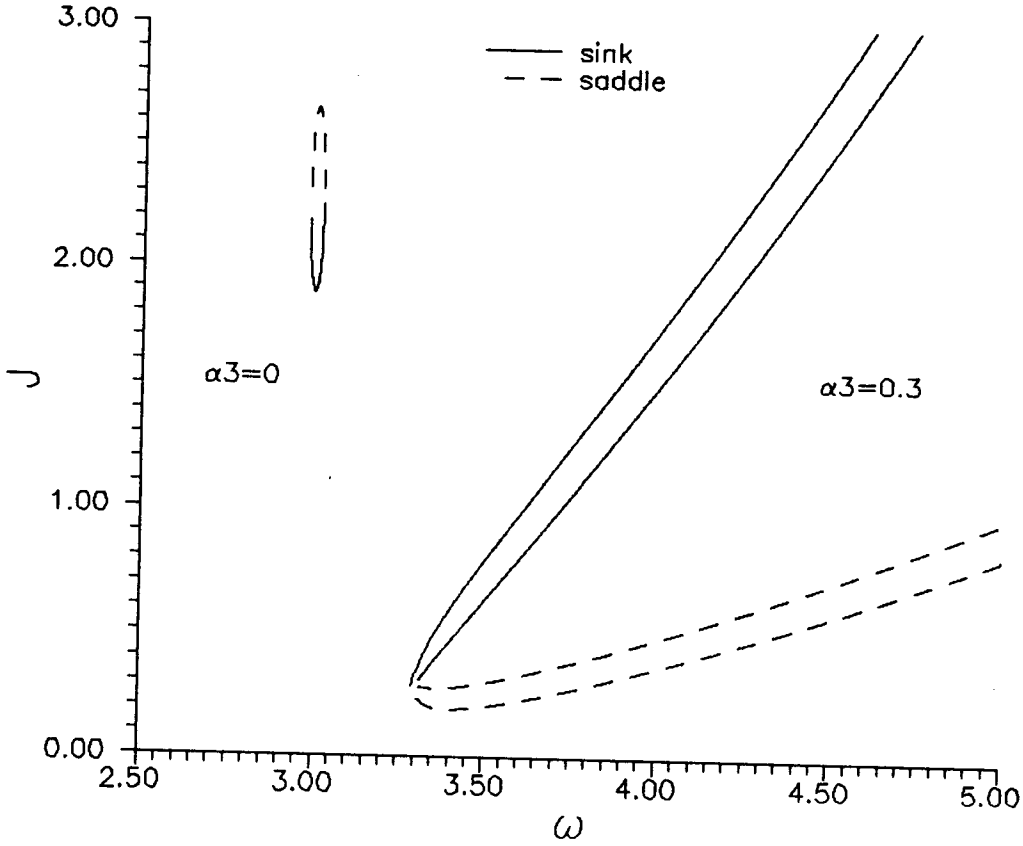

Fig.9 Subharmonic resonant structure of the forced Poincaré map (n/m=1/3)

Numerical simulations of the system (Eqn.19) verify the existence of secondary resonant responses for the values predicted above (Eqn.78). Examples are a subharmonic solution (Fig.10: n/m=1/3) and an ultrasubharmonic solution (Fig.11: n/m=7/5). Note the number of Poincaré points describing the order of subharmonic (Fig.10a: m=3) and the periodicity of the ultrasubharmonic (Fig.11a: m=5) and the peak with the largest energy content in the power spectra of both subharmonic and ultrasubharmonic solutions (Fig.10.b: $\omega_{max}=\omega/3$ and Fig.11.b: $\omega_{max}=7\omega/5$). The predictions are sensitive to the order of the initial system approximation (Eqn.45) and higher order averaging (Sanders and Verhulst, 1985) is needed to accurately describe large amplitude ultraharmonic and ultrasubharmonic solutions.

The near secondary resonant system exhibits both symmetric (Eqn.74, Eqn.76: n,m odd) and unsymmetric (Eqn.76: n,m even) nonlinear properties associated with the nonlinear properties of the drag perturbation. Note that unsymmetric system solution forms are (x,y,θ), $(x,y,\theta+m\pi/n\omega)$ whereas symmetric forms are (x,y,θ), $(-x,-y,\theta+m\pi/n\omega)$. Therefore, unsymmetric system solutions are portrayed by unsymmetric phase planes (Fig.12a,b: n/m=4/5) whereas symmetric solutions reveal self-similarity in the solutions (Fig.12.c), $[x(\theta),y(\theta)=-x(\theta+m\pi/n\omega),-y(m\pi/n\omega)]$ or multiple coexisting unsymmetric solutions differing by initial conditions (Fig.12,a,b). Thus, stability analysis of the Poincaré map define conditions for coexistence of periodic solutions near secondary resonances.

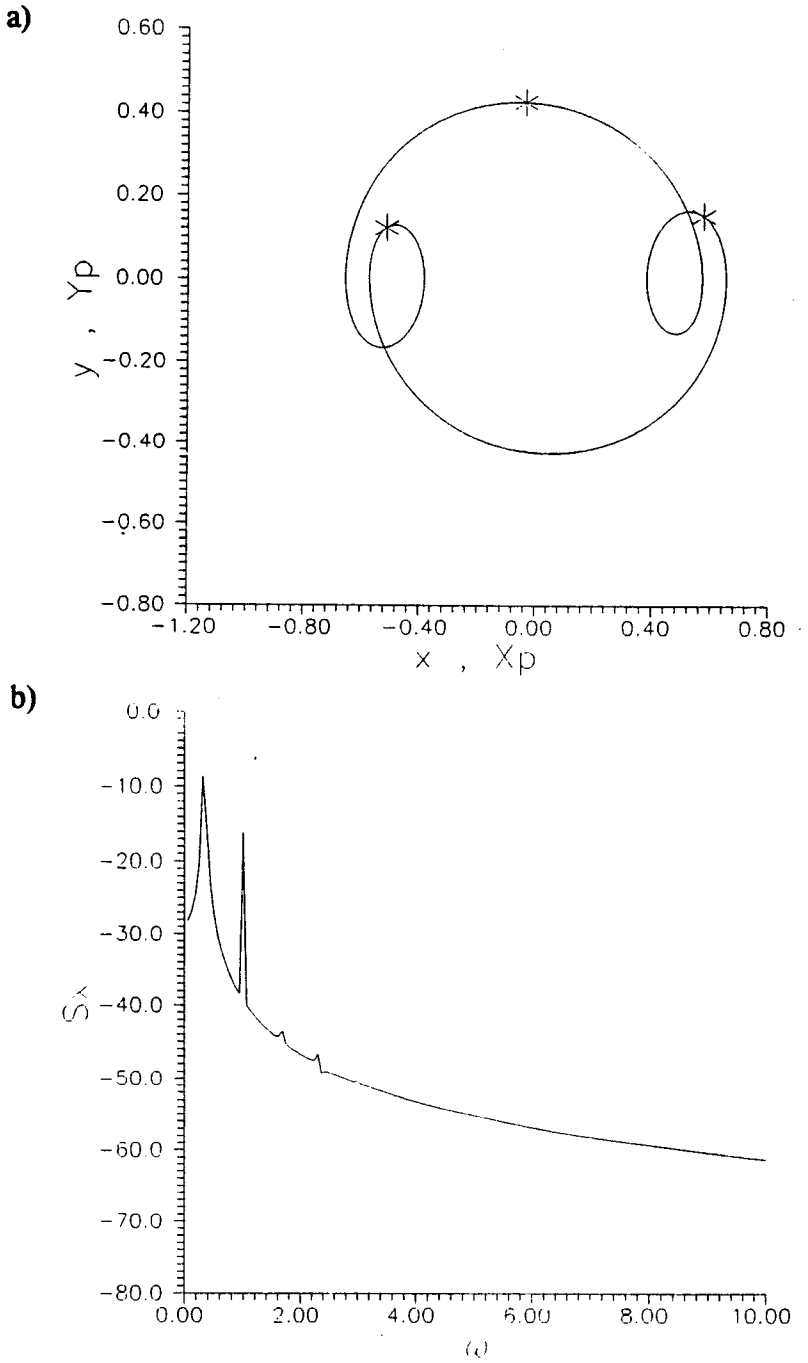

Fig.10 Subharmonic solution (n/m=1/3): a) phase plane, Poincaré map; b) power spectra

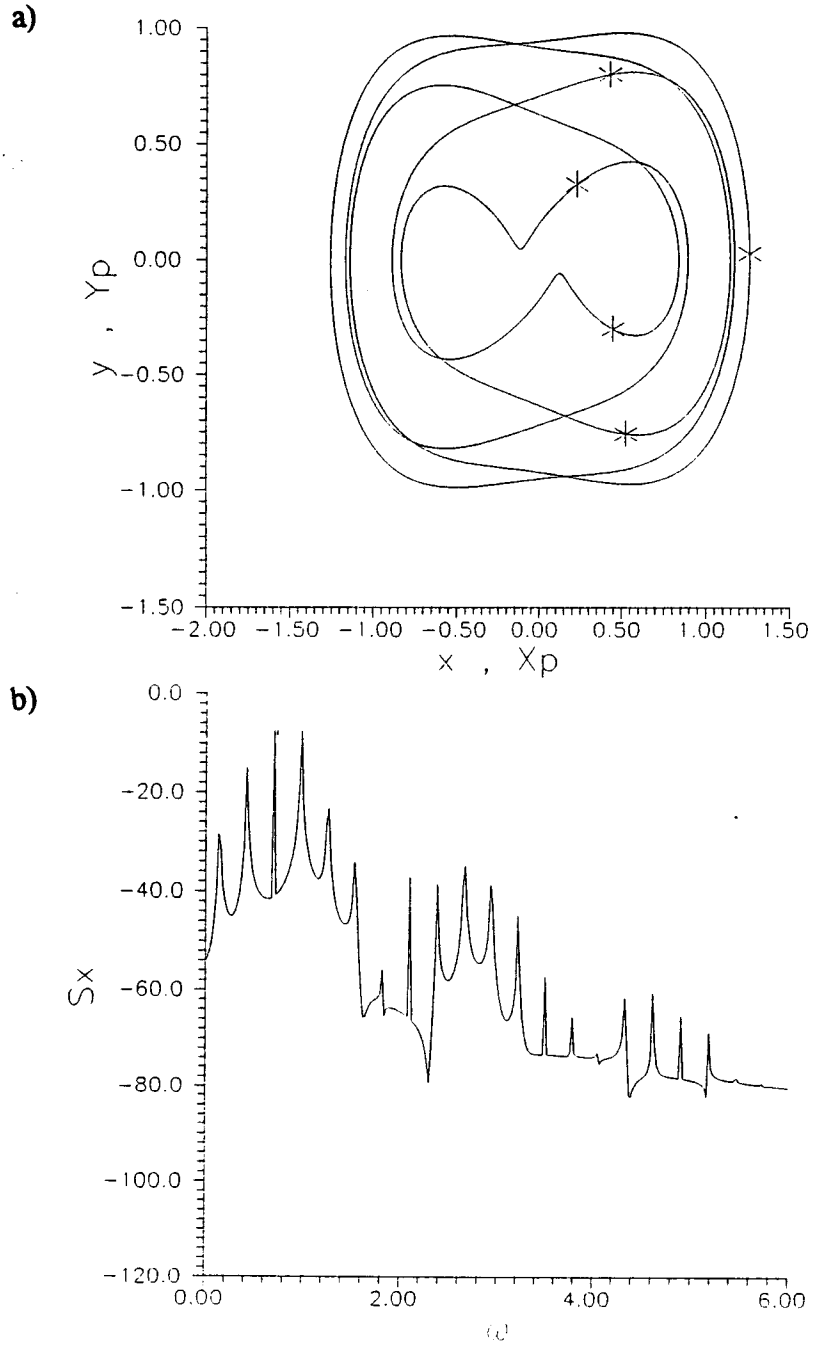

Fig.11 Ultrasubharmonic solution (n/m=7/5): a) phase plane, Poincaré map; b) power spectra

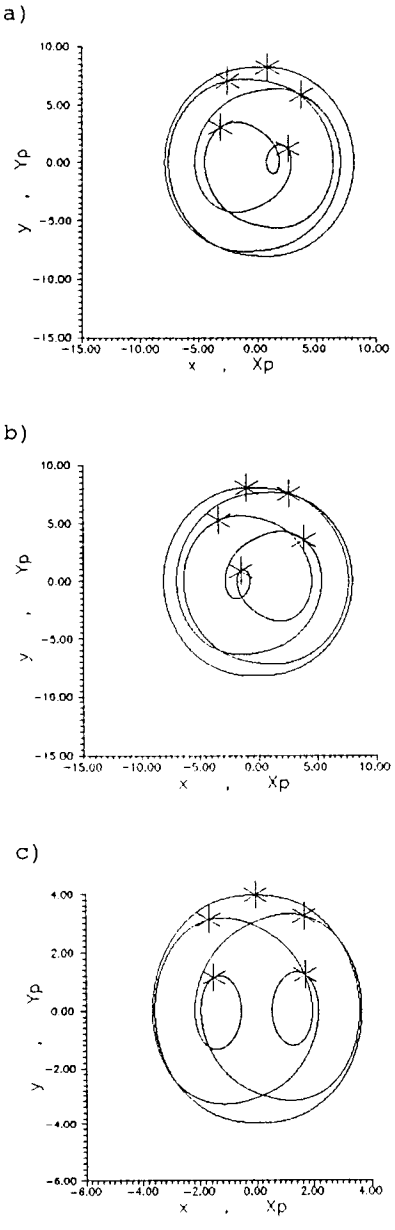

Fig.12 Coexistence (a,b) and self-similarity (c) of ultrasubharmonic solutions: a,b) (x(0),y(0))=(0,0);(-1,0), (n/m=4/5), c) (n/m=3/5)

4. LOCAL BIFURCATIONS

In order to investigate the stability of solutions which are not necessarily near resonance, a local variational approach is employed. This consists of perturbing an approximate system solution and evaluating its stability by analysis of the general Hill's system which is obtained after linearization of the corresponding variational. Due to the algebraic complexity of the geometric and quadratic drag nonlinearities, the approximate solution is obtained by the method of harmonic balance (Hayashi, 1964). The solution is formulated to account for the bias and even harmonic components induced by the hydrodynamic nonlinearity. Stability regions of the (m/n)T periodic solution are identified by Floquet theory (e.g. Ioos and Joseph, 1981). The first corresponds to the resonant tangent bifurcations which were found by generalized averaging in the previous chapter. The second consists of a symmetry breaking or period doubling bifurcations. The accuracy of the approximate analytical regions is verified by numerical calculation of the eigenvalues (Floquet multipliers) of the monodromy matrix associated with the fundamental solution of the linearized variational equation (Nayfeh and Sanchez, 1989).

Numerical simulations of system response (see detail in Appendix B) verify the harmonic balance approximations and validates results obtained by local stability analysis. The results are portrayed by phase planes describing loss of symmetry of ultraharmonic solutions, Poincaré maps of period doubled ultrasubharmonic and subharmonic solutions and power spectra which display the nonlinear harmonic content of the response.

4.1 Periodic Solutions

An approximate system solution can be obtained by a variety of methods (e.g. Nayfeh and Mook, 1979) but the method of harmonic balance (Hayashi, 1964) is chosen in order to account for the even harmonics which are induced by to the bias created by the nonlinear viscous drag and convective inertial forces. Thus, the following approximate solution form is assumed:

$$\begin{aligned} x_{0\frac{n}{m}} &= A_{0\frac{n}{m}} + \sum_{i}^{I} A_{i\frac{n}{m}} \cos\left(i \frac{n}{m}\theta + \Psi_{i\frac{n}{m}} \right) \\ y_{0\frac{n}{m}} &= -\omega\frac{n}{m} \sum_{i}^{I} i\, A_{i\frac{n}{m}} \sin\left(i \frac{n}{m}\theta + \Psi_{i\frac{n}{m}} \right) \end{aligned} \tag{81}$$

where $A_{0(n/m)}, A_{i(n/m)}, \Psi_{i(n/m)}$ are solution amplitudes and phases, I is the order of approximation (i=1,2,3,...,I) and n/m is the order of ultrasubharmonic.

The unknown amplitudes and phases are obtained by substitution of the approximate solution (Eqn.81) into the system (Eqn.19), squaring the resultant equation and comparing terms of equal harmonic order. Thus, the system is transferred into a finite nonlinear set of algebraic equations:

$$S_j\left(A_0 , A_{i\frac{n}{m}} , \Psi_{i\frac{n}{m}} \right) = 0 \tag{82}$$

where j=1,2,3,...,2I+1

[see Appendix A.2 for detail (S_j: j=1,2,3; n=m=1)].

The following is an example low order (I=1) set for the limiting case of a system characterized by a taut [$\tau=\frac{1}{2}\sqrt{(1+\beta^2)}$] mooring restoring force excited by a harmonic hydrodynamic exciting force obtained by linearization of the drag force for small amplitude wave kinematics [$F_{DI}=(8/3\pi)\mu\delta f_1(f_1-y/\omega)$, $F_I=-\mu\omega^2 f_1\sin\theta$].

$$
\begin{gathered}
A_0 = 0 \\
\left[\left(\frac{3}{2}\omega_0^2-\omega^2\right)A_1^2-f_1A_1\sin\Psi_1+2\alpha(1+\beta^2)^{1/2}\right]\left(f_1\cos\Psi_1-\gamma^*\omega A_1\right) = 0 \\
A_1\left\{\frac{3}{4}\left[\left(\omega_0^2-\omega^2\right)A_1-f_1\sin\Psi_1\right]^2+\frac{1}{4}\left(f_1\cos\Psi_1-\gamma^*\omega A_1\right)^2+\frac{\alpha^2}{1+\beta^2}\right\} \\
+\ \omega_0^2\left[\left(\omega_0^2-\omega^2\right)A_1-f_1\sin\Psi\right]\left[1+\beta^2+\frac{3}{4}A_1^2\right] = 0
\end{gathered}
\tag{83}
$$

where

$$\omega^2{}_0 = \alpha/\sqrt{(1+\beta^2)} \quad , \quad \gamma^* = \gamma + 8\mu\delta f_1/3\pi\omega$$

Solution of the set with an iterative Newton-Raphson procedure yields a frequency response relationship (ω-$A_{n/m}$). An unsymmetric solution includes even and odd harmonics [$x_0(\theta),y_0(\theta) \neq x_0(\theta+m\pi/n),y_0(\theta+m\pi/n)$; period=$2\pi$ ($T=2\pi/\omega$)] whereas a symmetric solution consists of only odd harmonics.

A low order solution (I=1) for a linearized mooring system ($\beta=10$ or $\alpha_{n>1}=0$) or for a weakly nonlinear small angle mooring configuration, results in the anticipated amplitudes and phase of a biased linear oscillator:

$$A_0 = \sqrt{\frac{3}{8}}\,\frac{\mu\delta}{\alpha_1}\left(f_1^2 + 2f_1A_1\sin\Psi_1 + A_1^2\right)$$

$$A_1 = \frac{\mu\,\omega^2\,f_1}{\sqrt{(\alpha_1-\omega^2)^2+(\gamma\omega)^2}} \qquad (84)$$

$$\Psi_1 = \tan^{-1}\left[-\frac{\alpha_1-\omega^2}{\gamma\omega}\right]$$

Note that the bias, A_0 is identified by the drag parameter to this order of approximation.

Numerical simulation of a taut system [$\tau=\frac{1}{2}\sqrt{(1+\beta^2)}$] excited by a linearized hydrodynamic exciting force [$F_D=(8/3\pi)\mu\delta(u-y/\omega)|u|$, $F_I=-\mu\omega^2 du/d\theta$; $u=f_0-f_1\sin\theta$] were performed using Runge-Kutta integration schemes (see Appendix B). Error control was achieved via the passage of the response through the exact fixed equilibrium point. The results for the 2π periodic response ($n=m=1$) show good agreement with low order approximations under wave and current excitation [$I=1$: $x_0=A_0+A_1\cos(\theta+\Psi_1)$] and under wave excitation alone [$I=1$: $x_0=A_1\cos(\theta+\Psi_1)$]. The low order (one term) approximation of a four-point system under wave excitation is sufficient for a large range of parameter conditions particularly for $\beta \approx 1$, however, more terms are needed to correctly model the response of a two-point system ($\beta=0$), near the primary resonance and in the low frequency secondary resonance range (Fig.13). It should be noted that the application of harmonic balance to strong nonlinear systems requires the calculation of an error term (e.g. ratio of amplitude norm of two consecutive approximations: $\Sigma\, A_k^2 \,/\, \Sigma\, A_{K+1}^2$) in order to determine solution convergence. The sensitivity of the approximate solution to the order of the approximation is similar to that of the Duffing equation without a linear term (Rahman and Burton, 1986).

a)

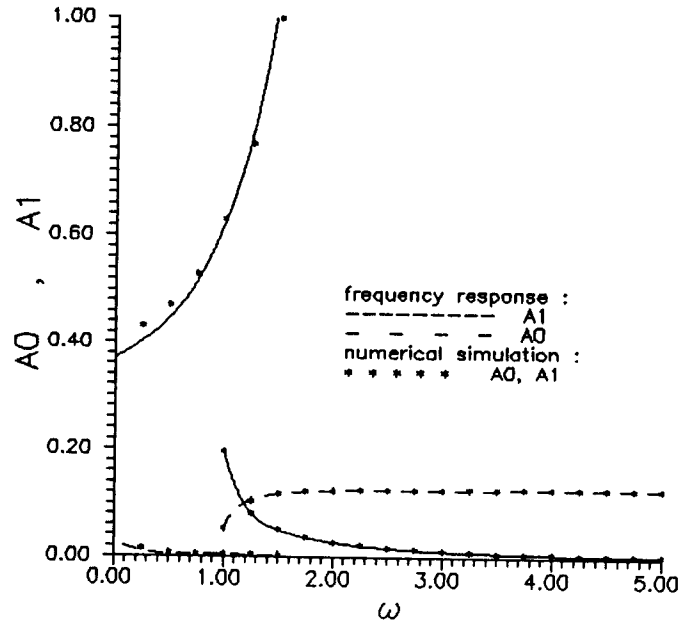

b)

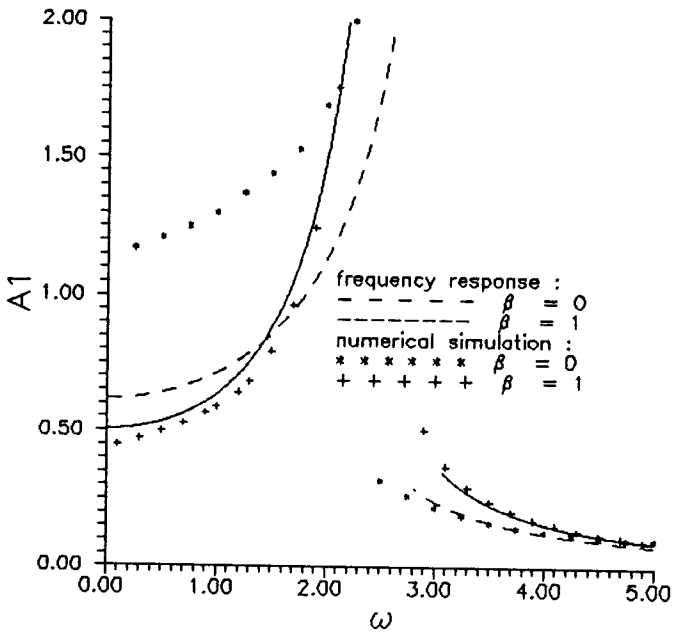

Fig13. Frequency response: a) wave and current, b) wave

4.2 Hill's Variational System

Local stability is determined by considering a perturbed solution $(x(\theta),y(\theta))$ where $(x_0(\theta), y_0(\theta))$ is an approximate solution and $(\epsilon(\theta), \eta(\theta))$ is a small variation.

$$\begin{aligned} x(\theta) &= x_0(\theta) + \epsilon(\theta) \\ y(\theta) &= y_0(\theta) = \eta(\theta) \end{aligned} \tag{85}$$

Substituting the solution $x(\theta),y(\theta)$ (Eqn.85) into the equations of motion (Eqn.19) and simplifying the resulting equation, leads to the following nonlinear variational equation:

$$\begin{aligned} \dot{\epsilon} &= \eta \\ \dot{\eta} &= D(\epsilon,\eta;x_0,y_0) + E(\epsilon,\eta;x_0,y_0) \end{aligned} \tag{86}$$

where

$$\begin{aligned} D(\epsilon,\eta) &= -\gamma\,\eta \\ &\quad + \mu\delta\left[\left(u-\frac{y}{\omega}\right)\left|u-\frac{y}{\omega}\right| - \left(u_0-\frac{y_0}{\omega}\right)\left|u_0-\frac{y_0}{\omega}\right|\right] \end{aligned} \tag{87}$$

$$\begin{aligned} E(\epsilon,\eta) &= \alpha\left[x_0-\tau\left\{\frac{\beta+x_0}{\sqrt{1+(\beta+x_0)^2}}-\frac{\beta-x_0}{\sqrt{1+(\beta-x_0)^2}}\right\}\right] \\ &\quad - \alpha\left[x-\tau\left\{\frac{\beta+x}{\sqrt{1+(\beta+x)^2}}-\frac{\beta-x}{\sqrt{1+(\beta-x)^2}}\right\}\right] \\ &\quad + \mu\omega^2\left\{\left(u'-u_0'\right)-\kappa\left[\left(u-\frac{y}{\omega}\right)u'-\left(u_0-\frac{y_0}{\omega}\right)u_0'\right]\right\} \end{aligned} \tag{88}$$

and

$$\begin{aligned} u &= f_0 + f_1 \cos[\kappa(x_0+\epsilon)-\theta] \quad ; \quad u_0 = u(\epsilon=0) \\ u' &= (1-\kappa\eta) f_1 \sin[\kappa(x_0+\epsilon)-\theta] \quad ; \quad u_0' = u'(\epsilon,\eta=0) \end{aligned} \tag{89}$$

Linearizing Eqns.87,88 yields the following first order linear ordinary differential system with periodic coefficient functions $H_{1,2}[x_0(\theta),y_0(\theta)]=H_{1,2}[x_0(\theta+2\pi),y_0(\theta+2\pi)]$:

$$\begin{aligned} \dot{\epsilon} &= \eta \\ \dot{\eta} &= H_1(x_0,y_0)\ \eta + H_2(x_0,y_0)\ \epsilon \end{aligned} \tag{90}$$

where

$$H_1 = -\gamma - 2\frac{\mu\delta}{\omega}\left| u_0 - \frac{y_0}{\omega}\right| + \mu\omega^2\kappa\left[\frac{1}{\omega} - 1 + \left[u_0 - \frac{y_0}{\omega}\right]\right] u_0' \tag{91}$$

$$\begin{aligned} H_2 = &-\alpha\left[1 - \tau\left\{\left[1+(\beta+x_0)^2\right]^{-3/2} + \left[1+(\beta-x_0)^2\right]^{-3/2}\right\}\right] \\ &- 2\mu\delta\kappa\left| u_0 - \frac{y_0}{\omega}\right| u_0' + \mu\omega^2\kappa^2\left\{(u_0-f_0)\left[\frac{1}{\kappa} - (u_0-y_0)\right] + u_0'^2\right\} \end{aligned} \tag{92}$$

Substituting the approximate solution (Eqn.81) in Eqns.91,92 and expanding $H_{1,2}(x_0,y_0)$ in a Fourier series $[H_{1,2}(\theta)]$ leads to the following generalized Hill's variational equation:

$$\begin{aligned} \dot{\epsilon} &= \eta \\ \dot{\eta} &= H_1(\theta)\ \eta + H_2(\theta)\ \epsilon \end{aligned} \tag{93}$$

where $H_{1,2}$ are calculated from the following:

$$H_1 = \xi_{0\frac{n}{m}} + \sum_j \xi_{Cj\frac{n}{m}} \cos\left[j\frac{n}{m}\theta\right] + \xi_{Sj\frac{n}{m}} \sin\left[j\frac{n}{m}\theta\right] \tag{94}$$

$$H_2 = \zeta_{0\frac{n}{m}} + \sum_j \zeta_{Cj\frac{n}{m}} \cos\left[j\frac{n}{m}\theta\right] + \zeta_{Sj\frac{n}{m}} \sin\left[j\frac{n}{m}\theta\right] \tag{95}$$

and (ξ_{Cj},ζ_{Cj}); (ξ_{Sj},ζ_{Sj}) are Fourier coefficients calculated from $H_{1,2}$:

$$\begin{bmatrix}\xi_{Cj\frac{n}{m}}\\ \zeta_{Cj\frac{n}{m}}\end{bmatrix} = \frac{1}{\pi}\int_{-\pi}^{\pi}\begin{bmatrix}H_1\left(\frac{n}{m}\theta\right)\\ H_2\left(\frac{n}{m}\theta\right)\end{bmatrix}\cos\left[j\frac{n}{m}\theta\right]\,d\theta$$
$$\begin{bmatrix}\xi_{Sj\frac{n}{m}}\\ \zeta_{Sj\frac{n}{m}}\end{bmatrix} = \frac{1}{\pi}\int_{-\pi}^{\pi}\begin{bmatrix}H_1\left(\frac{n}{m}\theta\right)\\ H_2\left(\frac{n}{m}\theta\right)\end{bmatrix}\sin\left[j\frac{n}{m}\theta\right]\,d\theta \tag{96}$$

Note that the approximation of the periodic coefficient x_0 (see Eqn.92) by the Fourier series is sensitive to the degree of geometric nonlinearity β (Fig.14). Isolation of the contribution of the restoring force to the Hill's equation (via $u \simeq f_1\cos\theta$ for small amplitude waves: $\kappa=0$ in Eqn.92) reveals that both $H_2(x_0)$ and $H_2(\theta)$ retain a singularity at $H_2(x_0=0)=\beta^2(1+\beta^2)^{-3/2}$ and for values of $x_0>\pi$, $H_2(x_0)$ is asymptotic to $\sqrt{(1+\beta^2)}$ (see Fig.14).

An example of a low order (J=1) 2π periodic Hill's system (m=n=1) for a limiting taut system excited by a nonlinear drag and harmonic inertial force is the following:

$$\begin{aligned}\dot{\epsilon} &= \eta\\ \dot{\eta} &= H_1(\theta)\,\eta + H_2(\theta)\,\epsilon\end{aligned} \tag{97}$$

where

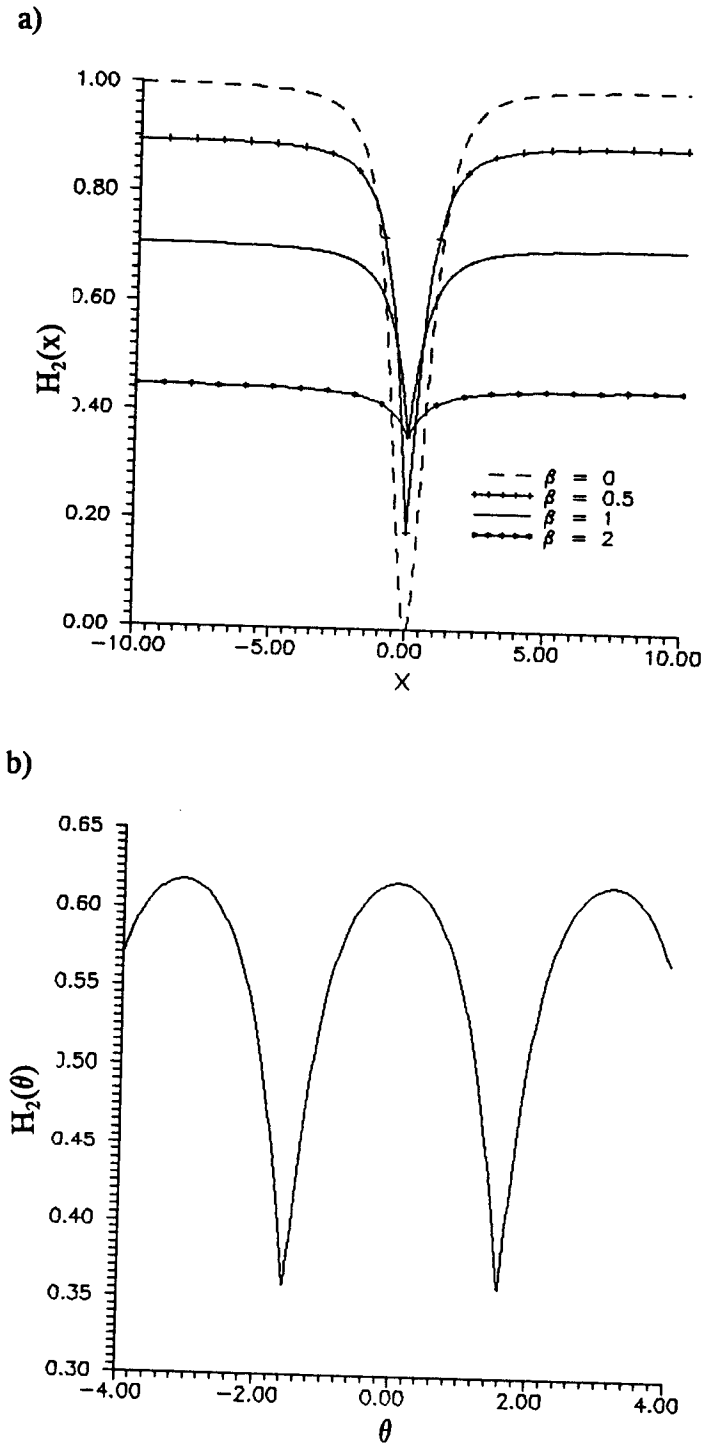

Fig.14 Hill's variational function: a) $H_2(x_0)$, b) $H_2(\theta)$

$$H_1(\theta) = -\gamma - 2\frac{\mu\delta}{\omega} \left| \xi_{C1}\cos\theta + \xi_{S1}\sin\theta \right| \tag{98}$$

$$H_2(\theta) = \zeta_0 + \zeta_{C1}\cos\theta + \zeta_{S1}\sin\theta \tag{99}$$

and

$$\begin{aligned} \xi_{C1} &= f_1 + A_1\sin\Psi_1 \quad ; \quad \xi_{S1} = A_1\cos\Psi_1 \\ \zeta_0 &= \alpha_1 + \frac{3}{2}\alpha_3\left(2A_0^2 + A_1^2\right) \\ \zeta_{C1} &= 6\alpha_3 A_0 A_1\cos\Psi_1 \quad ; \quad \zeta_{S1} = 6\alpha_3 A_0 A_1\sin\Psi_1 \\ \zeta_{C2} &= \frac{3}{2}\alpha_3 A_1^2\cos 2\Psi_1 \quad ; \quad \zeta_{S2} = \frac{3}{2}\alpha_1 A_1^2\cos 2\Psi_1 \end{aligned} \tag{100}$$

Note that H_1 portrays both linear structural damping and nonlinear drag whereas H_2 identifies contributions from the equivalent linear (α_1 in ζ_0) and cubic (α_3 in $\zeta_{0,1,2}$) coefficients of the restoring force.

4.3 Symmetry, Period Doubling and Tangent Bifurcations

The particular solution to (Eqn.93) is $\epsilon=\exp(\nu\theta)Z(\theta)$. Application of Floquet theory (Ioos and Joseph, 1981) yields two solution forms: $Z(\theta)=Z(\theta+2\pi m/n)$, $Z(\theta)=Z(\theta+4\pi m/n)$, which are due to the odd and even terms in (Eqn.81) respectively. Thus, two unstable regions are defined. The first unstable region, corresponding to $Z(\theta)=Z(\theta+2\pi m/n)$, is identified by the even terms (e.g. $j=2,4,6,\ldots$) in (Eqns.94,95) and coincides with the vertical tangent points defining primary ($n=m=1$) or secondary ($n,m\neq 1$) resonance on the frequency response curve. The second unstable region,

corresponding to $Z(\theta)=Z(\theta+4\pi m/n)$, is identified by the odd terms (e.g. $j=1,3,5,....$) and reveals an additional instability which consists of a period doubled solution.

The boundaries of the unstable regions can be obtained by assuming the following solution forms to the Hill's variational equation (Eqn.93) and applying the method of harmonic balance at the stability limit ($\nu=0$).

$$\epsilon\left[\frac{n}{m}\theta\right] = e_{0\frac{n}{m}} + \sum_j e_{j\frac{n}{m}} \cos\left[j\frac{n}{m}\theta + \psi_{j\frac{n}{m}}\right] \quad ; \quad Z\left[\theta + 2\frac{m}{n}\pi\right] \tag{101}$$

$$\epsilon\left[\frac{n}{2m}\theta\right] = \sum_j e_{j\frac{n}{2m}} \cos\left[j\frac{n}{2m}\theta + \psi_{j\frac{n}{2m}}\right] \quad ; \quad Z\left[\theta + 4\frac{m}{n}\pi\right] \tag{102}$$

The condition for a non-zero solution to Eqn.93 results in a determinant $[\Delta(\omega^2)=0]$ from which two hyperbolic stability curves defining the unstable primary and secondary resonance regions $[\Delta(\omega^2)<0$ for $\nu>0]$ are obtained. Intersection of the approximate stability curves with the frequency response curve define, in parameter space, the domain of stability loss of the $2m\pi/n$ periodic solution. The first stability region is obtained by the first solution form (Eqn.101: $j=2$):

$$\Delta = \begin{vmatrix} \zeta_{0\frac{n}{m}} & \frac{1}{2}\zeta_{C\frac{n}{m}} - \frac{n}{m}\frac{\omega}{2}\xi_{S1\frac{n}{m}} & \frac{1}{2}\zeta_{S1\frac{n}{m}} + \frac{n}{m}\frac{\omega}{2}\xi_{C1\frac{n}{m}} \\ \zeta_{C1\frac{n}{m}} & W_0 + W_{21} - \frac{n}{m}\frac{\omega}{2}\xi_{S2\frac{n}{m}} & \frac{n}{m}\omega\xi_{0\frac{n}{m}} + \frac{n}{m}\frac{\omega}{2}\xi_{C2\frac{n}{m}} \\ \zeta_{S1\frac{n}{m}} & -\frac{n}{m}\omega\xi_{0\frac{n}{m}} + \frac{n}{m}\frac{\omega}{2}\xi_{C2\frac{n}{m}} & W_0 - W_{22} + \frac{n}{m}\frac{\omega}{2}\xi_{S2\frac{n}{m}} \end{vmatrix} \tag{103}$$

where

$$W_0 = \zeta_{0\frac{n}{m}} - \left[\frac{n}{m}\omega\right]^2 \qquad (104)$$

$$W_{21} = \frac{1}{2}\left(\zeta_{C2\frac{n}{m}} + \zeta_{S2\frac{n}{m}}\right) \quad ; \quad W_{22} = \frac{1}{2}\left(\zeta_{C2\frac{n}{m}} - \zeta_{S2\frac{n}{m}}\right)$$

This region is identified by a tangent (saddle-node) bifurcation and corresponds to the bifurcation values obtained by generalized averaging in chapter 3 for primary (Eqn.71) and secondary (Eqn.78) near resonant solutions. The second stability region is obtained by the period doubled solution form (Eqn.102):

$$\Delta = \begin{vmatrix} \zeta_{0\frac{n}{m}} - \left[\frac{n}{m}\frac{\omega}{2}\right]^2 + \frac{1}{2}\zeta_{C1\frac{n}{m}} - \frac{n}{m}\frac{\omega}{4}\xi_{S1\frac{n}{m}} & \frac{n}{m}\frac{\omega}{2}\xi_{0\frac{n}{m}} + \frac{n}{m}\frac{\omega}{4}\xi_{C1\frac{n}{m}} + \frac{1}{2}\zeta_{S1\frac{n}{m}} \\ -\frac{n}{m}\frac{\omega}{2}\xi_{0\frac{n}{m}} + \frac{n}{m}\frac{\omega}{4}\xi_{C1\frac{n}{m}} + \frac{1}{2}\zeta_{S1\frac{n}{m}} & \zeta_{0\frac{n}{m}} - \left[\frac{n}{m}\frac{\omega}{2}\right]^2 - \frac{1}{2}\zeta_{C1\frac{n}{m}} + \frac{n}{m}\frac{\omega}{4}\xi_{S1\frac{n}{m}} \end{vmatrix} \qquad (105)$$

This region is identified by pitchfork or period doubling bifurcations which describe the transition from one to two stable solutions. The pitchfork bifurcation is caused by symmetry loss of a symmetric [$x(\theta) \neq -x(\theta + m\pi/n)$] or self similar solution (Eqn.81: $A_0=0$, $i=1,3,5,\ldots I$) whereas the period doubling bifurcation occurs for asymmetric [$x(\theta) = -x(\theta + m\pi/n)$] solutions (Eqn.81: $A_0 \neq 0$, $i=1,2,3,\ldots,I$).

Calculation of the eigenvalues of the monodromy matrix associated with the fundamental solution of the Hill's variational system, confirms the approximate analysis noted above (Nayfeh and Sanchez, 1988). The eigenvalues (or Floquet multipliers) characterize the stability of the perturbed solution ($|\lambda| < 1$). Loss of stability is obtained through saddle-node ($\lambda=1$) or pitchfork ($\lambda=-1$) bifurcations. The eigenvalues are

obtained by direct numerical integration of the Hill's variational system (Eqn.93).

A low order (I=1) 2π periodic two-term solution $x_0(\theta)=A_0+A_1\cos(\theta+\Psi_1)$ corresponding to excitation of a taut system by a linearized hydrodynamic exciting force consisting of small amplitude waves and weak current depicts (Fig.15a) both tangent and period doubled bifurcations. The primary resonance is derived from Eqn.103:

$$\omega^2=\frac{1}{2}\left\{\alpha\left(\zeta_0-\frac{\zeta_1^2}{\zeta_0}\right)\gamma^2\pm\sqrt{\gamma^4+2\alpha\gamma^2\left[\left(\frac{\zeta_1}{\zeta_0}\right)^2-1\right]+\alpha^2\left[\left(\frac{\zeta_1}{\zeta_0}\right)^2-\frac{\zeta_2}{\zeta_0}\right]^2}\right\} \tag{106}$$

where

$$\gamma' = \gamma + (8/3\pi)\mu\delta\sqrt{(f_0^2+f_1^2)}$$

and

$$\zeta_1 = \sqrt{(\zeta_{C1}^2+\zeta_{S1}^2)} \quad , \quad \zeta_2 = \sqrt{(\zeta_{C2}^2+\zeta_{S2}^2)}$$

For the undamped system, $\gamma'=0$, Eqn.106 simplifies to $\omega\approx\sqrt{(\alpha\zeta_0/2)}$.

The second stability region is derived from the period doubled Eqn.105:

$$\omega^2 = 2\left[\alpha\zeta_0-\gamma'^2\pm\sqrt{\gamma'^4-2\alpha\gamma'^2\zeta_0+\alpha^2\zeta_1^2}\right] \tag{107}$$

For the undamped system, $\gamma'=0$, Eqn.107 simplifies to $\omega\approx\sqrt{(2\alpha\zeta_0)}$.

A low order symmetric solution such as $x_0(\theta)=A_1\cos(\theta+\Psi_1)$, corresponding to the response of small amplitude wave excitation ($f_0=0$, $f_1\neq0$), does not exhibit a period doubling phenomenon but determines a pitchfork bifurcation in which the $Z(\theta)=Z(\theta+\pi)$ solution loses its stability (Fig.15b). This region is obtained from Eqn.103:

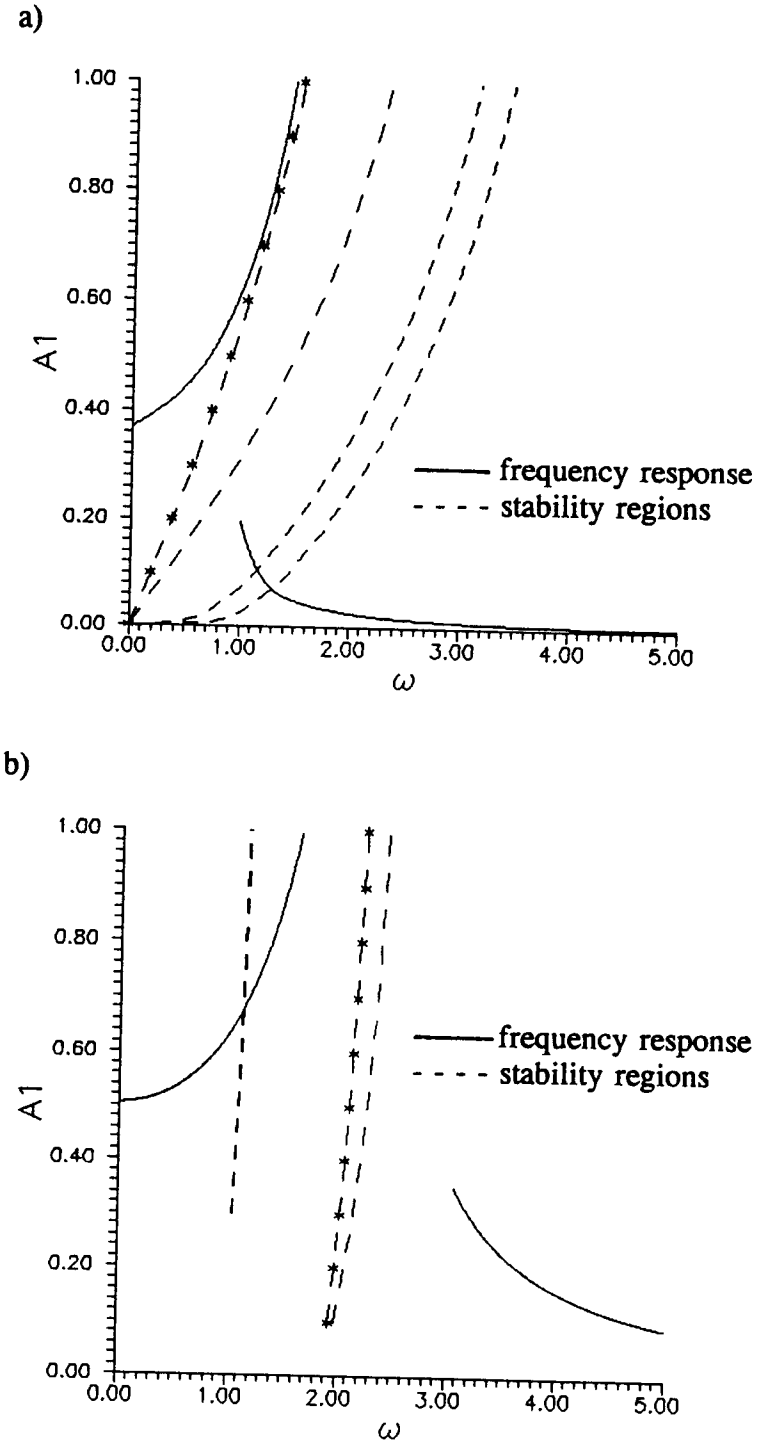

Fig 15. Stability diagram of nonlinear mooring with linearized excitation:

a) wave and current, b) wave

$$\omega^2 = \frac{1}{8}\left\{\alpha\left(\zeta_0 - \frac{\zeta_2^2}{\zeta_0}\right) - \gamma'^2 \pm \sqrt{\gamma'^4 + 2\alpha\gamma'^2\left[\left(\frac{\zeta_2}{\zeta_0}\right)^2 - 1\right] + \alpha^2\left[\left(\frac{\zeta_2}{\zeta_0}\right)^2 - 2\frac{\zeta_4}{\zeta_0}\right]^2}\right\} \qquad (108)$$

For the undamped system, $\gamma' = 0$, Eqn.108 simplifies to $\omega \approx \sqrt{(\alpha a_0/8)}$.

The stability loss of the symmetric solution is portrayed in the emergence of a low order unsymmetric solution $x_0(\theta) = A_0 + A_1\cos(\theta + \Psi_1) + A_2\cos(2\theta + \Psi_2)$ which yields (via Eqn.105) a period doubled solution $Z(\theta) = Z(\theta + 4\pi)$ similar to Eqn.106. This period doubling is associated with the appearance of an ultrasubharmonic (n/m=3/2). Note in Fig.15b the narrow domain of period doubling instability and the larger amplitude (A_1) of the 2π periodic solution in the ultrasubharmonic versus subharmonic domains.

Numerical simulations of system response at the stability limits depict the symmetry loss which occurs at the pitchfork bifurcation (Fig.16a-d) and the transition from a 2π periodic solution (Fig.17a, 18a) to a period doubled in both subharmonic (Fig.17b) and ultrasubharmonic (Fig.18b) domains.

Symmetry breaking of system response (n=m=1) to excitation by small amplitude waves ($f_0 = 0$, $f_1 \neq 0$) occurs with variation of exciting frequency in the parameter space predicted by Eqn.108. Loss of symmetry is apparent in the phase plane by the geometric shape of the response and the power spectra with the appearance of even harmonics (Fig.16b,c). Note that the pitchfork bifurcation is defined by the transition from and to a symmetric solution (Fig.16a,b and Fig.16c,d). Period doubling of subharmonic response (n/m=1/2) to excitation by small amplitude waves and a weak

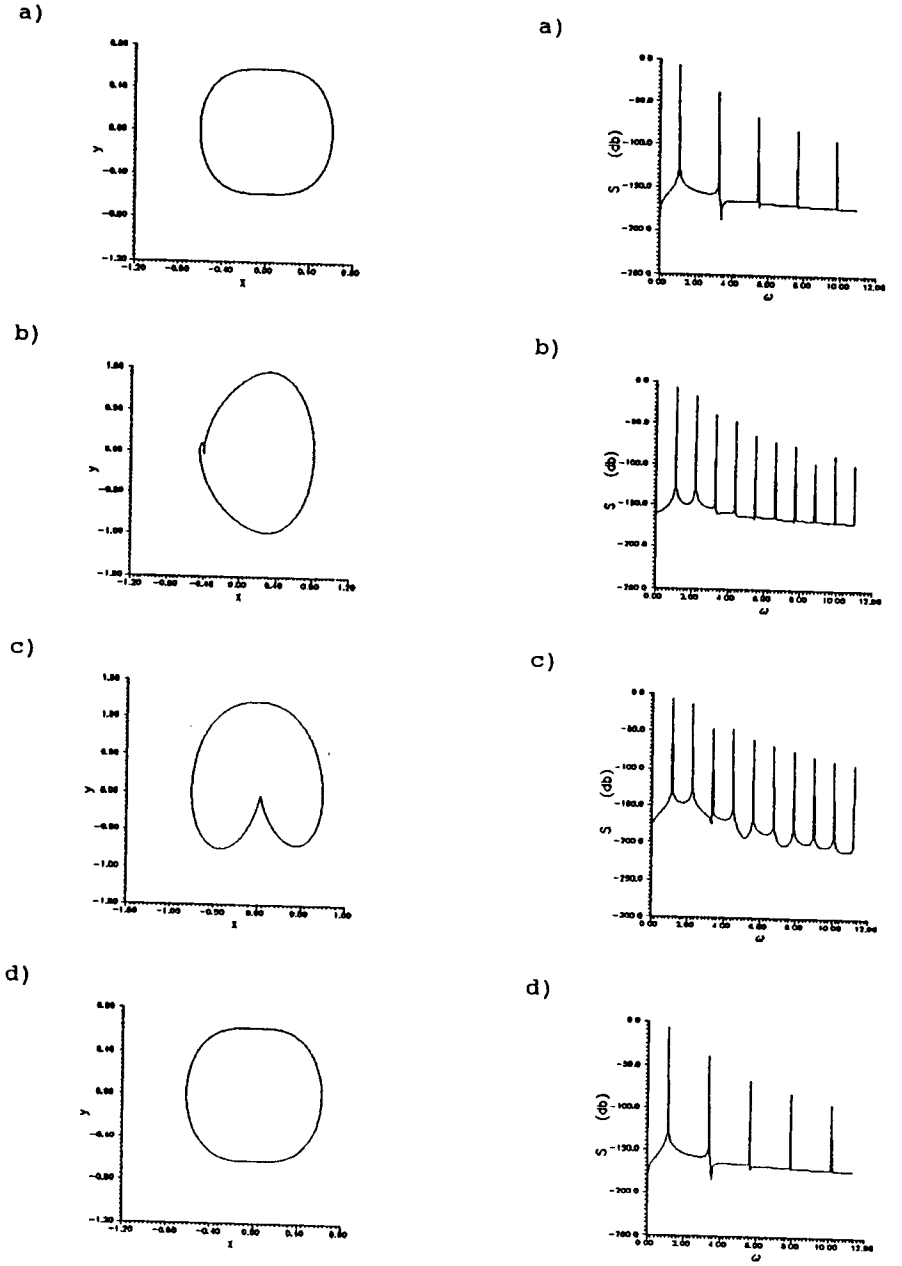

Fig.16 Symmetry loss in the unbiased system

[a) ω=1.09, b) ω=1.10 , c) ω=1.12, d) ω=1.13]

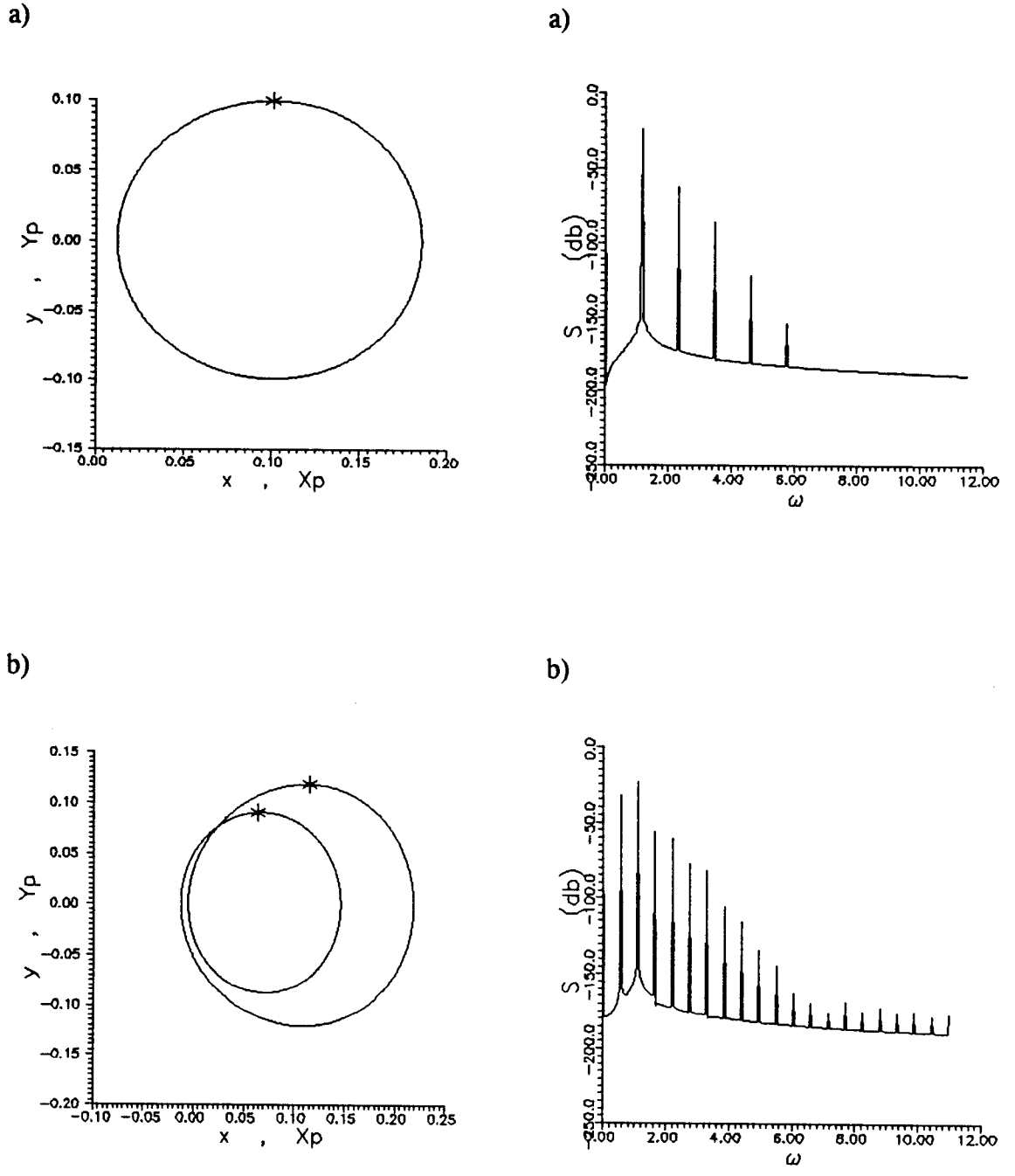

Fig.17 Period doubling in a system excited by current and waves:

a) $\omega=1.26$ (n=m=1), b) $\omega=1.24$ (n/m=1/2)

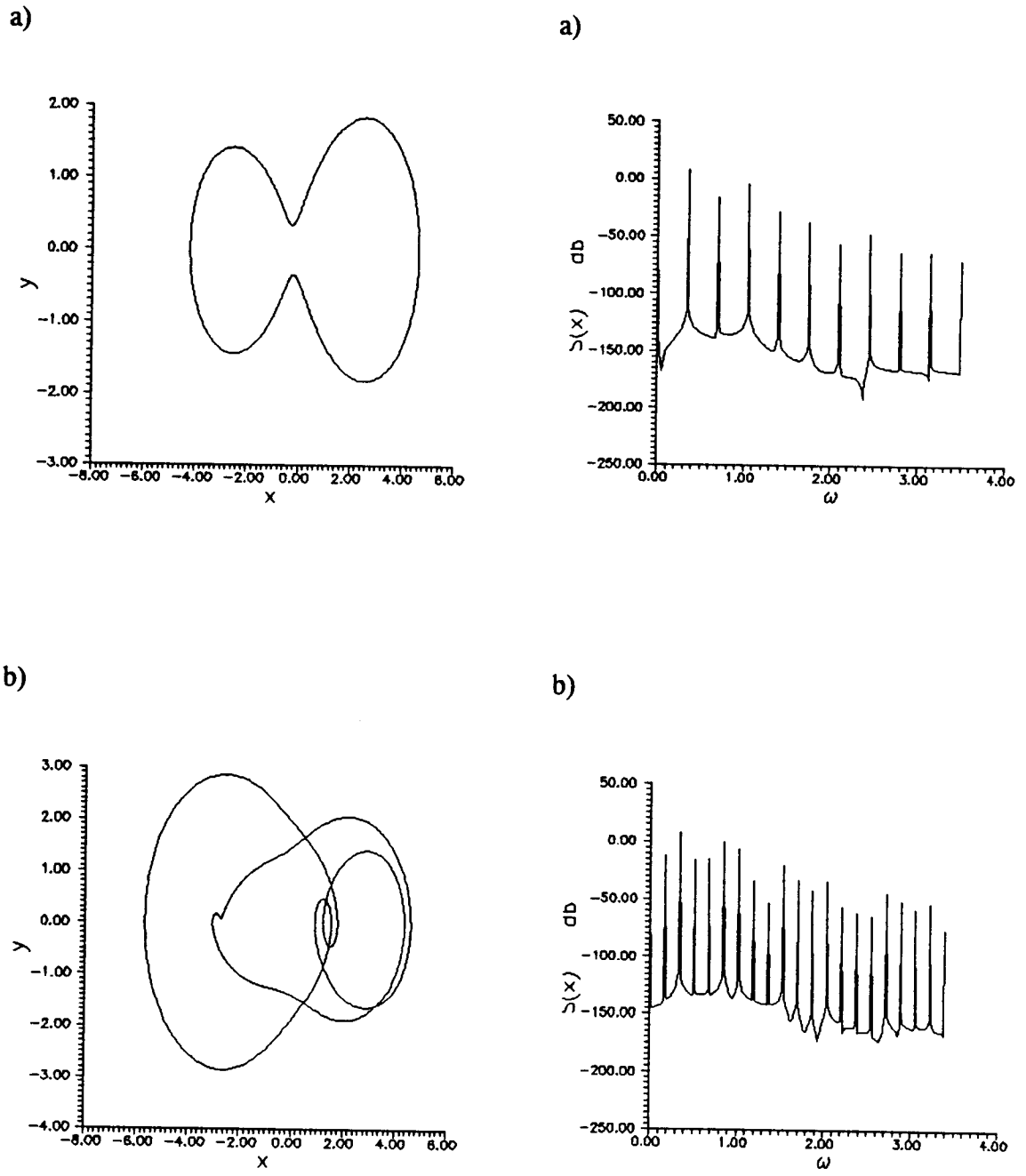

Fig. 18 Period doubling in a system excited by waves:

a) $\omega=0.35$ (n=m=1), b) $\omega=0.34$ (n/m=5/2)

colinear current ($f_0, f_1 \neq 0$) is predicted by Eqn.107. This transition is apparent with the appearance of a second Poincaré point and a high energy 4π component ($\omega/2$) in the power spectra (Fig.17b). Period doubling of an unsymmetric ultrasubharmonic response ($n/m=5/2$) to excitation by small amplitude waves (i.e. within the parameter space of a pitchfork bifurcation) is also depicted by the complexity of the $4\pi/5$ phase plane and with the appearance of a high energy $4\pi/5$ component ($5\omega/2$) in the power spectra (Fig.18b).

Loss of symmetry of a 2π periodic solution ($n=m=1$) can be viewed as a form of dynamic symmetry breaking (Parlitz and Lauterborn, 1985) as there is no symmetry loss in the static case of a single-well potential. Furthermore, recall (see chapter 3) that symmetric ($n=m=1$) or self-similar (n,m odd: $n,m \geq 1$) solutions are unique (e.g. Figs.8,10,11,12c) and unsymmetric (n,m even, $n,m \geq 1$) solutions appear in multiples (e.g. Fig.12a,b: $n/m=4/5$). Therefore, the transition from a symmetric (or self similar) solution to an unsymmetric solution consists of a pitchfork bifurcation describing the emergence of two stable periodic orbits. The two coexisting partner orbits are defined by different initial conditions and portray inverse symmetry in the phase plane (Fig.19). Coexistence of two period doubled partner solutions (Fig.20b,d) is also a consequence of dynamic symmetry breaking and is portrayed by inverse symmetry in the phase plane whereas the power spectra is the same. Note that although coexisting solutions (with different initial conditions) are found for an identical parameter space (Fig.20a-d) the magnitude of the near secondary resonance solutions ($n,m > 1$: Fig20b,d) is greater than that of the 2π periodic response ($n=m=1$: Fig.20a).

a)

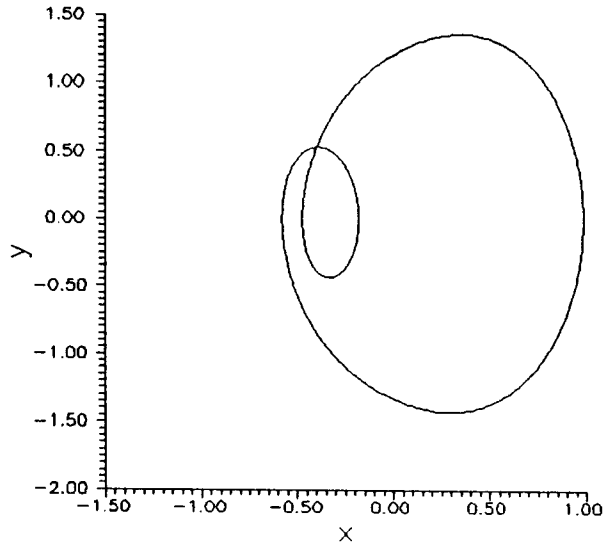

b)

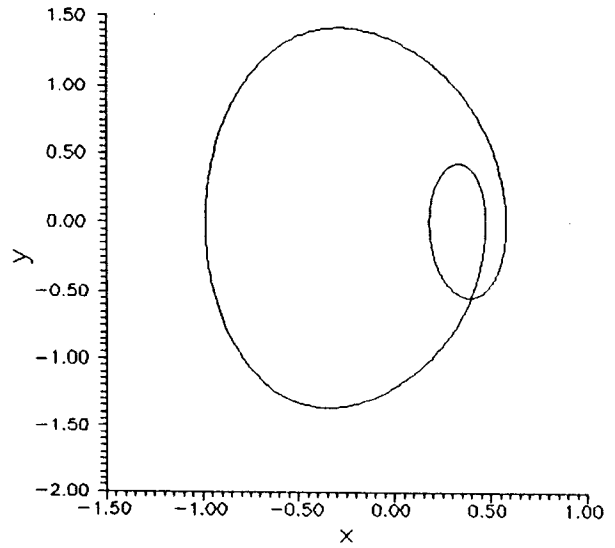

Fig.19 Coexistence of period 2π partner orbits (m=n=1):

a) (x(0),y(0))=(0,0), b) (x(0),y(0))=(1,1)

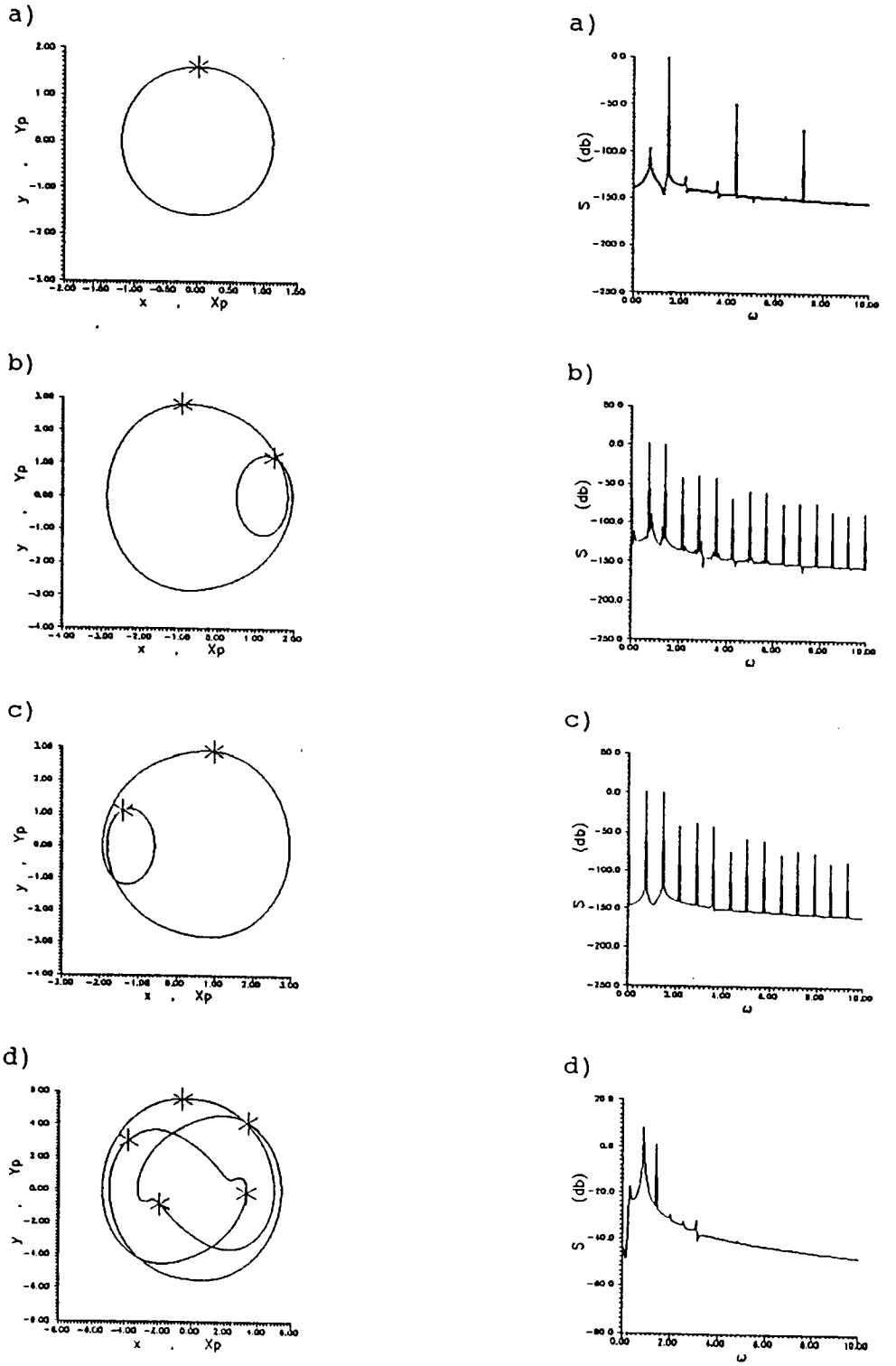

Fig.20 Coexistence of period 4π partner orbits: a) (x(0),y(0))=(0,0) (n=m=1), b,c) (x(0),y(0))=(-1,0),(1,1)(n/m=1/2), d) (x(0),y(0))=(-3,1)(n/m=3/5)

Analysis of the Hill's variational system (Eqns.97-99) derived for a taut system excited by harmonic waves ($f_0=0$) results in the following criterion for period doubling bifurcations:

$$\Delta(\omega^2) = \left[\zeta_0 - \left(\frac{\omega}{2}\right)^2\right]^2 - \frac{1}{4}\left(\zeta_{C1}^2+\zeta_{S1}^2\right) + \left(\frac{\gamma\omega}{2}\right)^2 + sgn(\sigma)\frac{\mu\delta}{2}\left(\xi_{C1}\zeta_{S1}+\xi_{S1}\zeta_{C1}\right) - \left(\frac{\mu\delta}{2}\right)^2\left(\xi_{C1}^2+\xi_{S1}^2\right) \tag{109}$$

where $\sigma=\xi_{C1}\cos\Psi_1+\xi_{S1}\sin\Psi_1$ and sgn (σ) denotes the sign of σ.

This criterion enables the investigation of the influence of the nonlinear hydrodynamic drag force (Fig.21a). Numerical simulations of system response at the stability limit [Fig.22: a) n=m=1, b) n/m=1/2] reveal the transition from a 2π periodic solution to a period doubled one depicted by the appearance of a strong bias in phase space and even harmonics in the power spectra (Fig.22b).

The stability criterion can be simplified for a weakly nonlinear small angle mooring configuration or for the linearized mooring system ($\beta=10$: $\zeta_0=\alpha_1$, $\alpha_{n>1}=0$) resulting in a narrower unstable region (Fig.21a: linearized restoring force).

$$\Delta(\omega^2) = \left[\alpha_1 - \left(\frac{\omega}{2}\right)^2\right]^2 + \left(\frac{\gamma\omega}{2}\right)^2 - \left(\frac{\mu\delta}{2}\right)^2\left(f_1^2+2f_1A_1\sin\Psi_1+A_1^2\right) \tag{110}$$

Thus, the unstable region defining the secondary resonance is shown to be

a)

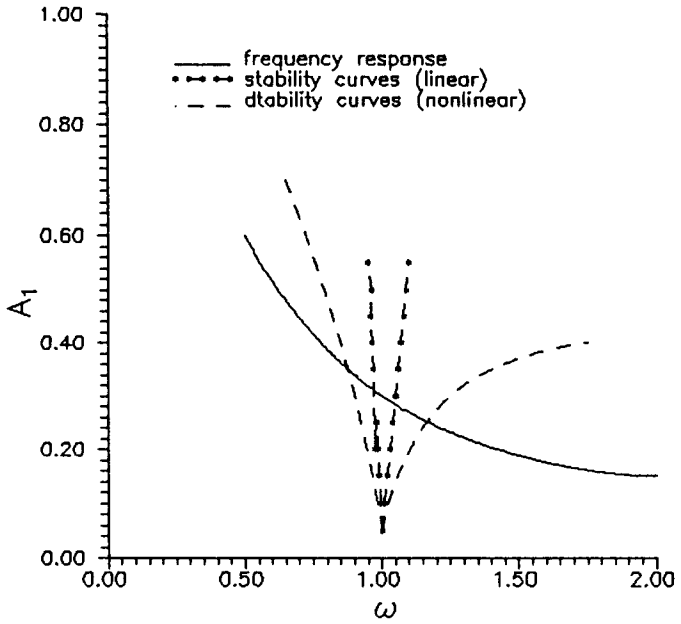

b)

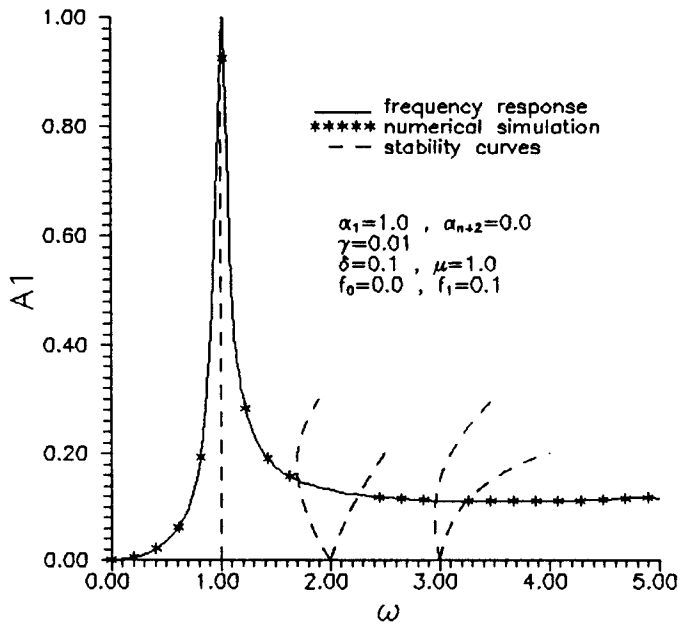

Fig.21 Stability diagram of linearized mooring with nonlinear excitation: a) influence of drag, b) influence of convective excitation

a)

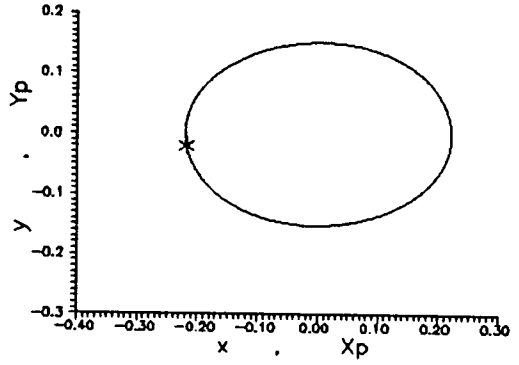

a)

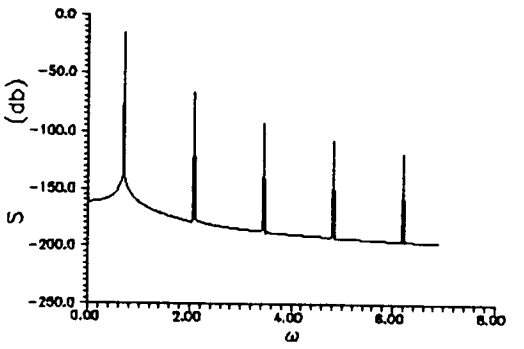

b)

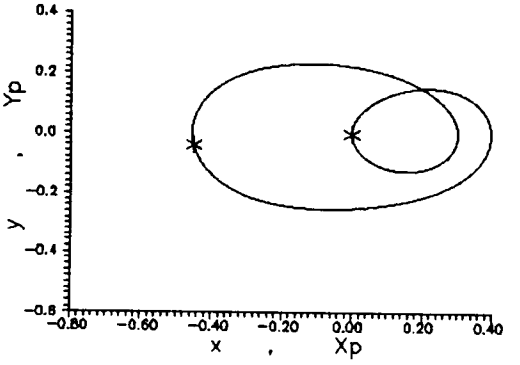

b)

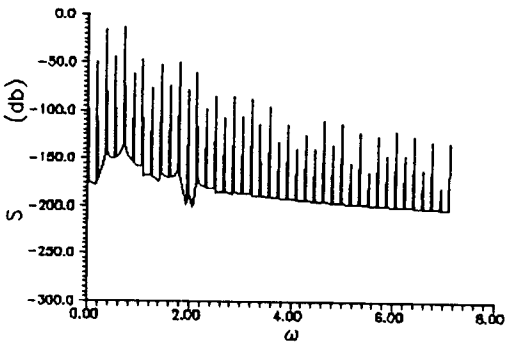

Fig.22 Period doubling - influence of nonlinear drag:

a) $\omega=0.85$ (n=m=1), b) $\omega=1.10$ (n/m=1/2)

confined between two hyperbolic functions [$\Delta(\omega)=0$, $\gamma << \delta$] and is found to be sensitive to the magnitude of the response as indicated by:

$$A_1 \propto f_1 + \left| \frac{4\alpha_1 - \omega^2}{2\mu\delta} \right| \tag{111}$$

Note that the stability region of the undamped system ($\gamma,\delta=0$ in Eqn.109) is defined by the following criterion: $\omega^2=4\zeta_0-2\sqrt{(\zeta_{C1}^2+\zeta_{S1}^2)}$, which is identical (to 1st order) to the secondary resonance stability region of the Duffing equation (Szemplinska-Stupnika, 1987).

The influence of the convective hydrodynamic nonlinearity is investigated by incorporating the complete solution in the stability criteria (Eqns.103,105). Results (Fig.21b) confirmed by numerical simulations (Fig.23) reveal a distinct widening of the bifurcation regions even for the linearized mooring system. Note that equivalent linearization of drag or convective terms would not have revealed the existence of period doubling instabilities (n/m=1/2) and resulted only in a unique approximate 2π periodic solution (n=m=1).

a)

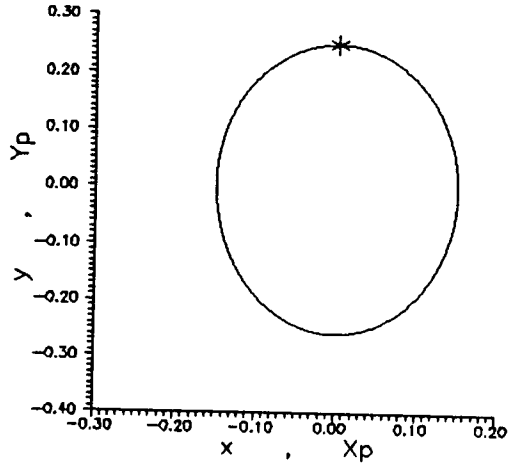

a)

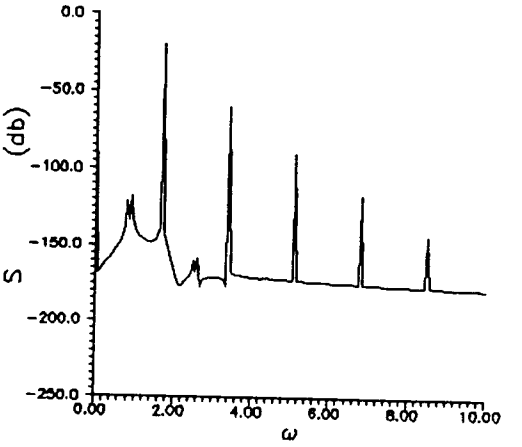

b)

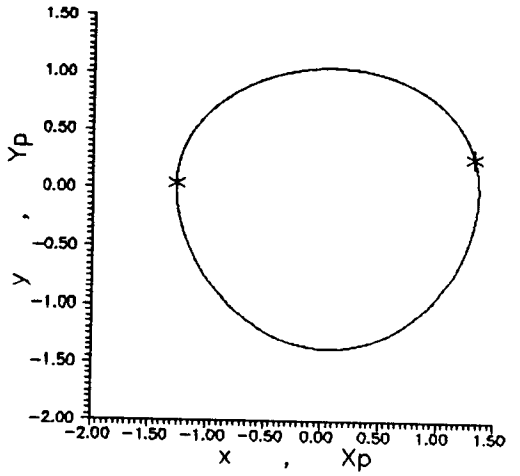

b)

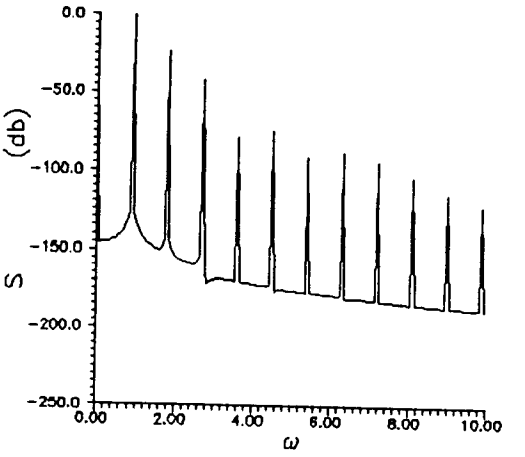

Fig.23 Period doubling - influence of nonlinear inertia:

a) $\omega=1.6$ (n=m=1), b) $\omega=1.9$ (n/m=1/2)

5. GLOBAL BIFURCATIONS

Global bifurcations are defined as qualitative changes in an orbit (or solution) structure of an extended region of phase space (e.g. Wiggins, 1988). Recall that while system response subject to weak excitation was shown to be structurally stable (section 2.3), local analysis of nonresonant (chapter 4) and near resonance (chapter 3) system response subject to larger excitation revealed a variety of stable and unstable coexisting phenomena. This chapter describes motion between or among the local equilibrium points that are not confined to a small region of the solution domain. Existence of homoclinic orbits enable application of Melnikov's method to the perturbed averaged system derived in chapter 3. Transverse intersections of the stable and unstable manifolds result in a criterion for Smale horseshoe type chaos of the 2π periodic response. This criterion is sensitive to the high frequency of the averaged system and only estimates for the separatrix splitting of the rapidly forced system are obtained semi-analytically.

Numerical simulations of system response reveal transient chaotic phenomena which alternates between the two coexisting attractors. Further analysis of the period doubling bifurcations found in chapter 4 reveals existence of a period doubling cascade. If the sequence of period doubling bifurcations is infinite with a finite accumulation point, the resulting motion is that of a steady state chaotic attractor with period $4^l\pi/n$ where $l \to \infty$. Numerical simulation of system response confirms the semi-analytical criteria for period doubling cascade. While the 1/m subharmonic and n/m

ultrasubharmonic solutions repeat after m intervals, the chaotic attractor does not, consequently generating a fractal map. The chaotic attractor is also characterized by a continuous spectra showing its "random like" behavior. The local transitions to and from stable coexisting steady state solutions are also shown to be sensitive to initial conditions. The transition is abrupt and numerical simulation of system response near secondary resonance reveal transient chaotic phenomena (i.e. crisis, c.f. Grebogi et al. 1983) and chaotic attractors (i.e. explosions, c.f. Ueda, 1981).

5.1 Existence of Transverse Homoclinic Orbits

Analysis of the perturbed averaged system derived in section 3.1 (Eqns.55-60) determined existence of stable and unstable hyperbolic orbits (Eqn.71). The averaged system representing the associated Poincaré map was formulated to consist of an integrable potential function perturbed by a damping mechanism. While the structure of the potential function was shown to be Hamiltonian (Eqn.61), the secondary resonances were found not to be excited by the averaged inertial forcing (Eqn.56: $r \neq 1$: $n,m > 1$). Consequently, only the phase plane of the near primary resonant Hamiltonian system contains two coexisting centers separated by the stable and unstable manifolds of a saddle. In order to determine whether the averaged 2π periodic system (Eqns.64-66) obtains a homoclinic orbit, the Bendixson criterion (Guckenheimer & Holmes, 1986) is employed (see section 2.3). The criterion is calculated from the trace of the system (Eqn.64) derivative matrix $[B=\partial(F_1(J,\Phi)+G_1(J,\Phi))/\partial J+\partial(F_2(J,\Phi)+G_2(J,\Phi))/\partial\Phi]$ which

results in the following:

$$B = -\gamma \mp 4\delta^* \sqrt{f_1^2 + 2f_1\sqrt{2J}\sin\Phi + 2J} \tag{112}$$

Consequently, for small structural damping ($\gamma < \delta$), the system near primary resonance contains homoclinic loops defined by the stable and unstable manifolds of the saddle. Note that homoclinicity is not limited to weak damping perturbation. Approximation of the damping perturbation (Eqn.66) by a lower bound representative of an equivalently linearized drag force [$G_1^L = -2(\gamma^* + f)J$, $G_2^L = 0$] results in the following constant negative value:

$$B^L = -\left(\gamma + \frac{\mu f_1 \delta}{\pi \omega}\right) < 0 \tag{113}$$

Thus, the hardening averaged system excited by a small amplitude linearized drag force does not contain a saddle connection. The approximation of the damping perturbation by an upper bound [$G_1^U = -2\gamma^* J - 4(2fJ\sin\Phi + (2J)^{3/2})/3$, $G_2^U = -2fJ\cos\Phi/3$] reveals existence of homoclinic orbits as the Bendixson criterion changes sign in the following:

$$B^U = -\gamma - 4\delta^*\sqrt{2J} - 2\delta^* f_1 \sin\Phi \tag{114}$$

The homoclinic orbits $q^0{}_{\pm}(\theta)$ of the near primary resonant averaged system (Eqn.64: $\delta^* = 0$) describe the following level set (H_0) obtained from the Hamiltonian energy [Eqn.61: $H(J,\Phi) = H(j_2, 3\pi/2) \equiv H_0$]:

$$H_0 = \Omega^* j_2 - \alpha_3^* j_2^2 - f_1\sqrt{2j_2} \tag{115}$$

The orbits $q^0_{\pm}(\theta)=(J_{\pm}(\theta),\Phi_{\pm}(\theta))$ are obtained by integrating the Hamiltonian system (Eqn.64: $\delta^*=0$) after incorporating the invariant energy (Eqn.61: r=1) on the saddle connection (Eqn.115). This is done by substitution of $\Phi_{\pm}(J_{\pm};H_0)$ obtained from $H(J_{\pm},\Phi_{\pm})=H_0$, into $F_1(J_{\pm}(\theta),\Phi_{\pm}(\theta))$ (Eqn.64) and integrating (with respect to θ) after separation of variables (e.g. Tabor, 1989; Nayfeh & Mook, 1979):

$$J_{\pm}(\theta): \qquad \theta-\theta_0 = \int_{J(\theta_0)}^{J_{\pm}(\theta)} \frac{dJ}{\sqrt{f_1^2(2J_{\pm})-\left(H_0-\Omega^* J_{\pm}+\alpha_3^* J_{\pm}^2\right)^2}} \tag{116}$$

$$\Phi_{\pm}(\theta) = \sin^{-1}\left(\frac{H_0-\Omega^* J_{\pm}+\alpha^{*3} J_{\pm}^2}{f_1\sqrt{2J_{\pm}}}\right) \tag{117}$$

Existence of transverse intersections of the stable and unstable manifolds of the homoclinc orbits is shown by application of Melnikov's method to the perturbed averaged system. The method does not guarantee the existence of a strange attractor or steady state chaos, but does give a bound in parameter space below which Smale horseshoe type chaos is unlikely to occur. The distance between the stable and unstable manifolds is given by (e.g. Guckenheimer & Holmes, 1986):

$$d(t_0;\delta^*) = \frac{\delta^* M(t_0)}{|f(q_0(0))|} + O(\delta^{*2}) \tag{118}$$

where $M(t_0)$ is the Melnikov function:

$$M(t_0) = \int_{-\infty}^{\infty} f(q_0(t)) \wedge g(q_0(t), t+t_0)\, dt \tag{119}$$

Consequently, when $M(t_0)$ has a simple zero $d(t_0)$ also has a simple zero and there exist transverse intersections of the stable and unstable manifolds.

The damping perturbation (Eqn.66) does not depend explicitly on time as the averaged system (Eqn.64) is autonomous. Therefore, the Melnikov function for the homoclinic orbits defined in Eqns. 116,117 simplifies to the following time independent function:

$$M = \int_{-\infty}^{\infty} (F_1 G_2 - F_2 G_1) \, d\theta \tag{120}$$

where

$$\begin{aligned} F_1 G_2 - F_2 G_1 &= 2\gamma J_{\pm}\left(-\Omega^* + 2\alpha_3^* J_{\pm} - f_1 \frac{\sin\Phi_{\pm}}{\sqrt{2J_{\pm}}}\right) \\ &+ \frac{4}{3}\sqrt{\Gamma_{\pm}}\left[(2J_{\pm})(-\Omega^* + 2\alpha_3^* J_{\pm})\left(1 + \frac{f_1 \sin\Phi_{\pm}}{\sqrt{2J_{\pm}}}\right) - f_1\sqrt{2J_{\pm}}\sin\Phi_{\pm} - f_1^2\right] \end{aligned} \tag{121}$$

and

$$\Gamma_{\pm} = f_1^2 + 2f_1\sqrt{2J_{\pm}}\sin\Phi_{\pm} + 2J_{\pm} \tag{122}$$

Numerical calculation of the Melnikov function (Eqn.120) results in a value M $[M \neq M(\theta_0)]$ which is a function of the parameter space determining existence of the perturbed homoclinic orbit (Eqns.116,117) as the stable and unstable manifolds of the hyperbolic saddle either do ($M=0$) or do not intersect ($M \neq 0$).

Note that the criterion obtained is sensitive to the high frequency of the averaged system θ/ϵ where ϵ is the measure of smallness employed in the averaging

transformation. Recall that application of averaging (chapter 3) transformed the system (Eqn.47) which was in the form of $d\mathbf{q}/d\theta=\epsilon\mathbf{f}(\mathbf{q},\theta)+\epsilon^2\mathbf{g}(\mathbf{q},\theta;\epsilon)]$ where $\mathbf{q}=(u,v)^T$, to the following form for the averaged system (Eqn.52): $d\mathbf{q}/d\theta=\epsilon\tilde{\mathbf{f}}(\mathbf{q})+\epsilon^2\tilde{\mathbf{g}}(\mathbf{q};\epsilon)$ where (for n=m=1) $2\pi\tilde{\mathbf{f}}(\mathbf{q})=_0\int^{2\pi}\mathbf{f}(\mathbf{q},\theta)d\theta$. Resealing time, $\theta\rightarrow\theta/\epsilon$, transforms the averaged system into $d\mathbf{q}/d\theta=\tilde{\mathbf{f}}(\mathbf{q})+\epsilon\tilde{\mathbf{g}}(\mathbf{q};\epsilon)$ (i.e. Eqn.55). Consequently, the Melnikov function (Eqn.120) depends implicitly on ϵ and the relatively high frequency of oscillation (i.e. period $2\pi\epsilon$) results in the Melnikov function being exponentially small in ϵ. Recently, Holmes et al. (1988) established upper and lower bounds for the separatrix splitting of rapidly forced systems and demonstrated the applicability of the Melnikov criterion to forced Hamiltonian saddle-node bifurcation problems exhibiting exponentially small splitting.

The value of the Melnikov function calculated for parameter values obtained from the bifurcation value defining coexistence of saddle-sinks (Eqn.72), was found to be sensitive to the magnitude of the excitation ($f^*=\mu\omega f/2$). As anticipated by the Bendixson criterion (Eqn.112), weak excitation does not generate transverse intersections whereas numerical simulation for large amplitude excitation reveals long duration (i.e. large number of cycles) of irregular transient behavior and sensitivity to initial conditions before the solution settles to one of the coexisting attractors. This is demonstrated by comparison of a Poincaré section comprised of the projection of the Poincaré amplitude X_P, onto the integer "time scale" N_P, representing sampling at each forcing cycle (Fig.24). Note that simulations incorporating initial conditions near the orbits described by the stable sinks of the Poincaré map [i.e. near $(j'_{1,3},\phi'_{1,3})$ in section 3.2] converge

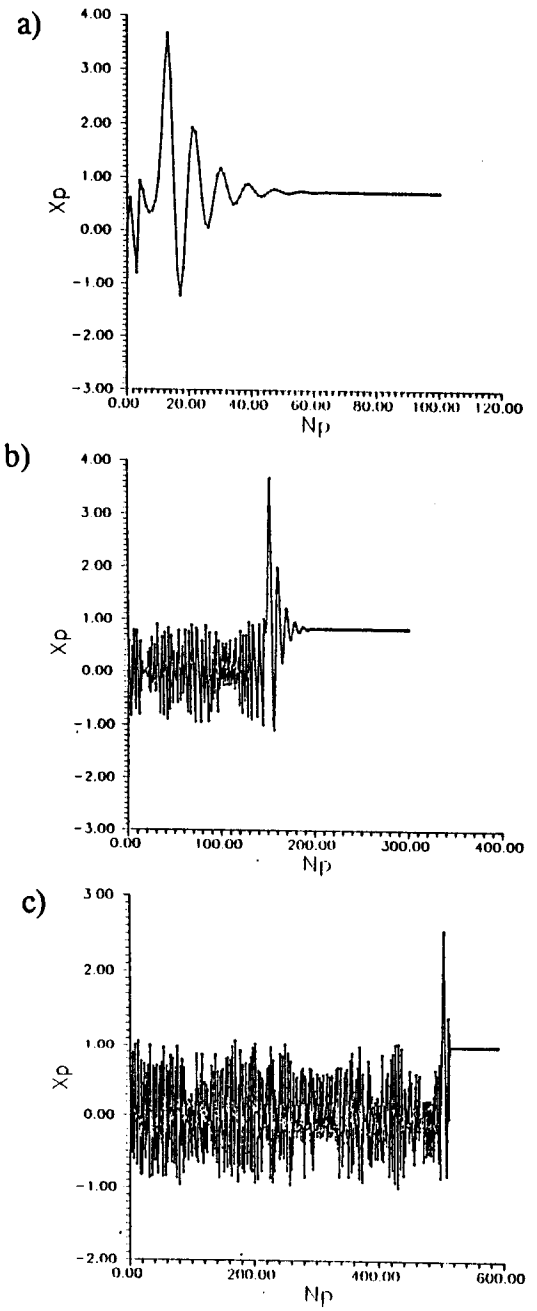

Fig.24 Transient chaotic response (n=m=1) - variability of initial conditions: a) (x(0),y(0))=(0,0), b) (x(0),y(0))=(-1,0), c) (x(0),y(0))=(-1,0.01)

to their respective steady states (attractors) rapidly (Fig.24a: $N_P \simeq 50$ forcing cycles) whereas initial conditions in the vicinity of the perturbed homoclinic orbit [i.e. near (j'_2, ϕ'_2)] exhibit lengthy transient chaotic behavior before settling to one of the coexisting attractors (Fig.24b,c: $N_P \simeq$ 100-500 forcing cycles).

5.2 Existence of a Period Doubling Cascade

Existence of a period doubling cascade is shown by further stability analysis of the period doubled subharmonic solution found in the previous chapter by local bifurcation analysis. A low order (I=2) subharmonic solution is substituted in the $x_{1/2}(\theta) = A_0 + A_{1/2}\cos(\theta/2 + \Psi_{1/2}) + A_1\cos(\theta + \Psi_1)$ (Eqn.81: n/m=1/2), Hill's variational equation for a taut system (Eqns.97-99) to obtain the following subharmonic Hill's system:

$$\begin{aligned} \dot{\epsilon} &= \eta \\ \dot{\eta} &= H_1(\theta)\ \eta + H_2(\theta)\ \epsilon \end{aligned} \tag{123}$$

where

$$H_1(\theta) = -\gamma - 2\frac{\mu\delta}{\omega}\left|\sum_{j=1}^{2} \xi'_{Cj\frac{1}{2}} \cos\left(j\frac{1}{2}\theta\right) + \xi'_{Sj\frac{1}{2}} \sin\left(j\frac{1}{2}\theta\right)\right| \tag{124}$$

$$H_2(\theta) = \zeta'_0 + \sum_j \zeta'_{Cj\frac{1}{2}} \cos\left(j\frac{1}{2}\theta\right) + \zeta'_{Sj\frac{1}{2}} \sin\left(j\frac{1}{2}\theta\right) \tag{125}$$

and

$\xi' = \xi'(A_0, A_j, \Phi_j)$, $\zeta' = \zeta'(A_0, A_j, \Phi_j)$ are in Appendix A.3.

As in the previous stability analysis (chapter 4), a low order three term solution generates two unstable regions. The first region, $Z(\theta+4\pi)$, is identified by the $\cos\theta$ term in Eqns.114,115 and corresponds to the secondary 4π tangent resonance whereas the lowest order unstable region, $Z(\theta+8\pi)$, corresponds to an 8π resonance and is identified by the period doubling term $\cos(\theta/2)$. The boundaries of the unstable regions can be obtained by solving the 4π subharmonic variational equation (Eqn.112) with low order approximations (Eqns.101, 102: $n/m=1/2$, $j=3$) resulting in stability equations defining existence of the 4π subharmonic tangent bifurcation (Eqn.103: $n/m=1/2$ near secondary resonance) and the evolution of a 8π subharmonic within the boundaries of the region defined by Eqn.105 ($n/2m=1/4$). Consequently, a build up of period doubled components can be expected as the low order 8π subharmonic solution (Eqn.81: $j=4$, $n/m=1/4$) will also generate two stable regions corresponding to $Z(\theta+8\pi)$ and $Z(\theta+16\pi)$. The ultrasubharmonic Hill's variational equations (Eqns.93-95: $n,m>1$) were numerically integrated over time [θ:(0, $2m\pi/n$)] to determine the regions of stability loss. The resulting eigenvalues defined saddle-node ($\lambda=1$) and period doubled ($\lambda=-1$) bifurcation points thus confirming the approximate analysis. Thus, the subharmonic ($n=1$,$m>1$) and the ultrasubharmonic ($n,m>1$) Hill's equation suggests the possible cascade of period doubling. If the period doubling sequence is infinite, the resulting motion is chaotic (Feigenbaum, 1980).

Numerical simulations of system response identify a variety of 8π subharmonic and $8\pi/n$ ultrasubharmonic solutions adjacent in parameter space to the period doubled solutions described in the previous chapter. These solutions in part evolve to a strange

attractor. The taut mooring system excited by an unbiased linearized exciting force exhibits a cascade of period doubling from a 4π subharmonic (Fig.17b: n/m=1/2) and a $4\pi/5$ ultrasubharmonic (Fig.18b: n/m=5/2) to period 8π solutions in the subharmonic (Fig.25a: n/m=1/2) and ultrasubharmonic (Fig.25b: n/m=5/2) domains. Note that the peak with the largest energy content remains identical to that of the fundamental generating subharmonic (compare Fig.17b: $\omega_{max}=\omega/2$ to Fig.25a: $\omega_{max}=2\omega/4$) and ultrasubharmonic (compare Fig.18b to Fig.25b: $\omega_{max}=10\omega/4$) solutions. The period doubling cascade evolves directly to a chaotic attractor (Fig.26) whereas the subharmonic response converges to a period doubled solution. Investigation of system response to a nonlinear hydrodynamic drag force incorporating a weak bias, reveals evolution of a period doubling cascade from a 4π subharmonic (Fig.22: n/m=1/2) to an 8π (Fig.27a,b: n/m=1/2) subharmonic resulting in a chaotic attractor (Fig.28). The influence of convective terms reveals a continuous period doubling cascade from a 4π subharmonic (Fig.23:n/m=1/2) to 8π and 16π (Fig.29a,b: n/m=1/2) subharmonics, culminating with a chaotic attractor over a large domain (Fig. 30).

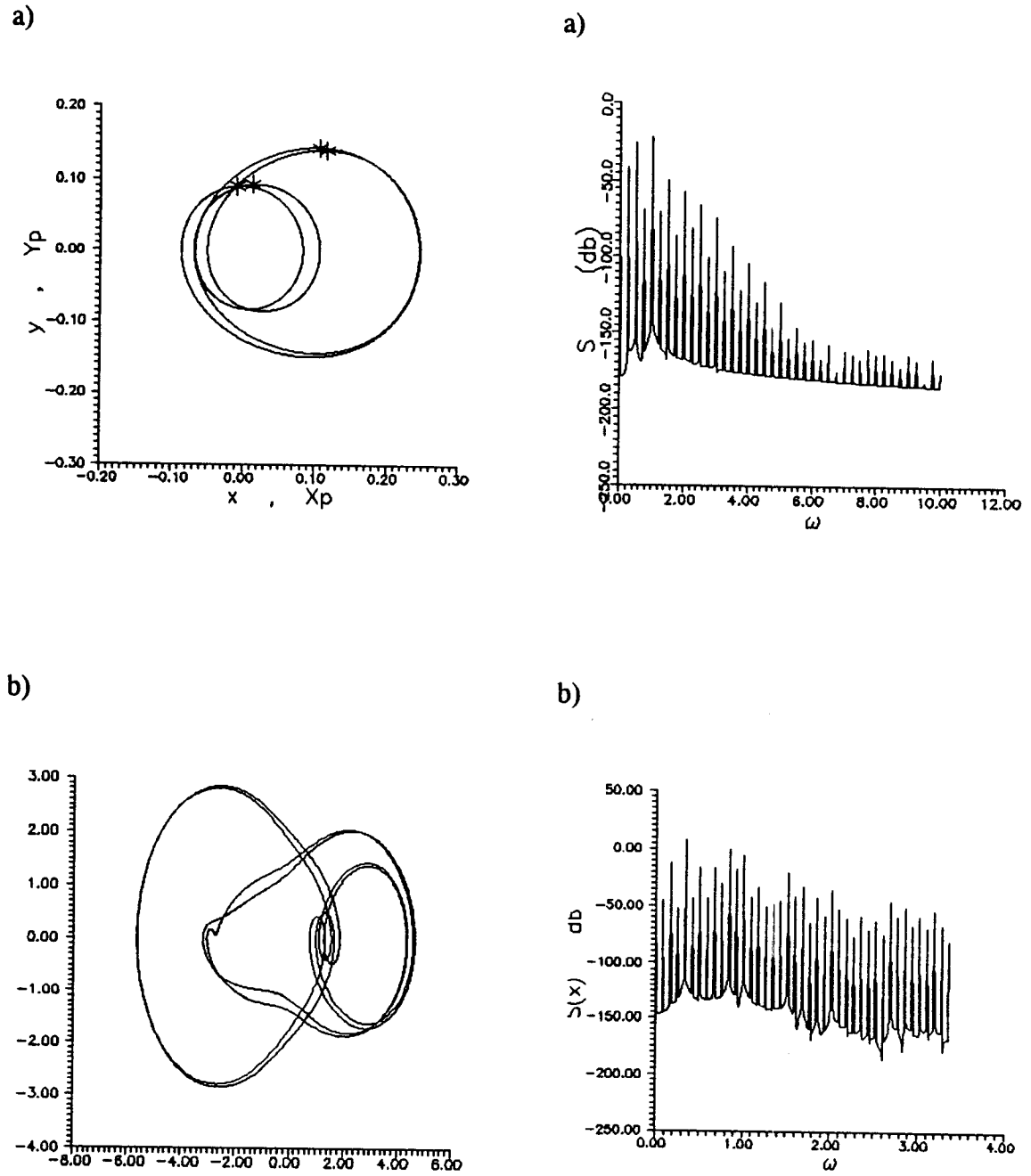

Fig.25 Period quadrupling in a system subject to linearized excitation:

a) $\omega=1.23$ (n/m=1/4), b) $\omega=0.337$ (n/m=5/4)

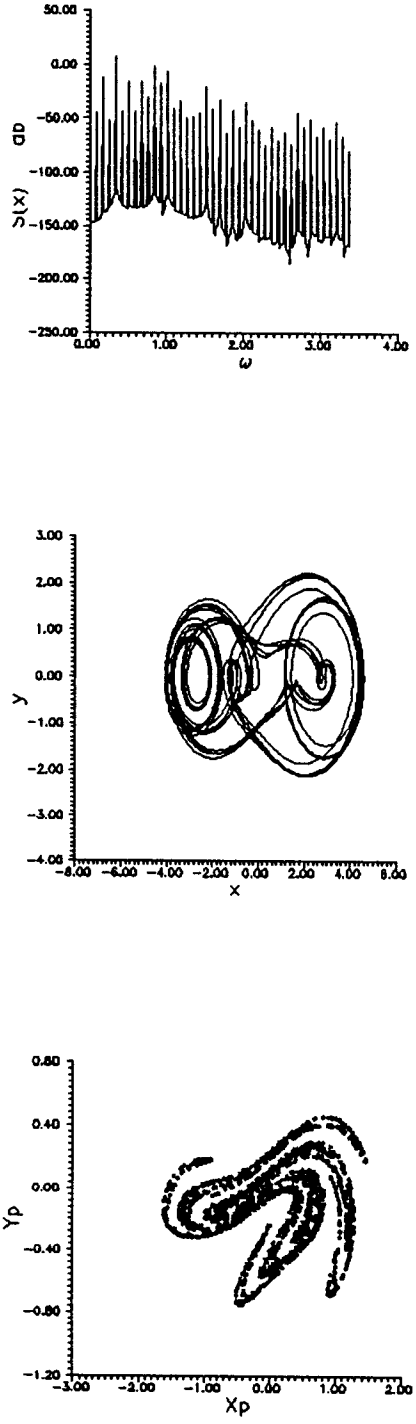

Fig.26 Chaotic attractor in a system subject to linearized excitation (ω=0.335)

a)

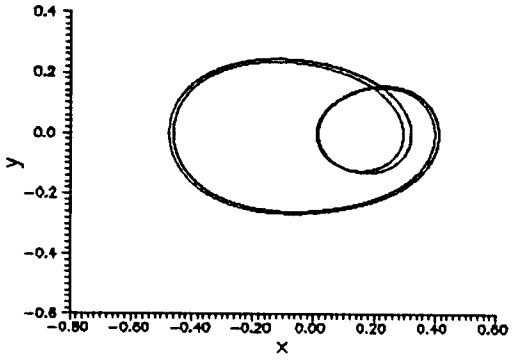

a)

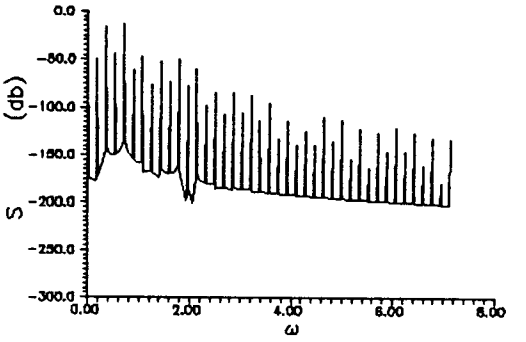

b)

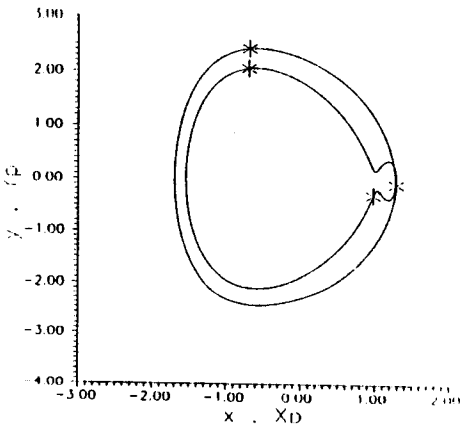

b)

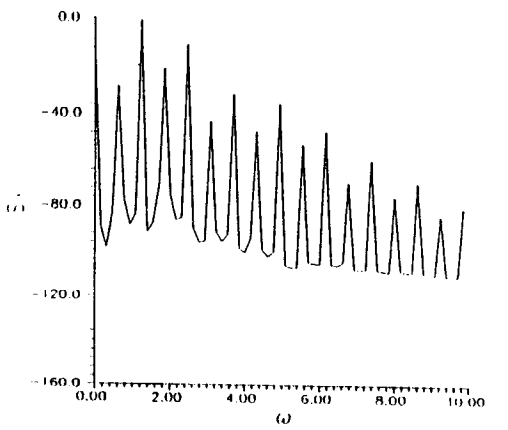

Fig.27 Period quadrupling in a system subject to nonlinear drag excitation:

a) ω=0.92 (n/m=1/4), b) ω=2.33 (n/m=1/4)

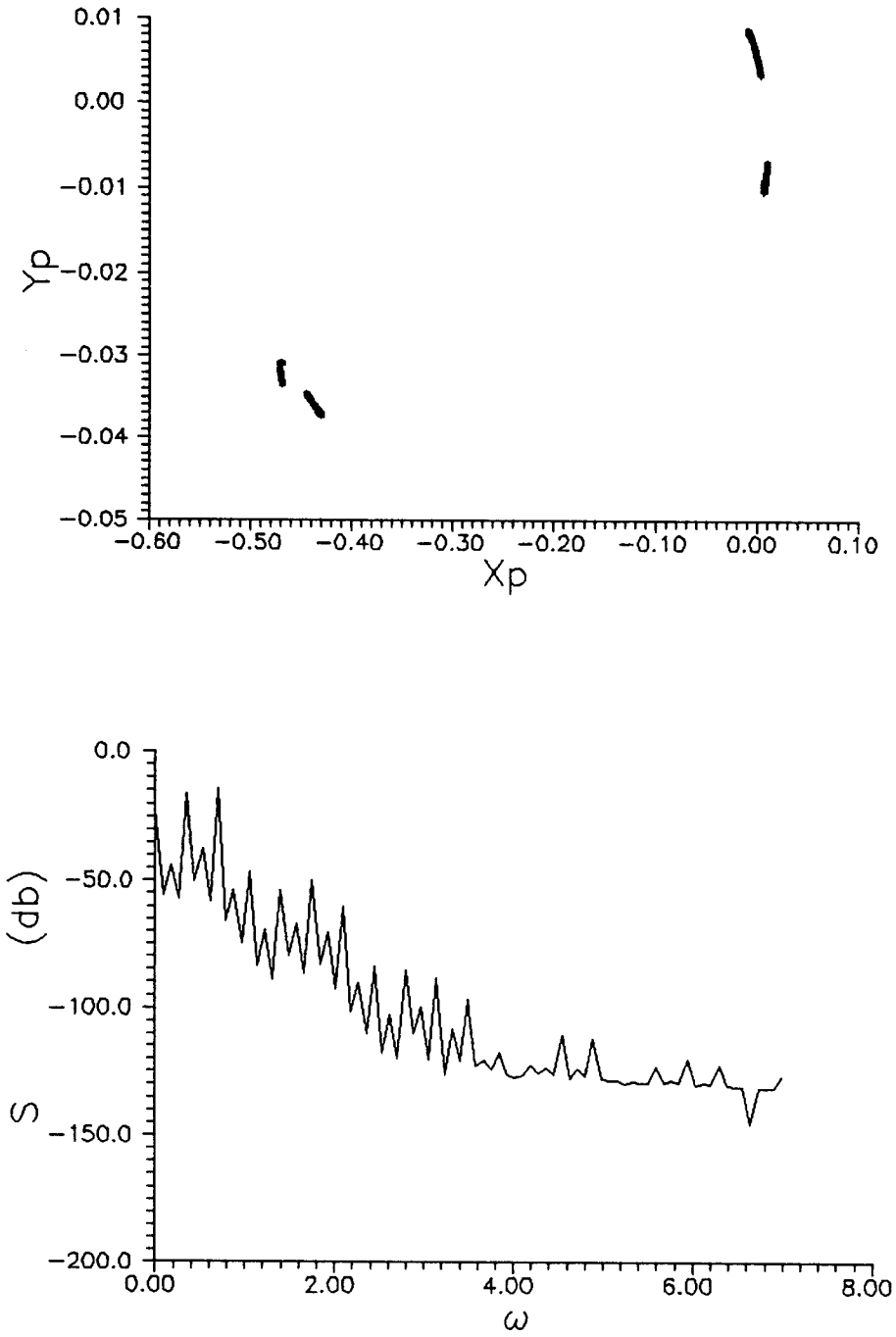

Fig.28 Chaotic attractor in a system subject to nonlinear drag excitation (ω=2.41)

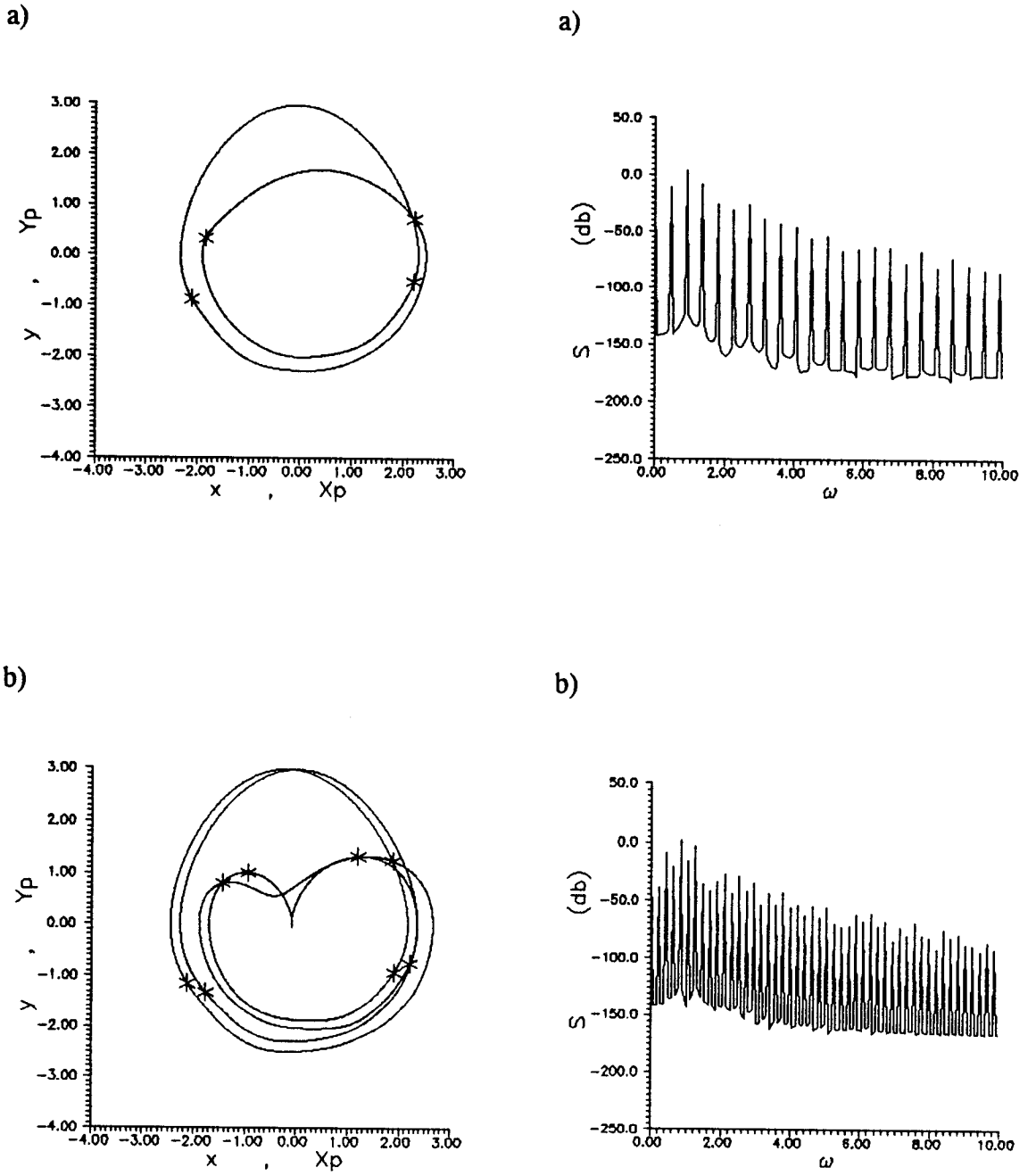

Fig.29 Period doubling cascade in a linearized system subject to nonlinear drag and convective excitation: a) $\omega=1.70$ (n/m=1/4), b) $\omega=1.68$ (n/m=1/8)

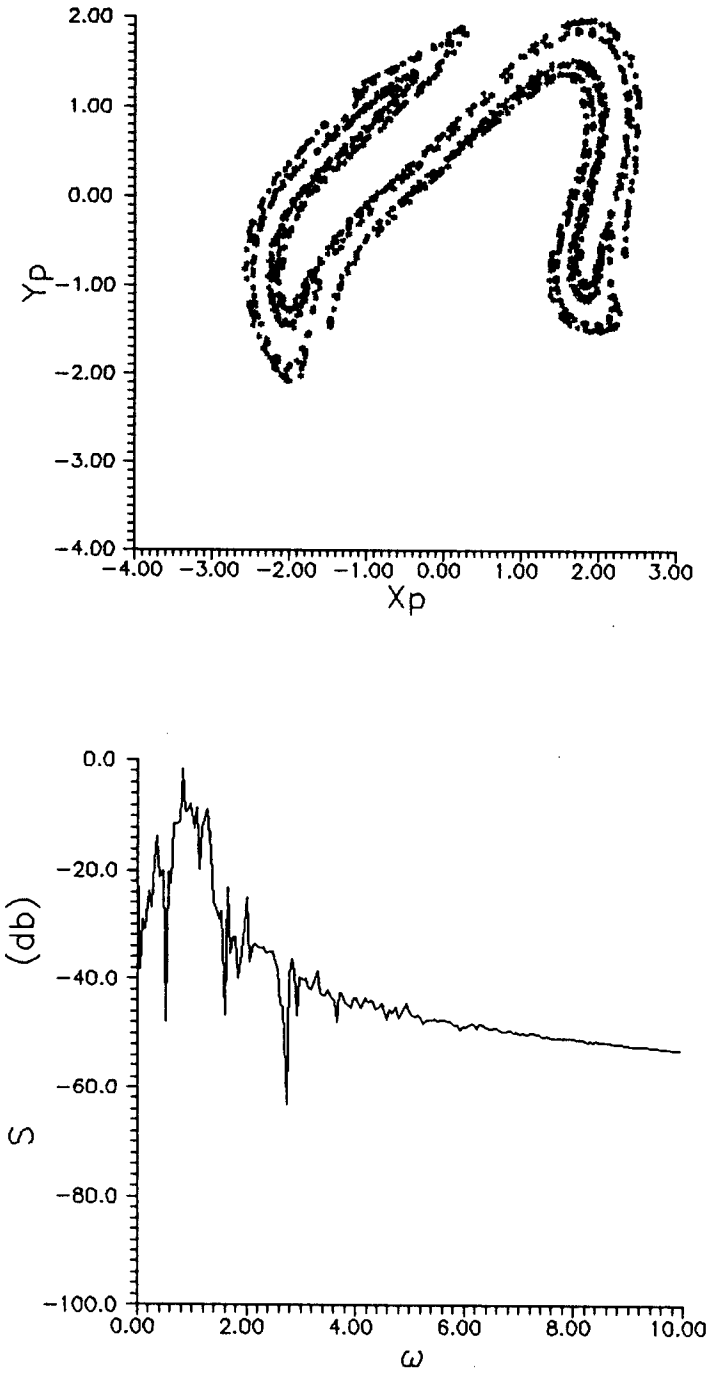

Fig.30 Chaotic attractor in a linearized system subject to nonlinear drag and convective excitation (ω=1.65)

5.3 Crisis and Transitions Between Coexisting States

Numerical investigation of the transition states near the predicted tangent subharmonic and ultrasubharmonic bifurcations (Eqn.79) reveals lengthy transient solutions and sensitivity to initial conditions associated with the abrupt change from neighboring periodic motions (e.g. Grebogi et al., 1983). This phenomena is associated with contraction of a subharmonic attractor in phase space before settling to 2π periodic motion (Fig.31: n/m=1/3). Note that the contraction is depicted by a sharp decrease in the size of the attractor. The sharp transition to and from neighboring states is accompanied by lengthy transients which are sensitive to initial conditions (Fig.32). The transients can last for a long duration before converging to one of the coexisting solutions (Fig.31: n/m=1/3). The Poincaré section (Figs.32a: N_P,X_P) and map (Fig.33b: X_P,Y_P) was found to be sensitive to initial conditions and did not remain constant under various parameter conditions. Although this structure is not portrayed by a steady state fractal dimension characteristic of a strange attractor, positive Liapunov exponents (Wolf et al., 1985) calculated from both time series (x(t)) and Poincaré section ($X_P(N_P)$) reveal the erratic behavior of the response. Furthermore, when a unique solution exists for certain values in parameter space, the transients evolve to a chaotic attractor (Fig.33). This attractor appears suddenly and has a limited domain of existence in parameter space. Note that although both transient and "explosive" steady state chaotic phenomena are associated with the tangent bifurcations, Melnikov's method cannot be applied due to the lack of explicit homoclinicty in the ultrasubharmonic system (Eqns.73-76).

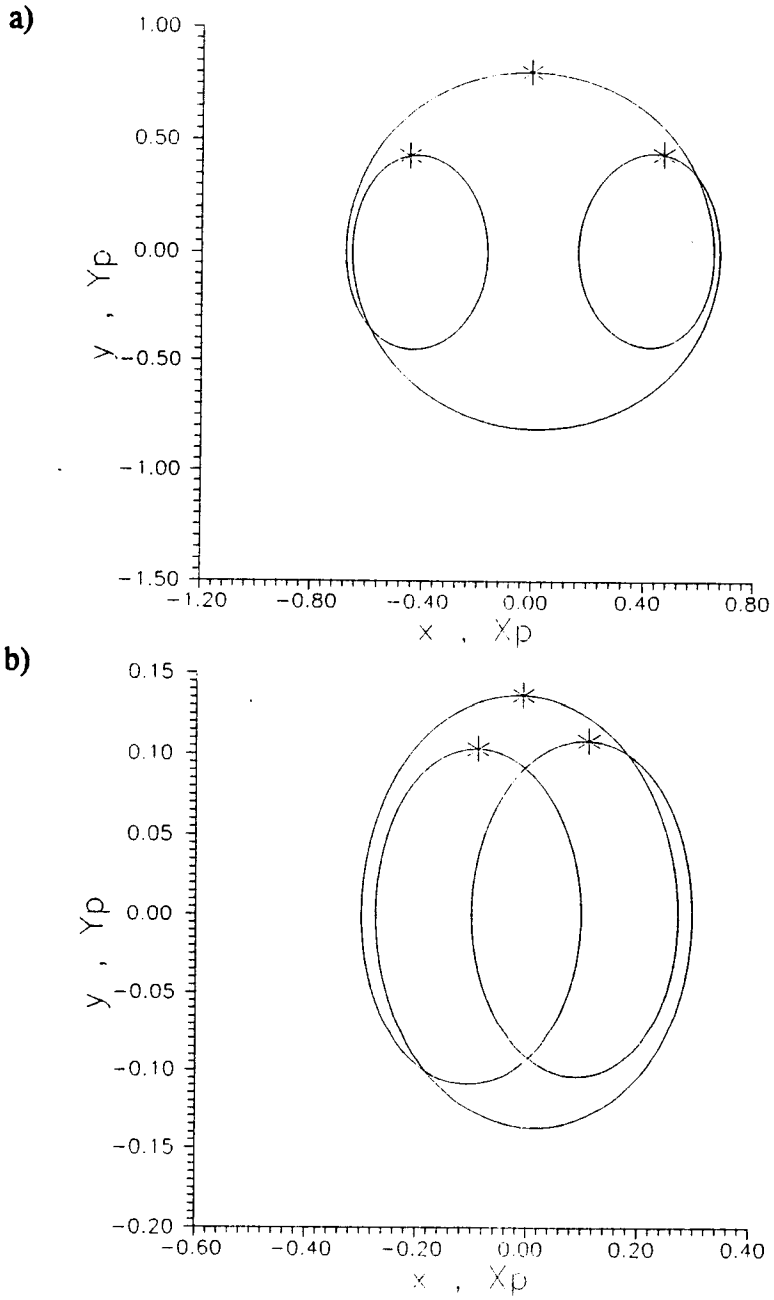

Fig.31 Contraction of ultrasubharmonics (n/m=7/3): a) ω=0.47, b) ω=0.32

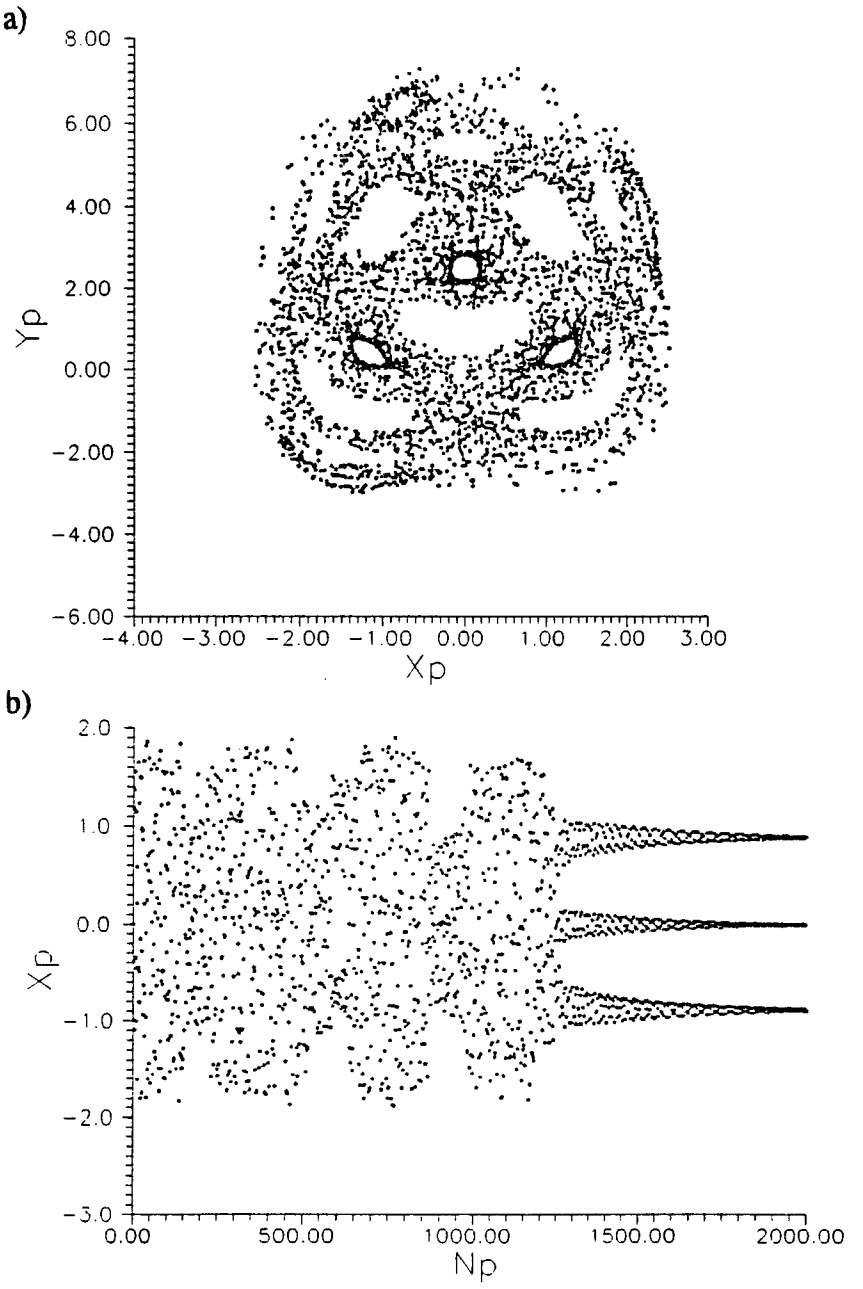

Fig.32 Transient chaotic response in the subharmonic domain (n/m=1/3):

a) Poincaré map, b) Poincaré section

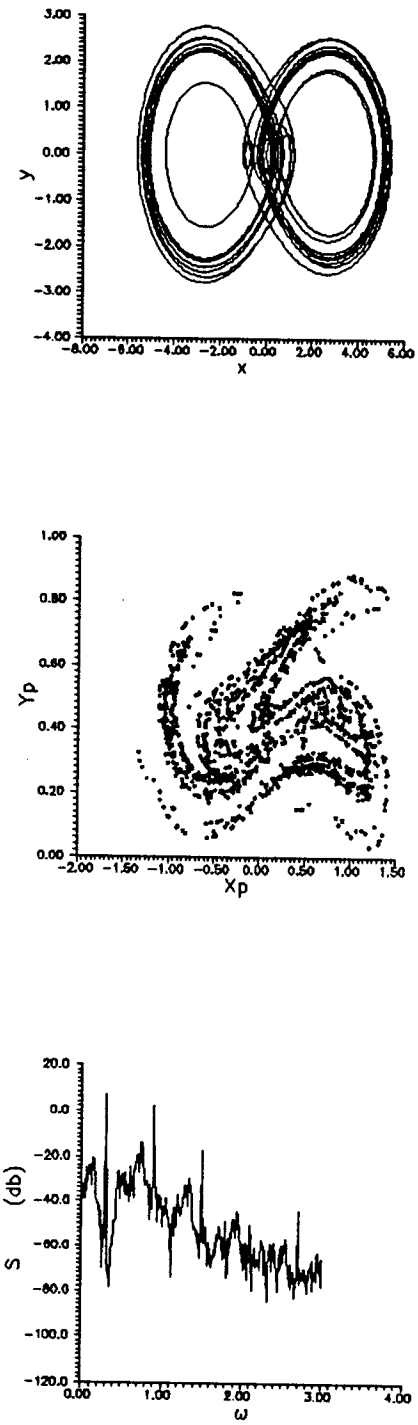

Fig.33 Chaotic attractor in an ultrasubharmonic domain (ω=0.33, n/m=7/3)

6. SUPERSTRUCTURE IN THE BIFURCATION SET AND ROUTES TO CHAOS

Analysis of the bifurcation criteria obtained reveals a periodic recurrence of a fine structure, or superstructure in the bifurcation set (e.g. Parlitz & Lauterborn, 1985). This structure identifies a similar bifurcation pattern of coexisting solutions in the subharmonic, ultraharmonic and ultrasubharmonic domains. Within this structure strange attractors appear when a period doubling bifurcation sequence is infinite (Feigenbaum, 1980) and when an abrupt change in the size of a unique attractor (Ueda, 1981) occurs near a tangent bifurcation value. The superstructure is closely related with the nonlinear resonances of the system and enables identification of routes to chaos and their relationship with other instabilities for given environmental conditions.

6.1 Identification of a Superstructure

Identification of a superstructure in the bifurcation set of a nonlinear system enables a comprehensive overview of its behavior. While a large number of dynamical systems exhibit at first glance a nonlinear structure similar to that of one dimensional maps (e.g. Simoyi et al., 1982), detailed numerical analysis of continuous dynamical systems reveals that at least a codimension two bifurcation analysis is needed to adequately describe nonlinear system behavior. In particular, stable coexisting attractors typical of nonlinear systems (e.g. Figs.8,20) cannot be explained by an equivalent one dimensional map in which at most one stable orbit exists for a given parameter set.

Furthermore, Holmes and Whitley (1984), revealed that the bifurcation sequence for periodic orbits of two dimensional families is quite different than that of one dimensional maps. They demonstrated that although local tangent and period doubling bifurcations behave similarly in one and two dimensional maps, global bifurcations, in which homoclinic cycles are created, dominate the bifurcation set of the two dimensional map. Parlitz and Lauterborn (1985) demonstrated numerically the existence of a superstructure in the bifurcation set of a single well potential Duffing equation. They related their findings to ultraharmonic (n/m=n/1) and ultrasubharmonic (n/m=n/3) resonant properties of the system and conjectured that the superstructure is universal to a large class of forced nonlinear oscillators. Recently, Ueda et al. (1990) demonstrated global bifurcations organizing behavior of the double well potential Duffing equation. By numerically investigating the fractal basin boundary bifurcations (Grebogi et al., 1987; Thompson and Soliman, 1990) of their system (n/m=1/1,1/3), they determine generic codimension two patterns and also conjecture similar behavior in forced dissipative systems.

Investigation of the tangent bifurcation criteria (Eqns.79,103) in parameter space [α=1, β:(0,1), τ=½$\sqrt{}$(1+β^2), $\gamma<\delta$=0.1, μf, ω] reveals a similar bifurcation pattern for subharmonic, ultraharmonic and ultrasubharmonic near resonant solutions (Fig.34). The pattern consists of intersecting "resonance horns" that portray asymptotic behavior for large excitation (μf). Intersecting resonance lines (tangent and homoclinic bifurcations) describing coexisting solutions were also derived for the Hénon map by a number of investigators (e.g. Holmes and Whitley, 1984). Note that bifurcations of

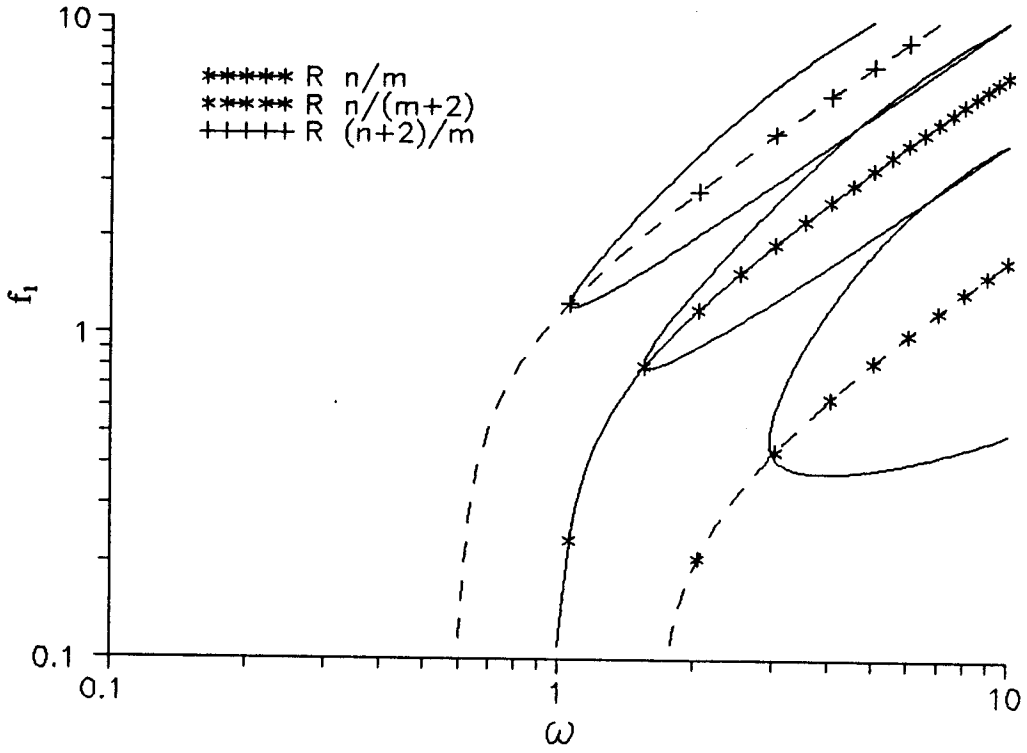

Fig.34 Superstructure in the bifurcation set

equivalent periodic families (e.g. n/m=n/3) intersect and posses the same slope. The width of the horn was found to be governed by the relative damping ratio ($\gamma^* \propto \gamma/\delta$). Thus a control space defined by parameters describing a nondimensional relationship between excitation and structural parameters (μf, ω/ω_0 where $\omega_0=\omega_0(\alpha,\beta)$, γ/δ) was derived. Note that the codimension two bifurcations of Ueda (1980) and Ueda et al. (1990) are defined in parameter space by damping versus excitation amplitude whereas Parlitz and Lauterborn (1985) describe their ultraharmonic resonances in terms of excitation amplitude versus frequency.

Classification of the bifurcations defining the superstructure is typically done by a describing bifurcation number. Holmes and Whitley (1984) extend the conventions of one dimensional maps in their analysis of the two dimensional Hénon map [i.e. s_m^j where index m is the period determined by Sarkovski's theorem (e.g. Devaney, 1986) and j is the order of appearance calculated by kneading theory (e.g. Guckenheimer and Holmes, 1986)]. Ueda et al. (1990) define suffices describing the periodicity (m) and an arbitrary index to distinguish between types of solutions whereas Parlitz and Lauterborn (1985) define an ultraharmonic index (i.e. number of maximum periodic solutions in one forcing period) complemented by periodicity index to define ultrasubharmonics.

In order to classify the bifurcation pattern of subharmonic, ultraharmonic and ultrasubharmonic solutions, the nonlinear resonance relationship $n\omega \approx m\sqrt{\alpha_1}$ is utilized to determine the first index [*n/m*], of the resonance number. Recall (chapter 3) that the ratio n/m (i.e. an inverse one dimensional winding number) is a relatively prime

integer. Consequently a second index [*j*], is required to determine the order of ratios with non-common factors. Note that m denotes periodicity of the response and an irrational value for n/m defines aperiodic solutions (i.e. quasi-periodic). Finally, a third index is required to determine the dimension [*d*] of the response (i.e. integer deterministic versus fractal chaotic). Note that the fractal dimension may not by itself establish the chaotic nature of the motion (e.g. when it is close to an integer value) and a multi-fractal representation (Feder, 1989) is needed to quantify strangeness of systems with two or more degrees-of-freedom [e.g. the quasi-periodic response of an experimental attractor for thermal convection (Jensen et al., 1985)]. Thus, a resonance number $R_{(n/m,\,j,\,d)}$ describing a repeating global bifurcation pattern is defined. Note that the indices of this number are consistent with the semi-analytical local and global tangent bifurcation criteria derived previously (Eqns.72,79,103,105).

The following table is constructed to display the complex superstructure in the bifurcation set. The superstructure enables identification of coexisting solutions and pitchfork or period doubling bifurcations. The table displays the index of the fundamental resonant structure [*n/m*] followed by the index of ordering [*j*]. Note that the upper row and the first column describe the ultra [*n*] and sub [*m*] indices respectively. The index [*j*] identifies the order of equal ratios [e.g. (n/m,j)= (1/2,1) at (column,row)=(1,2) versus (n/m,j)= (1/2,2) at (column,row)=(2,4)]. Thus, the table diagonal divides between the ultraharmonic and subharmonic domains. Coexistence found by local analysis [e.g. Fig.20b (n/m=1/2) and Fig.20d (n/m=3/5)], can be determined by resonance numbers $R_{(n/m,\,j)}$ with similar n/m ratios (e.g. $R_{1/2,1}$ and $R_{3/5,1}$).

Table 1: Order of superstructure in the bifurcation set

$R_{n/m}$	1	2	3	4		n
1	1/1,1	2/1,1	3/1,1	4/1,1		n/1,j
2	1/2,1	1/1,2	3/2,1	2/1,2		n/2,j
3	1/3,1	2/3,1	1/1,3	4/3,1		n/3,j
4	1/4,1	1/2,2	3/4,1	1/1,4		n/4,j
m	1/m,j	2/m,j	3/m,j	4/m,j		1/1,j

Note that ultraharmonic solutions described by an even descriptor (n or m) are unsymmetric [e.g. Fig.12a (n/m=4/5), Fig.17b (n/m=1/2)] whereas odd descriptors describe symmetric or self-similar solutions [e.g. Fig.12c (n/m=3/5)].

The pitchfork bifurcation (Eqn.108, Figs.15b) describes stability loss of a symmetric solution (e.g. Fig.16a) and its evolution in parameter space to two partner orbits (e.g. Fig.19a,b). This bifurcation is described by the ordering index j:1,2 for n/m=2/1 (e.g. $R_{2/1,1} \rightarrow R_{2/1,2}$) in the ultraharmonic domain. Similarly, the period doubling bifurcation (Eqn.107 and Figs.15a,17) is described by the ordering index in the subharmonic domain j:1,2 for n/m=1/2 (e.g. $R_{1/2,1} \rightarrow R_{1/2,2}$). Note that period doubling in the ultraharmonic domain (e.g. Fig.18) is described by j:2,3 for n/m=2/1 (e.g. $R_{2/1,2} \rightarrow R_{2/1,3}$).

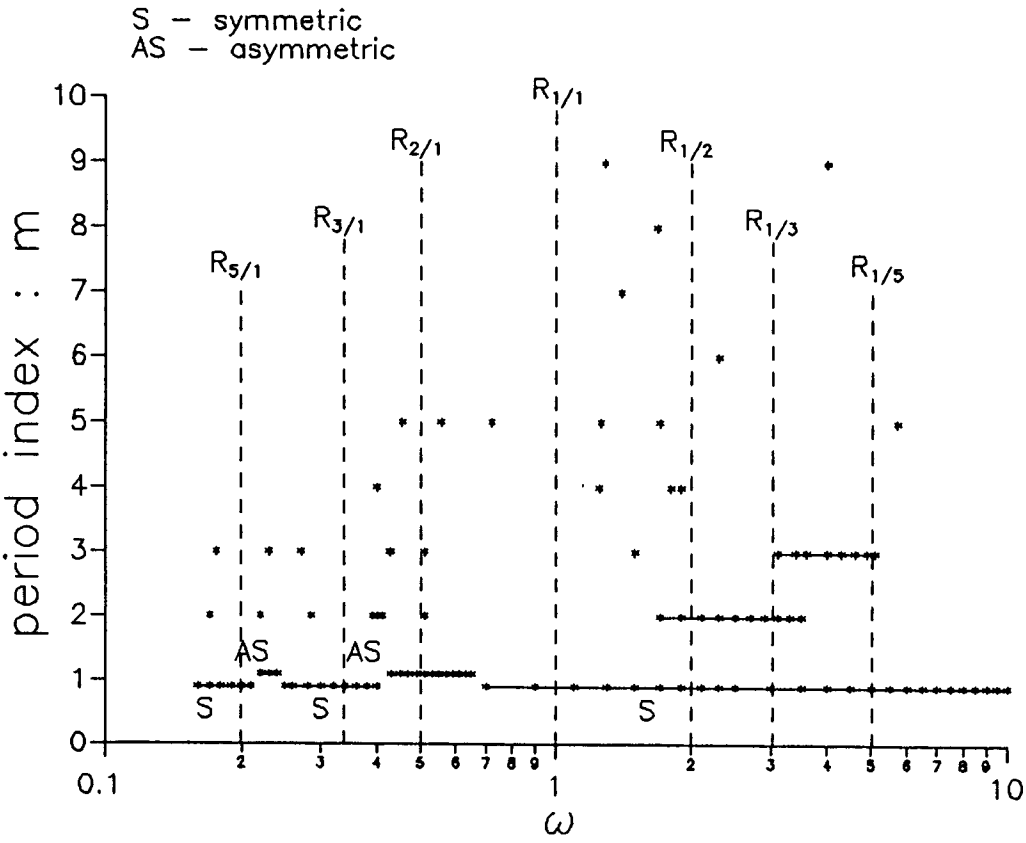

Fig.35 Schematic bifurcation diagram

Numerical simulations of system response enable construction of the following schematic bifurcation diagram (Fig.35). The simulations consist of changing one control (ω) for a given parameter space under various sets of initial conditions. The diagram depicts existence of periodic orbits throughout the domain described by a variety of subharmonic and ultrasubharmonic solutions. Solutions are separated by a common periodicity index m. Symmetric (S) and asymmetric (AS) solutions (n/m=n/1) describing pitchfork bifurcation transitions are also depicted. For convenience, resonance lines ($R_{n/m}$: dashed lines) are added to highlight solution ordering. An example is the $R_{7/3,1}$ ultra-subharmonic response (Fig.35: $\omega \simeq 4$, n/m=7/3) found between the resonance lines of $R_{3/1}$ and $R_{2/1}$. While not all of the ultrasubharmonics predicted by the resonance number ordering were found, the dominant harmonic and lower order subharmonic and ultrasubharmonic solutions were found to be accurately described. Note that in order to obtain the complete nonlinear steady state response, fractal basin boundaries describing all possible initial conditions need to be considered.

6.2 Routes to Chaotic Response

Two routes to chaotic response describe the evolution of a strange attractor defined in chapter 5. These routes can be described by evolution of unsymmetric and symmetric solutions as is evident by the spectral content of the pre-chaotic and post-chaotic motions.

The first route is a smooth and continuous period multiplying route. This route

includes period doubling (Figs.23,29,30) and can be trace in the superstructure by the ordering index j:2,4,8...(e.g. $R_{1/2,1} \rightarrow R_{1/2,2} \rightarrow R_{1/2,4} \rightarrow R_{1/2,8}$). Similarly, a period tripling route is identified j:3,9 (e.g. $R_{1/3,1} \rightarrow R_{1/3,2}$ ...) and verified numerically (Fig.36). The period doubling and tripling routes to chaotic motion is are observed with the appearance of additional even (Fig.37) and odd (Fig.36) harmonics respectively. Consequently, the period multiplying scenario describes an accumulation of internal resonance horns in the bifurcation set. Note that when the multiplying sequence is infinite the dimension index [d], describing the number of systems degrees-of-freedom, does not retain its integer value and is replaced by a characteristic fractal dimension (i.e. $R_{\cdot 1/2\cdot,\infty,\cdot 2.31\cdot}$, Fig.37c).

Another route to chaotic motion is observed in the abrupt change to and from neighboring periodic motions (e.g. $R_{1/1,1} \rightarrow R_{1/3,1}$). This occurs near the local tangent bifurcation values and as described previously, is associated with contraction of the $2m\pi/n$ ultrasubharmonic. This route is short lived in parameter space and culminates to a strange attractor when a "collision" occurs between two neighboring attractors separated by a saddle (i.e. bifurcation defined as a hetroclinic tangency). Consequently, strange attractors were found for odd (m and n odd) self-similar subharmonic (e.g. $R_{\cdot 1/3\cdot,\infty,\cdot 2.57\cdot}$, Fig.38b) and ultrasubharmonic (e.g. $R_{\cdot 7/3\cdot,1,\cdot 2.63\cdot}$, Fig.33) scenarios while even (m or n even) ultrasubharmonic scenarios of unsymmetric solutions were portrayed only by transient chaotic behavior.

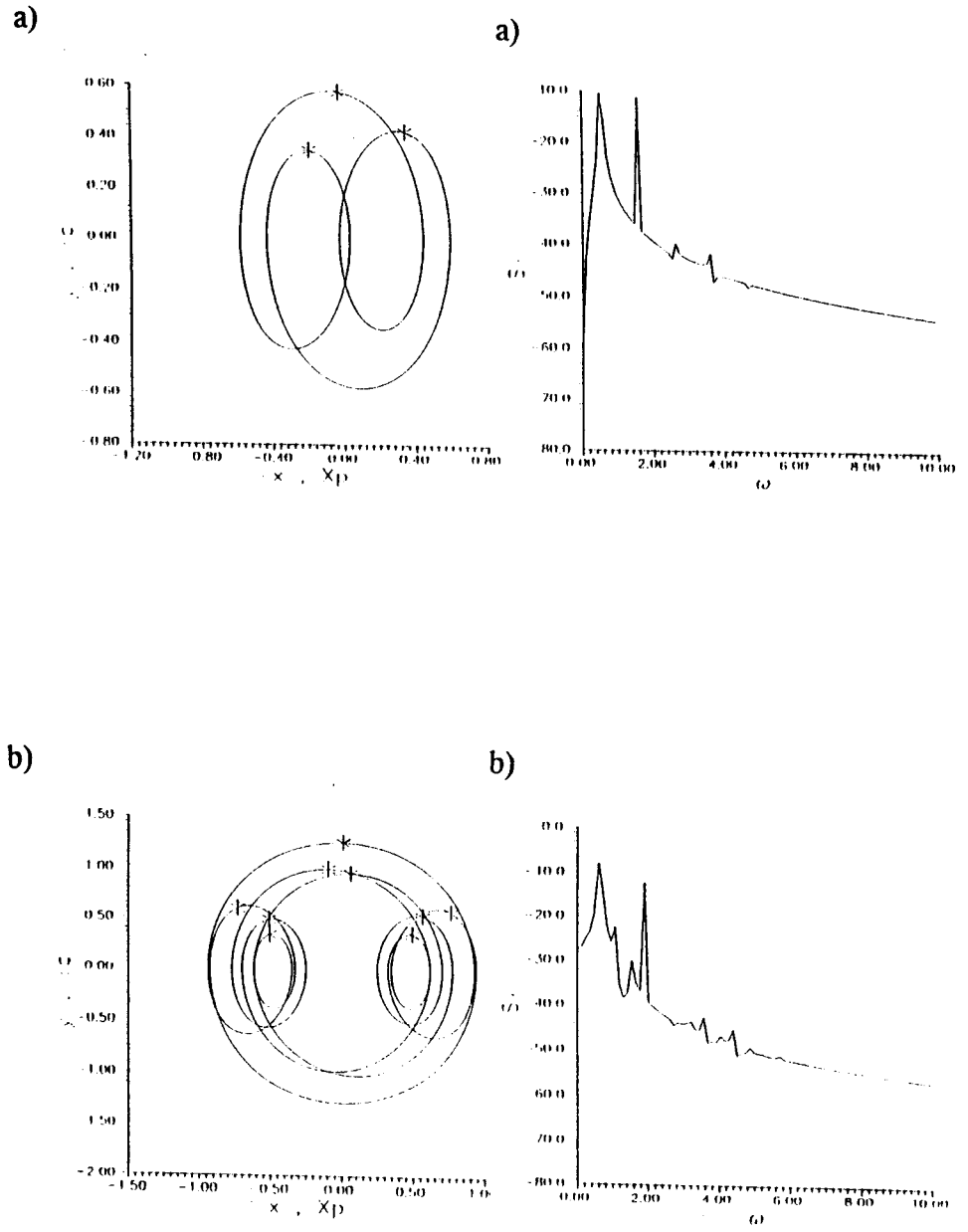

Fig.36 Period tripling: a) $\omega=1.62$ (n/m,j)=(1/3,1), b) $\omega=1.87$ (n/m,j)=(1/3,2)

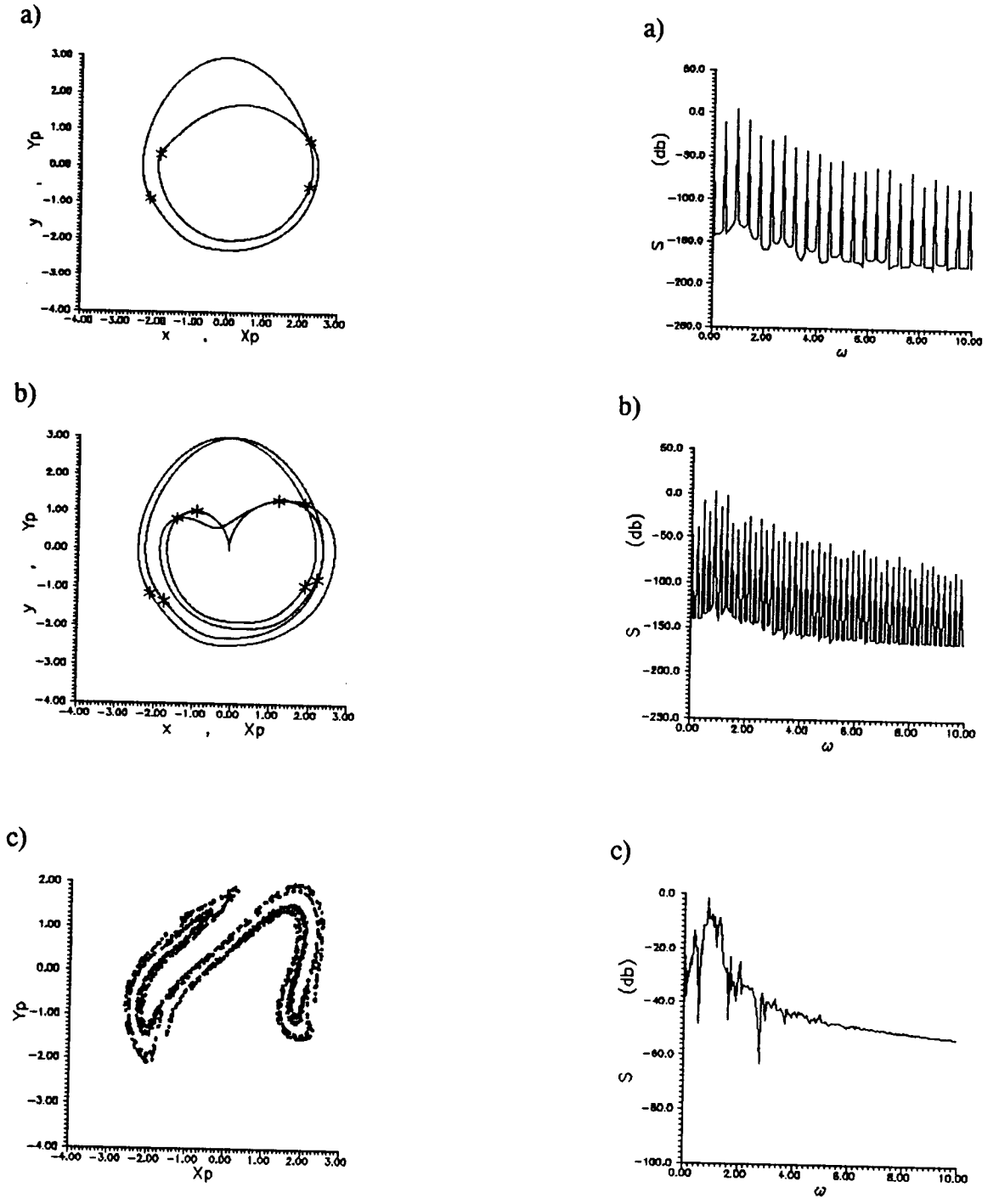

Fig.37 Evolution of a chaotic attractor via period doubling: a) $\omega=1.7$ (n/m,j=1/2,2), b) $\omega=1.68$ (n/m,j=1/2,4), c) $\omega=1.65$ (n/m,j="1/2",∞)

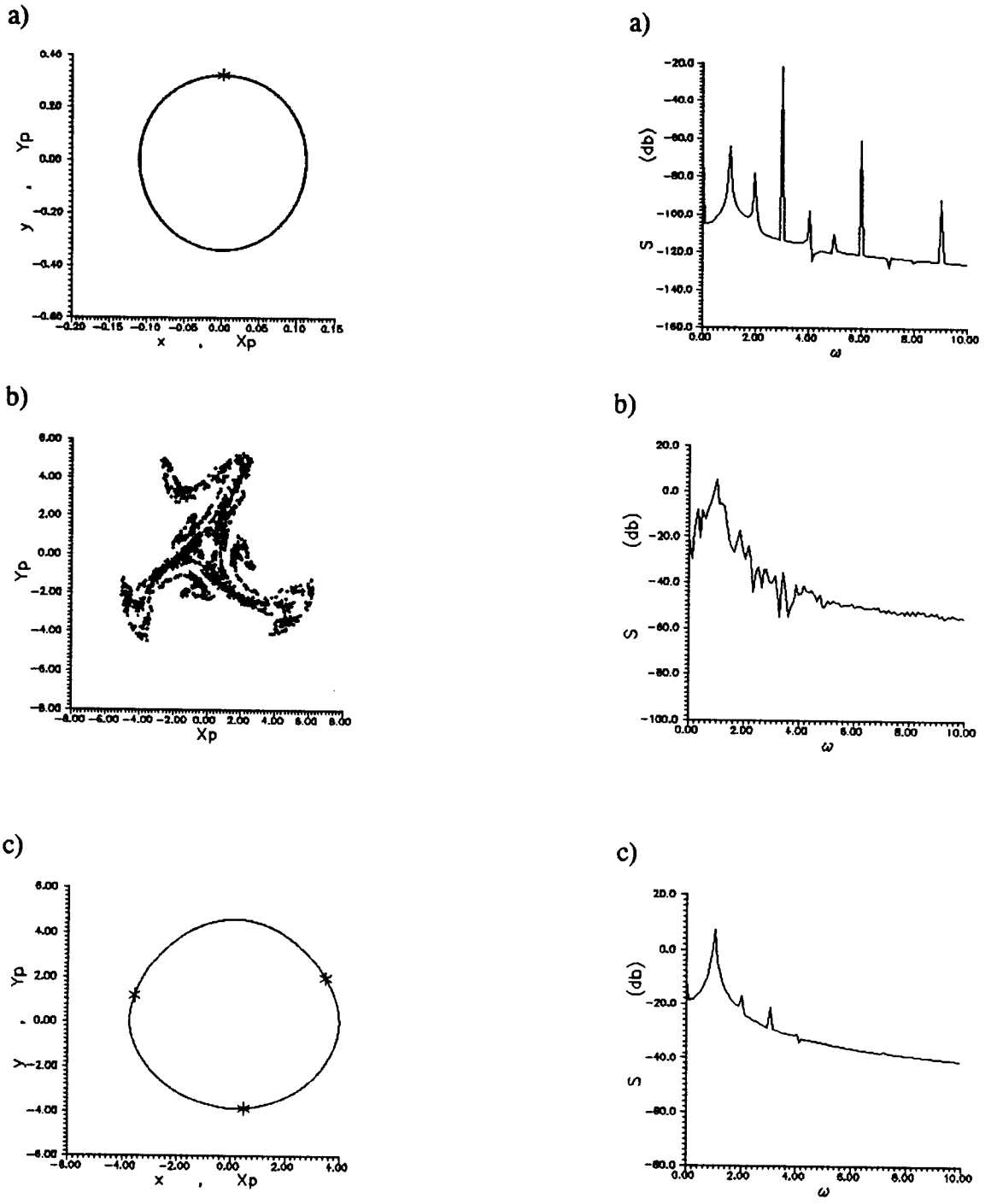

Fig.38 Evolution of a chaotic attractor via an explosion: a) ω=3.05 (n=m=1), b) ω=3.10 (n/m,j="1/3","1"), c) ω=3.15 (n/m,j=1/3,1,2)

6.3 Parametric Control of System Instabilities

Investigation of the controlling mechanisms for the local and global bifurcations identified in the previous chapters for the single degree of freedom system (Eqn.19) was performed by numerical investigation of the parameter set near the bifurcation values. Period doubling was found to be sensitive to the magnitude of the drag induced bias $[\mu\delta(f_0^2+\frac{1}{2}f_1^2)]$ for weak excitation whereas the instabilities generated by the convective terms governing combined parametric $[\mu\omega^2\kappa(1+f_0)f_1]$ and external $[\mu\omega^2(1+\kappa^2)f_1]$ excitation dominate system behavior for larger excitation. Comparison of results to system response in which the drag nonlinearity was equivalently linearized (resulting in linear damping and a change in excitation phase) does not reveal the bias induced instabilities. Note that the bias is a function of both current or waves. Consequently, equivalent linearization of the hydrodynamic drag force will not account for even subharmonic or ultrasubharmonic instabilities. Furthermore, local period doubling and subharmonic tangent instabilities were found in a linearized ($\beta>>1$ or $\alpha_{1>1}=0$) mooring configuration (Eqns.80,110). These instabilities exist in limited parameter space (Fig.9) and were not found to be sensitive to initial conditions.

The symmetric and unsymmetric solutions are usually associated with symmetric and unsymmetric system nonlinearities (Szemplinska-Stupnika, 1987) which are found in both drag and inertial components of the exciting force. However, combined parametric and external excitation exhibit chaotic subharmonic dynamics due to tangent bifurcations in a system with a quadratic nonlinearity (Holmes, 1980) and generate

period doubling bifurcations in a system with a symmetric nonlinearity (HaQuang et al., 1987). Investigation of parameters influencing the instabilities of the system show that the period doubling route to chaos is sensitive to the magnitude of the inertial force whereas the tangent route is controlled by the relationship between the restoring force and both drag and inertial components of the exciting force. The system with the linearized restoring force was found to be dominated by the inertial force which controls both tangent and period doubling routes to chaotic motion.

The influence of coupling of degrees of freedom was done by numerical simulation of the two degree of freedom system (Eqn.12). Recall that the coupling appeared in the restoring forces [$l_{1,2} \propto \sqrt{(x_1^2+x_3^2)}$] and exciting forces due to the hydrodynamic velocity potential [$u_{1,3} \propto u_{1,3}(\exp(\pm x_3),\cos(\kappa x_1-\theta)$]. Furthermore, system reduction to a single degree of freedom system by employing symmetry conditions ($\sigma=0$) enabled identification of fundamental nonlinearities in a limiting single degree of freedom system (Eqn.19). Therefore, investigation of degree-of-freedom coupling was first performed on the taut strongly nonlinear ($\alpha=1$, $\beta=0$, $\tau=1$) neutrally buoyant ($\sigma=0$, $\mu_1=1$) symmetric ($\gamma_1=\gamma_3$) system where symmetry of the exciting field ($f_0=0$) was maintained by choice of identical values for the hydrodynamic coefficients ($\delta_1=\delta_3,\mu_1=\mu_3$). Note that the system described has identical natural frequencies in both surge and heave directions. Results of analysis near the critical bifurcation values of the single-degree-of-freedom system reveal similar behavior to that of the limiting system including the transition to a chaotic attractor [Fig.39: a) Eqn.19, b) Eqn.12]. Note that although the superstructure in the bifurcation set did not change, the instability regions

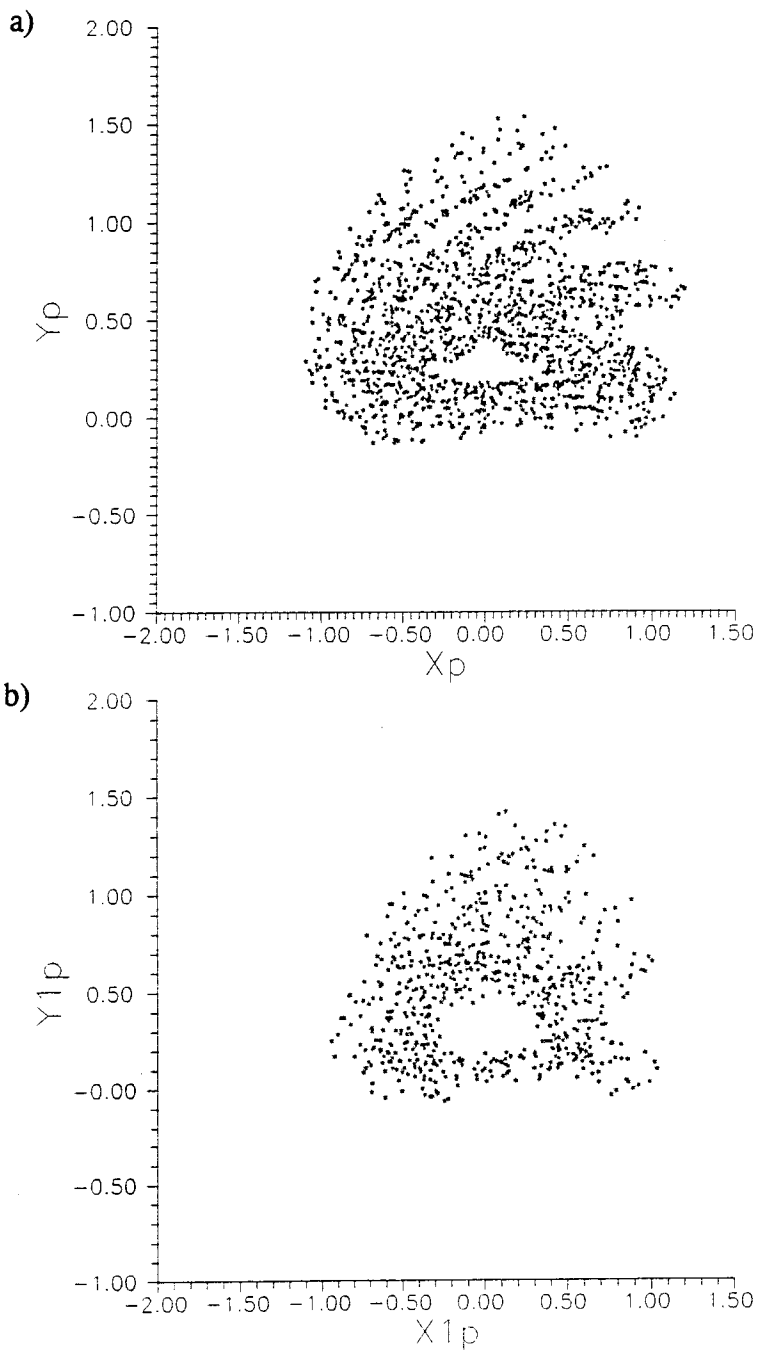

Fig.39 Comparison of chaotic attractors (ω=0.81): a) single-degree-of-freedom system (Eqn.19), b) two-degree-of-freedom system (Eqn.12).

widened as a direct consequence of the coupling and quasiperiodic solutions were discovered for a large parameter space (Fig.40). This phenomena can be viewed as additional parametric excitation to the system. Investigation of system response governed by a nonsymmetric parameter set reveals additional bifurcations associated with the two internal resonant mechanisms as the natural frequencies for heave and surge differ for a buoyant system ($\sigma \neq 0$). Furthermore, doubling of the quasiperiodic motion was also observed for a limited parameter space (Figs.41,42).

Thus, the superstructure of the bifurcation set is further complicated and requires additional nondimensional values to completely define parameter space [μf, ω/ω_1, ω_1/ω_3 where $\omega_1=\omega_1(\alpha,\beta)$, $\omega_3=\omega_3(\alpha,\beta,\sigma)$, $\gamma_{1,3}/\delta_{1,3}$]. The complexity can be shown in a displacement diagram depicting heave (x_3) versus surge (x_1) for periodic and aperiodic motions (Fig.43).

The mechanisms governing system instabilities and the onset of transient and steady state chaotic response have been identified via the superstructure in the bifurcation set which is constructed by a nonlinear resonance (tangent bifurcation) formulation of the fundamental single-degree-of-freedom system. Analysis of coupling of the degrees of freedom reveals existence of quasiperiodic motions within the resonant superstructure. Consequently, control of system instabilities including competing coexisting solutions and the onset of chaotic response, is achieved by enforcing a change in parameter space. Two examples are an increase in structural damping (γ) governing the relative damping parameter for control of small amplitude period doubling instabilities and a combination of damping (γ) and mooring (α,β,τ) behavior in order

to control the influences of combined parametric and external excitation and further coupling in the two-degree-of-freedom system. The former example can be viewed as a problem governed by an additive controller whereas the latter example requires a control policy combining additive and multiplicative control variables.

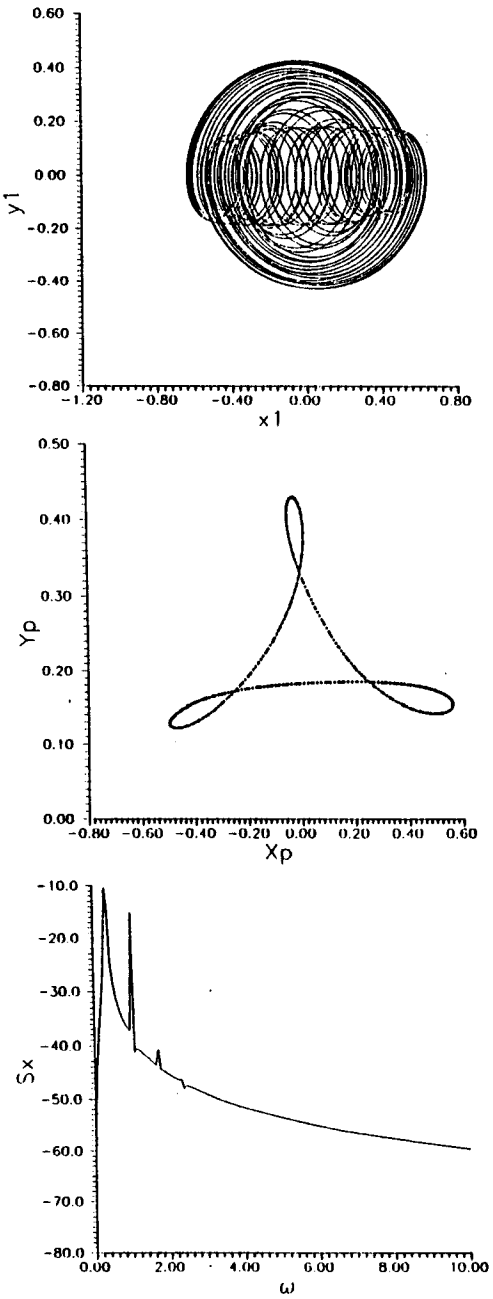

Fig.40 Quasiperiodic period tripling [ω=1.01 (n/m,j)$\approx$("1/3",1)]

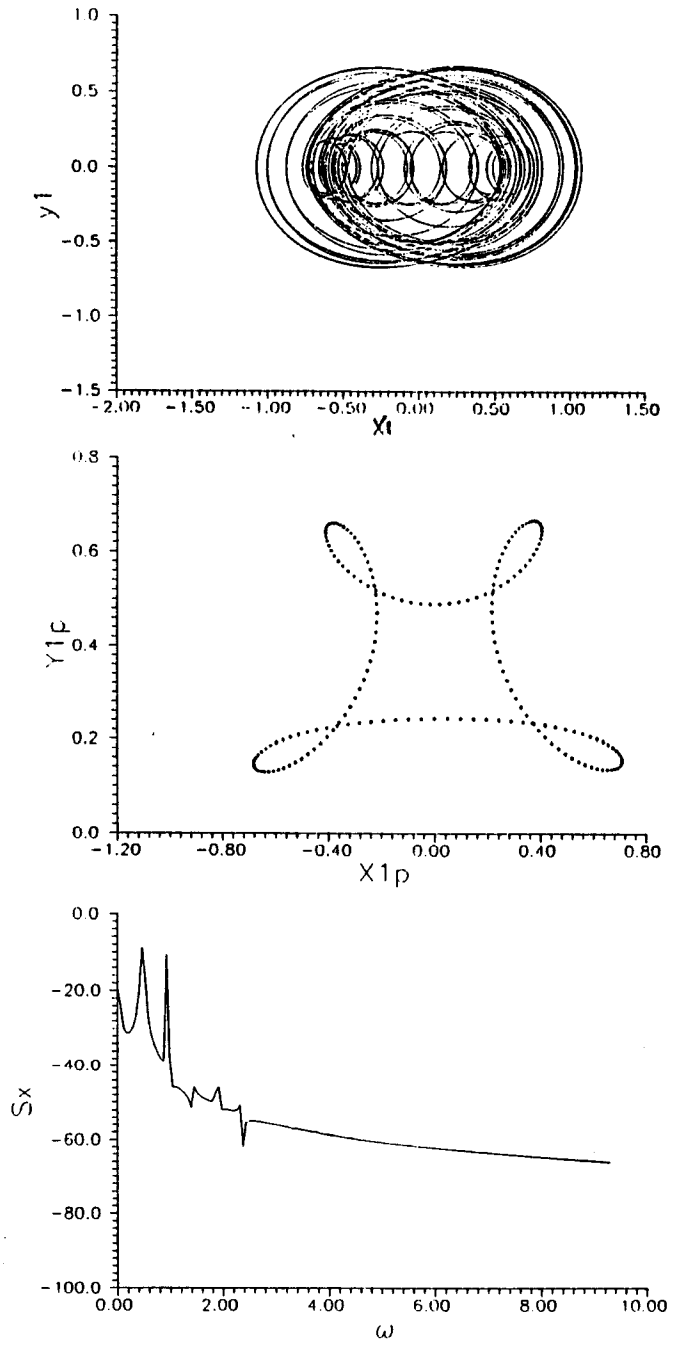

Fig.41 Quasiperiodic period doubling [ω=0.87 (n/m,j)$\approx$("1/2",1)]

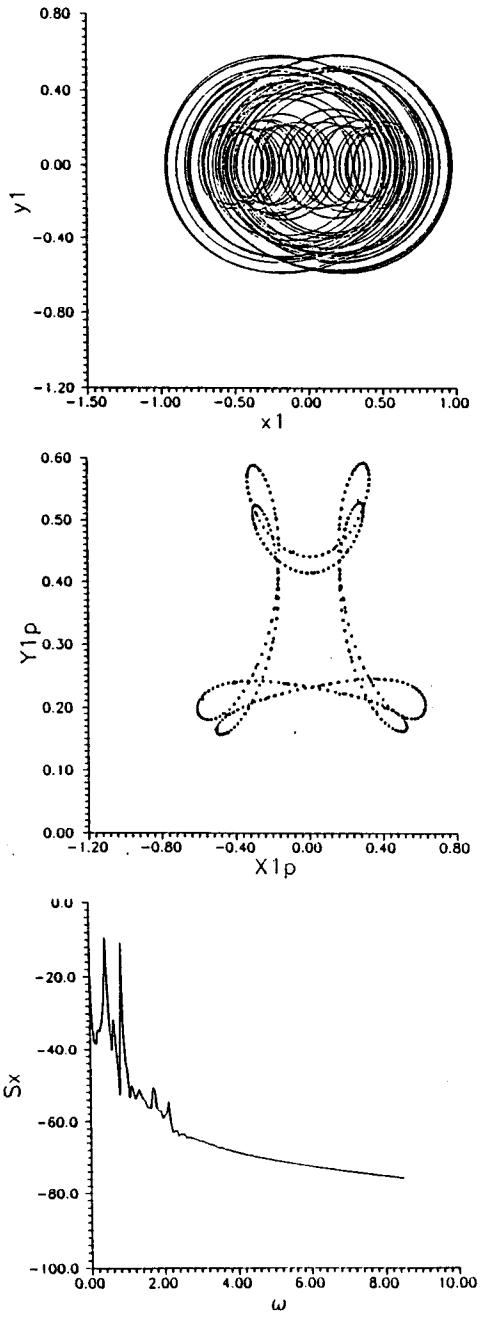

Fig.42. Quasiperiodic period quadrupling [ω=0.85 (n/m,j)$\approx$("1/2",2)]

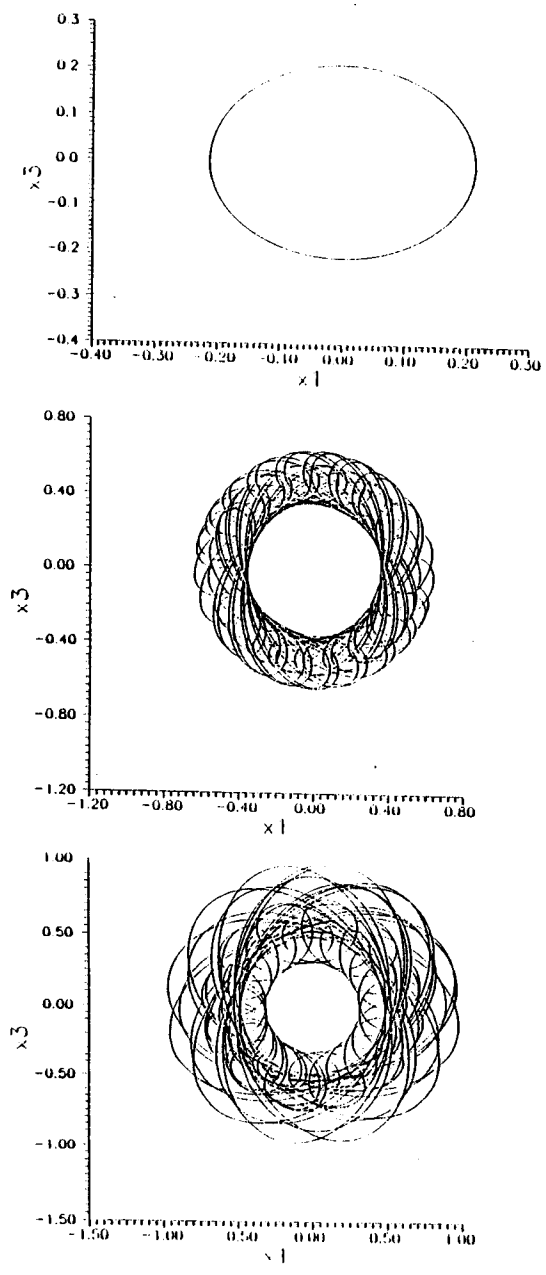

Fig.43 Displacement diagram: quasiperiodic heave vs. surge: a) $\omega=0.7$ (n=m=1), b) $\omega=1.01$ (n/m,j)≈("1/3",1), c) $\omega=0.85$ (n/m,j)≈("1/2",2)

7. CONCLUSIONS AND FUTURE RESEARCH

This final chapter includes a summary, observations and conclusions obtained from the study. The potential applications of the study are in the analysis, design and control of nonlinear ocean mooring and towing systems and of equivalent mechanical systems subjected to similar environmental conditions. This study provides a basis for comparison and guidelines for future research of nonlinear ocean systems.

7.1 Summary

Complex nonlinear periodic and aperiodic phenomena are predicted and investigated by semi-analytical methods in a general class of ocean mooring system models. The models describe systems that are characterized by a nonlinear restoring force and a coupled fluid-structure interaction exciting force. The restoring force consists of a single well potential and classifies the system as one belonging to a class of degenerate bifurcation problems. The environmental nonlinearites include coupled hydrodynamic viscous drag and convective inertial wave components. Coupling of the degrees of freedom further complicate the already strongly nonlinear system. The need for the study arises with the development of large motion dynamical ocean systems and the lack of consistent existing nonlinear ocean systems analysis portrayed by detailed numerical models and by simplified models where the exciting forces are approximated or in part equivalently linearized.

The overall goal of this study was to investigate ocean mooring systems by developing analytical and numerical procedures which would enable determination of existence and prediction of complex nonlinear periodic and aperiodic system behavior. This goal is obtained by formulating and investigating system models incorporating the exact form of both structural and hydrodynamic nonlinearities, as system instabilities are not always adequately described by approximate models. Furthermore, sensitivity to initial conditions or loss of predictability in system behavior, cannot be obtained in systems described by an equivalently linearized formulation.

The investigation includes development and application of local and global bifurcation techniques to the ocean system. Formulation of the system Poincaré map enables identification of transverse homoclinic orbits depicted by transient chaotic dynamics. Stability analysis of coexisting subharmonic, ultraharmonic and ultra-subharmonic solutions reveals existence of a cascade of period doubling. Analysis of the bifurcation criteria complemented by numerical simulation enables identification of a superstructure in the bifurcation set. Within this superstructure, strange attractors appear when a period doubling sequence is infinite and when an abrupt change in size of the attractor occurs. The superstructure defines routes to chaotic motion and their relationship with other instabilities for a given set of environmental conditions. Investigation of the governing nonlinear mechanisms enable identification and control of system instabilities and the onset of chaotic response.

Thus, the semi-analytical methods described in this study predict complex nonlinear periodic and aperiodic response which cannot be obtained through evaluation

of an approximate or equivalently linearized system and can significantly reduce the efforts of a numerical search in parameter space otherwise needed to complete the analysis of the strongly nonlinear system considered.

7.2 Observations and Conclusions

System model and global attraction - The choice of a symmetric nonlinear continuous small body mooring configuration subject to excitation by a deterministic linear monochromatic two dimensional field, enabled formulation of a three-degree-of-freedom system. A fundamental limiting single-degree-of-freedom oscillator was shown to characterize the multi-point mooring system as a coupled strongly nonlinear system subject to combined biased, parametric and external excitation. Stability analysis by a Liapunov function approach revealed global attraction for small excitation.

Generality of bifurcation techniques - Evaluation of system stability in the context of the Poincaré map is limited to a weakly nonlinear near resonance formulation. Analysis of the map described by a potential Hamiltonian perturbed by a damping mechanism identifies homoclinicity. The criterion for the existence of transverse homoclinic orbits is sensitive to the high frequency of the averaged system. Consequently, the estimates for the separatrix splitting of the forced system are obtained. The estimates, verified by numerical simulation, show sensitivity to initial conditions depicted by transient chaotic behavior. Note that although an analytical criterion for transverse intersections

of ultrasubharmonic resonances was not attainable, numerical simulation revealed equivalent transient behavior before settling to a strange attractor characterized by an explosion. Investigation of nonresonant solutions by a variational approach is not limited to a weak formulation and existence of a period doubling cascade was found to be a fundamental instability mechanism.

Superstructure in the bifurcation set - Investigation of the bifurcation criteria complemented by numerical simulation, reveals a steady state superstructure in the bifurcation set. A resonance number consisting of suffices describing the nonlinear content and dimension of solutions within the superstructure is derived. The superstructure enables identification of the mechanisms governing system stability and the onset of strange attractors. The controlling mechanisms are a bias governing small amplitude motion instabilities and combined parametric and external excitation governing large amplitude motion. The influence of coupling of degrees of freedom consists of additional parametric excitation widening unstable regions. Although comparison of single-degree and two-degree-of-freedom systems depict identical nonlinear phenomena, the coupling complicates the bifurcation set and quasiperiodic solutions are found coexisting in parameter space.

Importance of physical parameters - Investigation of system response semi-analytically reveals the importance of the physical parameters governing the nonlinearities.

- Mooring restoring force: defined by governing geometric nonlinearity, pretension

and buoyancy which describe a variable multiplicative control to hydrodynamic induced instabilities.

- Structural damping: linear additive control of resonant mechanisms (i.e. large amplitude ultrasubharmonics and strange attractors in their domain).
- Hydrodynamic drag force: defined by a relative motion quadratic nonlinearity that governs period doubling instabilities via a bias for small amplitude motion. Note that even a linearized mooring system is subject to drag induced instabilities which are not attainable by equivalent linearization techniques.
- Hydrodynamic inertia force: defined by second order relative motion convective nonlinearity which controls response via combined parametric excitation. Note that the convective terms cannot be neglected for large amplitude response where kinematics are evaluated at the displaced position.
- Coupling of degrees of freedom: generates parametric excitation and enhances quasiperiodic response in ultrasubharmonic regions of instability.

7.3 Future Research

In this study a variety of assumptions and choices were made in order to enable development of the analysis techniques. The following list includes topics for future investigation based on generalizing both the mooring system and the environmental field:

System - The system consists of moorings and body. Recall that selection of small body

was due to the lack of explicit formulation of the hydrodynamic exciting force and choice of a pretensioned mooring configuration was due to the need of a continuous restoring force. Consequently, two topics for research are the applicability of the fundamental results of this study to: a) Large body (e.g. diffracting) attached to the mooring assembly. Recall that extension to large body requires simultaneous solution of system and field. Therefore, an intermediate step can be selection a semi-analytical quasiperiodic formulation for the hydrodynamic exciting force. b) Moorings including material discontinuities and nonlinear elastic properties. Note that an equivalent topic is that of ocean towing as the nonlinearities are geometric and discontinuous.

Another topic of great importance is structural control of hydrodynamic induced instabilities. Investigation of structural damping mechanisms (e.g. quadratic damping feedback) will enable an optimum parametric control of system instabilities and the onset of chaotic response.

Field - The hydrodynamic ocean environment is nonlinear and stochastic. Consequently, the hydrodynamic exciting force is further complicated. Two topics for research are the influence of these complications on the fundamental results obtained in this study:

a) deterministic field: nonlinear (linear). b) stochastic field: nonlinear (linear). An additional stochastic topic for analysis is the evaluation of the drag coefficient and the influence of its variability (in deterministic and random fields) on system response.

BIBLIOGRAPHY

Abkowitz, M.A. (1972). Stability and Motion Control of Ocean Vehicles. MIT Press, Cambridge.

ABS (1975). Single Point Mooring Systems - Rules for Building and Classing.

Ansari, K.A and Khan, N.U. (1986). The effect of cable dynamics on the station-keeping response of a moored offshore vessel. *ASME Proc. 5 Int. Offshore Mech. Arctic Eng. Symp.*, 3, 514-521.

API (1987). Analysis of spread mooring systems for floating drilling units.

Arnold, V.I. (1965). Small denominators: I. Mapping of the circumference onto itself. *Am. Math. Soc. Transl. Ser.*, 2, 46, 213-284.

Arnold, V.I. (1978). Mathematical Methods of Classical Mechanics. Springer Verlag, New York.

Bernitsas, M.M. and Chung, J.S. (1990). Nonlinear stability and simulation of two-line ship towing and mooring. *App. Ocean Res.*, 11, 153-166.

Bernitsas, M.M. and Papoulias, F.A. (1986). Stability of single point mooring systems. *App. Ocean Res.*, 8, 49-58.

Bishop, S.R. and Virgin, L.N. (1988). The onset of chaotic motions of a moored semi-submersible. *ASME J. Offshore Mech. Arctic Eng.*, 110, 205-209.

Bogliubov, N.N. and Mitropolski, Y.A. (1961). Asymptotic Methods in the Theory of Nonlinear Oscillations. Gordon and Breach, New York.

Burton, T.D. and Hassan, A. (1991). Harmonic balance applied to strongly nonlinear oscillators. *Second Int. Conf. Industrial Applied Math.*, Abstracts, 1, 31.

Burton, T.D. and Rahman, Z. (1986). On the multi-scale analysis of strongly nonlinear forced oscillators. *Int. J. Nonlinear Mech.*, 21, 135-146.

Chakrabarti, S.K. (1987). Hydrodynamics of Offshore Structures. Springer-Verlag.

Chen, M.C. and Chou, F. (1986). Dynamic mooring system comparison for a deepwater semi-submersible. *ASME Proc. 5 Int. Offshore Mech. Arctic Eng. Symp.*, 3., 479-486.

Chiou, R. (1989). Nonlinear hydrodynamic response of curved singly-connected cables. PhD Disssertation, Oregon State University.

Choi, H.S, and Lou, J.Y.K. (1991). Nonlinear behavior of an articulated loading platform. *App. Ocean Res.*, 13, 63-74.

Clemens, H. and Wauer, J. (1981). Free and forced vibrations of a snap-through oscillator. *Proc. 9th Int. Conf. Nonlinear Oscillations*, 128-133.

Devaney, R.L. (1986). An introduction to Chaotic Dynamical Systems. Benjamin Cummings Publication Co.

Eckmann, J.P. and Kamphorst, S.O. (1986). Liapunov Exponents from time series. *Phys. Rev.*, A, 29, 3.

Falzarano, J.M. (1990). Predicting Complicated Dynamics Leading to Vessel Capsizing. PhD Dissertation, The University of Michigan.

Feder, J. (1989). Fractals. Plenum.

Feigenbaum, M.J. (1980). Universal behavior in nonlinear systems. Los Alamos Sci., 1, 4-27.

Fujino, M. and Sagara, N. (1990). An Analysis of Dynamic Behavior of an Articulated Column in Waves - Effects of Nonlinear Hydrodynamic Drag Force on the Occurrence of Subharmonic Oscillation. *J. Japan Society of Naval Architects*, 103-112 (in Japanese).

Garrison, C.J. (1978). Hydrodynamic loading of large offshore structures, three dimensional source distribution methods. in Numerical Methods in Offshore Engineering, eds. Zienkiewiez, O.C., Lewis, R.W. and Stagg, K.J., Chichester, 375-397.

Goldstein, H. (1980). Classical Mechanics. Addison Wesley, Reading.

Grassberger, P. and Procaccia, I. (1983). Measuring the strangeness of strange attractors. *Physica*, 9, 189-208.

Grebogi, C., Ott, E. and York, J.A. (1983). Crises, sudden changes in chaotic attractors and transient chaos. *Physica D*, 7, 181-200.

Grebogi, C., Ott, E. and York, J.A. (1987). Basin boundaries metamorphoses: changes in accessible boundary orbits. *Physica D*, 24, 243-262.

Guckenheimer, J. and Holmes, P. (1986). Nonlinear Oscillations, Dynamical Systems and Bifurcation of Vector Fields. Springer-Verlag, New York.

Hagedorn, P. (1978). Nonlinear Oscillations. Oxford University Press, Oxford.

HaQuang, N., Mook, D.T. and Palut, R.H. (1987). A nonlinear analysis of interactions between parametric and external excitations. *J. Sound Vibrt.*, 118, 425-439.

Hayashi, C. (1964). Nonlinear Oscillations in Physical Systems. McGraw-Hill, New York.

Holmes, C. and Holmes, P. (1981). Second order averaging and bifurcations to subharmonics in Duffing's equation. *J. Sound Vibrat.*, 78, 161-174.

Holmes, P. (1979). A nonlinear oscillator with a strange attractor. *Philos. Trans. R. Soc.*, A292, 419-448.

Holmes, P. (1980). Averaging and chaotic motions in forced oscillations. *SIAM J. Appl. Math.* 38, 1, 65-80.

Holmes, P. (1984). Bifurcation sequences in horseshoe maps: infinitely many routes to chaos. *Phys. Lett.* A, 104, 6, 299-302.

Holmes, P., Marsden, J. and Scheurle, J. (1988). Exponently small splitting of separatrices with applications to KAM theory and degenerate bifurcations. *Contemporary Mathematics*, 81 213-244.

Holmes, P. and Whitley, D. (1984). Bifurcations of one and two dimensional maps. *Philos. Trans. R. Soc.*, A, 311, 43-102.

D'Humieres, D., Beasly, M.R., Huberman, B.A. and Libchaber, A. (1982). Chaotic states and routes to chaos in the forced pendulum. *Phy. Rev.*, A, 26, 6, 3483-3496.

Ioos, G. (1989). Local techniques in bifurcation theory and nonlinear dynamics. in Chaotic Motions in Nonlinear Dynamical Systems, ed. Szemplinska-Stupnika, Ioos and Moon. Springer-Verlag. 137-193.

Ioos, G. and Joseph, D.D. (1981). Elementary Stability and Bifurcation Theory. Springer-Verlag.

Isaacson, M. de St. Q. (1979). Nonlinear inertia forces on bodies. *ASCE J. Waterway, Port, Coastal and Ocean Div.*, 103, 2, 213-227.

Jensen, M.H., Kadanoff, L.P., Libchaber, A, Procaccia, I. and Savans, J. (1985). Global universality at the onset of chaos: Results of a forced Rayleigh-Bénard experiment. *Phys. Rev. Lett.*, 55, 2798-2801.

Jiang, T. (1991). Investigation of nonlinear ship dynamics involving instability and chaos in examples from offshore technology. Institut fur Schiffbau der Universitat Hamburg, Report no. 512 (in German).

Jiang, T. and Schellin, T.E. (1990). Motion prediction of single-point moored tanker subjected to current, wind and waves. *ASME J. Offshore Mech. Arctic Eng.*, 112, 83-90.

Jiang, T., Schellin, T.E. and Sharma, S.D. (1987). Maneuvering simulation of a tanker moored in a steady current including hydrodynamic memory effects and stability analysis. *RINA Proc. Int. Conf. on Ship Maneuverability*, 1, paper no. 25.

Jordan, D.W. and Smith, P. (1977). Nonlinear Ordinary Differential Equations. Oxford University Press, Oxford

de Kat, J.O. and Wichers, E.W. (1991). Behavior of a moored ship in unsteady current, wind and waves. *Marine Tech.*, 28, 251-264.

La Salle, I.P. and Lefschetz, S. (1981). Stability Methods by Liapunov Direct method. Academic Press, New York.

Leonard, J.W. and Young, R.A. (1985). Coupled response of compliant offshore platforms. *Eng. Struc.* 7, 74-84.

Leonard, J.W. (1988). Tension Structures, Behavior and Analysis. McGraw-Hill, New York.

Lewis, E.V. (1988). Principles of Naval Architecture. SNAME, New York.

Li, T-Y. and Yorke, J.A. (1979). Period three implies chaos. *Am. Math. Monthly*, 82, 985-992.

Liaw, C.W. (1988a). Chaotic and periodic responses of a coupled wave-force and structure system. *Computers and Structures.*, 30, 4, 985-993.

Liaw, C.W. (1988b). Bifurcations of subharmonics and chaotic motions of articulated towers. *Eng. Struct.*, 10, 117-124.

Lichtenberg, A.J. and Lieberman, M.A. (1983). Regular and Stochastic Motion. Springer-Verlag, New York.

Lou, J.Y.K. and Choi, H.S. (1990). Nonlinear response of an articulated offshore loading platform. OTRC Report No. 6/90-a-2-100.

Meirovitch, L. (1970). Methods of Analytical Dynamics. McGraw-Hill, New York.

Melnikov, V.K. (1963). On the stability of the center for time periodic perturbations. *Trans. Moscow Math. Soc.*, 12, 1-56.

Miles, J.W. (1988). Resonance and symmetry breaking for the pendulum. *Physica D*, 31, 252-268.

Miles, J.W. (1984a). Resonant motion of spherical pendulum. *Physica D*, 11, 309-323.

Miles, J.W. (1984b). Resonantly forced motion of two quadratically coupled oscillators. *Physica D*, 13, 247-260.

Moon, F.C. (1980). Experimental models for strange attractor vibration in elastic systems. in New Approaches to Nonlinear Problems in Dynamics, Holmes, P. (ed.), 487-495.

Moon, F.C. (1987). Chaotic Vibrations, an Introduction for Applied Scientist and Engineers. Wiley, New York.

Moon, F.C. (1989). Experiments in chaotic dynamics. in Chaotic Motions in Nonlinear Dynamical Systems, ed. Szemplinska-Stupnika, Ioos and Moon. Springer-Verlag. 1-50.

Morozov, A.D. (1976). A complete qualitative investigation of Duffing's equation. *Diff. Eqn.*, 12, 164-174.

Nayfeh, A.H. (1988). On the undesirable roll characteristics of ships in regular seas. *J. Ship Res.* 32, 2, 92-100.

Nayfeh, A.H. (1973). Perturbation Methods. Wiley, New York.

Nayfeh, A.H. and Khdeir, A.A. (1986a). Nonlinear rolling of ships in regular beam seas. *Int. Shipbldg. Prog.* 33, 40-49.

Nayfeh, A.H. and Khdeir, A.A. (1986b). Nonlinear rolling of biased ships in regular beam waves. *Int. Shipbldg. Prog.* 33, 84-93.

Nayfeh, A.H. and Mook, D.T. (1979). Nonlinear Oscillations. Wiley, New York.

Nayfeh, A.H. and Sanchez, N.E. (1989). Bifurcations in a forced softening Duffing oscillator. *Int. J. Nonlinear Mech.*, 24, 6, 483-497.

Newman, J.N. (1977). Marine Hydrodynamics. MIT Press, Cambridge.

Papoulias, F.A. (1988). Dynamic analysis of mooring systems. PhD Dissertation, The University of Michigan.

Papoulias, F.A. and Bernitsas, M.M. (1988). Autonomous oscillations, bifurcations and chaotic response of moored vessels. *J. Ship Res.*, 32, 220-228.

Papoulias, F.A. and Bernitsas, M.M. (1986). Stability of motions of moored ocean vehicles. *Dynamics and Stability of Systems*, 1, 4, 323-341.

Parlitz, U. and Lauterborn, W. (1985). Superstructure in the bifurcation set of the Duffing equation. *Phys. Lett.* A, 107, 8, 351-355.

Patel, M.H. (1989). Dynamics of Offshore Structures. Butterworths, London.

Pauling, J.R. (1980). An equivalent linear representation of the forces exerted on the OTEC cold water pipe by combined effects of waves and current. ASME Ocean Engineering for OTEC, 21-28.

Poddar, B., Moon, F.C. and Mukherjee, S. (1986). Chaotic motion of an elastic-plastic beam. *J. App. Mech.*, 55, 185-189.

Rahman, Z. and Burton, T.D. (1986). Large amplitude primary and superharmonic resonances in the Duffing oscillators. *Int. J. Nonlinear Mech.*, 110, 363-380.

Raty, R., von Boehm, J. and Isomaki, H.M. (1984). Absence of inversion-symmetric limit cycles of even periods and the chaotic motions of Duffing's oscillator. *Phys. Let.*, 103A, 6, 289-291.

Rosenberg, R.M. (1977). Analytical Dynamics of Discrete Systems. Plenum Press.

Salam, F.M.A. and Sastry, S.S. (1985). Dynamics of the forced Josephson circuit: the regions of chaos. *IEEE Trans. Cir. Sys.*, 32, 8, 784-796.

Sanders, J.A. (1982). Melnikov's method and averaging. *Celestial Mech.*, 28, 171-181.

Sanders, J.A. and Verhulst, F. (1985). Averaging Methods in Nonlinear Dynamics. Springer-Verlag, New York.

Sarpkaya, T. and Isaacson, M. de St. Q. (1983). Mechanics of Wave Forces on Offshore Structures. Van Nostrand Reinhold.

Schellin, T.E., Jiang, T. and Sharma, S.D. (1990). Motion simulation and dynamic stability of an anchored tanker subject to current, wind and waves. *J. Ship Tech. Res.*, 37, 2, 64-84.

Schmidt, G. and Tondl, A. (1986). Nonlinear Vibrations. Cambridge University Press.

Sharma, S.D., Jiang, T. and Schellin, T.E. (1988). Dynamic instability and chaotic motions of a single-point moored tanker. *Proc. 17th ONR Symposium on Naval Hydrodynamics*, 543-563.

Shaw, S.W. and Wiggins, S. (1988). Chaotic dynamics of a whirling pendulum. *Physica D*, 31, 190-210.

Simoyi, R.H., Wolf, A. and Swinney, H.L. (1982). One dimensional dynamics in a multicomponent chemical reaction. *Phys. Rev. Lett.*, 49, 245-248.

Skop, R.A. (1988). Mooring systems: a state of the art review. *ASME J. offshore Mech. Arctic Eng.*, 110, 365-372.

Szemplinska-Stupnicka, W. and Bajkowski, J. (1986). The 1/2 subharmonic resonance and its transition to chaotic motion in a nonlinear oscillator. *Int. J. Nonlinear Mech.* 21, 401-419.

Szemplinska-Stupnicka, W. (1987). Secondary resonances and approximate models of routes to chaotic motions in nonlinear oscillators. *J. Sound Vibrat.*, 113, 155-172.

Szemplinska-Stupnicka, W. (1988). Bifurcations of harmonic solution leading to chaotic motions in the softening type Duffing's oscillator. *Int. J. Nonlinear Mech.*, 23, 257-277.

Szemplinska-Stupnicka, W. (1989). Chaotic and regular motions in nonlinear vibrating systems. in Chaotic Motions in Nonlinear Dynamical Systems, ed. Szemplinska-Stupnika, Ioos and Moon. Springer-Verlag. 51-136.

Szemplinska-Stupnicka, W. (1990). The Behavior of Nonlinear Vibrating Systems, Vol. I, Fundamental Concepts and Methods: Applications to Single-Degree-of Freedom Systems. Kluwer Academic Press, Dordrecht.

Szemplinska-Stupnicka, W. (1990). The Behavior of Nonlinear Vibrating Systems, Vol. II, Advanced Concepts Applications to Multi-Degree-of Freedom Systems. Kluwer Academic Press, Dordrecht.

Tabor, M. (1989). Chaos and Integrability in Nonlinear Dynamics. Wiley, New York.

Tang, D.M. and Dowel, E.H. (1988). On the threshold force for chaotic motions for a forced buckled beam. *ASME J. Appl. Mech.*, 55, 190-196.

Thompson, J.M.T. (1983). Complex dynamics of compliant offshore structures. *Proc. R. Soc. Lond.*, A, 387, 407-427.

Thompson, J.M.T., Bokaian, A.R. and Ghaffari, R. (1984). Subharmonic and chaotic motions of compliant offshore structures and articulated mooring towers. *ASME J. Energy Resources Tech.*, 106, 191-198.

Thompson, J.M.T. and Soliman, M.S. (1990). Fractal control boundaries of driven oscillators and their relevance to safe engineering design. *Proc. R. Soc. Lond.*, A, 428, 4-13.

Thompson, J.M.T. and Stewart, H.B. (1986). Nonlinear Dynamics and Chaos. Wiley, Chichester.

Timoshenko, S., Young, D.H. and Weaver, W. (1974). Vibration Problems in Engineering. Wiley, New York.

Troger, H. and Hsu, C.S. (1977). Response of a nonlinear system under combined parametric and forcing excitation. *ASME J. App. Mech.*, 44, 179-181.

Ueda, Y. (1980). Steady motions exhibited by duffing's equation: a picturebook of regular and chaotic motions. in New Approaches to Nonlinear Problems in Dynamics, Holmes, P. (ed.), 311-322.

Ueda, Y. (1981). Explosions of strange attractors exhibited by Duffing's equation. *Ann. N.Y. Acad. Sci.*, 357, 422-434.

Ueda, Y., Yoshida, S., Stewart, H.B., Thompson, J.M.T. (1990). Basin explosions and escape phenomena in the twin-well Duffing oscillator: compound global bifurcations organizing behavior. *Phil. Trans. R. Soc. Lond.*, A, 332, 169-186.

Virgin, L.N. (1987). The nonlinear rolling response of a vessel including chaotic motions leading to capsize in regular seas. *App. Ocean Res.*, 9, 89-95.

Virgin, L.N. and Bishop, S.R. (1988). Complex dynamics and chaotic responses in the time domain simulations of a floating structure. *Ocean Eng.*, 15, 71-90.

Wehausen, J.V. (1971). The motions of floating bodies. *Ann. Rev. Fluid Mech.*, 3, 237-268.

Wichers, J.E.W. (1988). A simulation model for a single point moored tanker. Maritime Res. Inst. Netherlands, Report no. 797.

Wiggins, S. (1988). Global Bifurcations and Chaos - Analytical Methods. Springer-Verlag, New York.

Wiggins, S. (1990). Introduction to Applied Nonlinear Dynamical Systems and Chaos. Springer-Verlag, New York.

Witz, J.A., Ablett, C.B. and Harrison, J.H. (1989). Nonlinear response of semi-submersibles with nonlinear restoring moment characteristics. *App. Ocean Res.*, 11, 153-166.

Wolf, A., Swift, J.B., Swinney, H.L. and Vastano, J.A. (1985). Determining Lyapunov exponents from a time series. *Physica D*, 16, 285-317.

Yagasaki, K., Sakata, M. and Kimura, K. (1990). Dynamics of a weakly nonlinear system subjected to combined parametric and external excitation. *ASME J. App. Mech.*, 57, 209-217.

APPENDICES

Appendix A - Nonlinear Functions

This appendix includes the following nonlinear functions (A.1), equations (A.2) and coefficients (A.3):

A.1:

Coefficients of the nonlinear functions $F_1(x,\theta)$ and $F_2(x,y,\theta)$ of Eqns.30,31 (chapter 2):

$$F_1(x,\theta) = \sum_l \left[B_l + K_l(\theta)\right] x^l \tag{1}$$

where

$$\begin{aligned}
K_0 &= \mu f_1 \left\{ \omega^2 \left[-\left(1-\frac{f_0}{\omega}\right)\sin\theta + \frac{1}{2} f_1 \sin 2\theta \right] \right. \\
&\left. + sgn(u-y)\,\delta \left[2\frac{f_0}{\omega}\cos\theta - \frac{1}{2} f_1 \cos 2\theta \right] \right\} \\
K_1 &= \mu f_1 \left\{ \omega^2 \left[\left(1-\frac{f_0}{\omega}\right)\cos\theta + f_1 \cos 2\theta \right] \right. \\
&\left. + sgn(u-y)\,\delta \left[2\frac{f_0}{\omega}\sin\theta - f_1 \cos 2\theta \right] \right\} \\
K_2 &= \mu f_1 \left\{ \omega^2 \left[\frac{1}{2}\left(1-\frac{f_0}{\omega}\right)\sin\theta - f_1 \sin 2\theta \right] \right. \\
&\left. + sgn(u-y)\,\delta \left[-\frac{f_0}{\omega}\cos\theta + f_1 \cos 2\theta \right] \right\} \\
K_3 &= \mu f_1 \left\{ \omega^2 \left[-\frac{1}{6}\left(1-\frac{f_0}{\omega}\right)\cos\theta - \frac{2}{3} f_1 \cos 2\theta \right] \right. \\
&\left. + sgn(u-y)\,\delta \left[-\frac{1}{3}\frac{f_0}{\omega}\sin\theta - \frac{2}{3} f_1 \sin 2\theta \right] \right\}
\end{aligned} \tag{2}$$

$$B_0 = \mu\,\delta\ sgn(u-y)\left[\left(\frac{f_0}{\omega}\right)^2 + \frac{1}{2}f_1^2\right] \qquad (3)$$
$$B_{2l+1} = -\alpha_{2l+1} \quad ; \quad B_{2l} = 0$$

and

$$F_2(y,xy,\theta) = \sum_l \Gamma_l\, y^l + \left[\Lambda_l(\theta)\ x^l\right] y \qquad (4)$$

where

$$\Gamma_0 = 0 \quad ; \quad \Gamma_1 = -\left[\gamma + 2\left(\frac{f_0}{\omega^2}\right)\right] \qquad (5)$$
$$\Gamma_2 = \left(\frac{1}{\omega^2}\right) \quad ; \quad \Gamma_{l\geq 3} = 0$$

$$\Lambda_0 = \mu f_1\left[-\omega\sin\theta - 2sgn(u-y)\left(\frac{\delta}{\omega}\right)\cos\theta\right]$$
$$\Lambda_1 = \mu f_1\left[\omega\cos\theta - 2sgn(u-y)\left(\frac{\delta}{\omega}\right)\sin\theta\right] \qquad (6)$$
$$\Lambda_2 = \frac{1}{2}\mu f_1\left[\omega\sin\theta + 2sgn(u-y)\left(\frac{\delta}{\omega}\right)\cos\theta\right]$$
$$\Lambda_3 = \frac{1}{6}\mu f_1\left[-\omega\cos\theta + 2sgn(u-y)\left(\frac{\delta}{\omega}\right)\sin\theta\right]$$

A.2

Amplitude equations of Eqn.82 (chapter 4):

$$S_j\left(A_0\tfrac{n}{m}, A_i\tfrac{n}{m}, \Psi_i\tfrac{n}{m}\right) = 0 \tag{7}$$

where $\quad j=3,\ n=m=1\ :\ x = A_0 + A_1\cos(\omega t + \Psi_1)$

or

$$\begin{gathered} R_0^2+\frac{1}{2}\left(R_{1S}^2+R_{1C}^2+R_{2C}^2+R_{3C}^2\right)-\frac{3}{8}(\mu\delta)^2\left(S_{4C}^2+S_{4S}^2\right)=0 \\ 2R_0R_{1C}+R_{2C}(R_{1C}+R_{3C}) = 0 \\ 2R_0R_{1S}-R_{1S}R_{2C} = 0 \end{gathered} \tag{8}$$

where

$$\begin{aligned} R_0 &= \alpha_1 A_0+\alpha_3\left(A_0^3+\frac{3}{2}A_1^2\right) \\ R_{1C} &= (\alpha_1-\omega^2)A_1+3\alpha_3\left(A_0^2A_1+\frac{1}{4}A_1^3\right)+\mu\omega^2 f\sin\Psi_1 \\ R_{1S} &= -\omega\gamma A_1-\mu\omega^2 f\cos\Psi_1 \\ R_{2C} &= \frac{3}{2}\alpha_3 A_0A_1^2 \\ R_{3C} &= \frac{1}{4}\alpha_3 A_1^3 \end{aligned} \tag{9}$$

$$\begin{aligned} S_c &= f\cos\Psi_1 \\ S_S &= f\sin\Psi_1+A_1 \end{aligned} \tag{10}$$

A.3

Coefficients of Eqns.124,125 (chapter 5):

$$\xi_{C\frac{1}{2}} = \frac{1}{2}A_{1/2}\sin\Psi_{1/2} \quad ; \quad \xi_{S\frac{1}{2}} = \frac{1}{2}A_{1/2}\cos\Psi_{1/2}$$
$$\xi_{C1} = f + A_1\sin\Psi_1 \quad ; \quad \xi_{S1} = A_1\cos\Psi_1 \tag{11}$$

$$\zeta_0 = -\alpha_1 - \frac{3}{2}\alpha_3\left(2A_0^2 + A^{2_{vn}} + A_1^2\right)$$
$$\zeta_{C\frac{1}{2}} = -3\alpha_3\left[2A_0A_{1/2}\cos\Psi_{1/2} + A_{1/2}A\cos\left(\Psi_1 - \Psi_{1/2}\right)\right]$$
$$\zeta_{S\frac{1}{2}} = 3\alpha_3\left[2A_0A_{1/2}\sin\Psi_{1/2} + A_{1/2}A_1\sin\left(\Psi_1 - \Psi_{1/2}\right)\right] \tag{12}$$
$$\zeta_{C1} = -3\alpha_3\left[\frac{1}{2}A^{2_{vn}}\cos\left(2\Psi_{1/2}\right) + 2A_0A_1\cos\Psi_1\right]$$
$$\zeta_{S1} = 3\alpha_3\left[\frac{1}{2}A^{2_{vn}}\sin\left(\Psi_{1/2}\right) + 2A_0A_1\sin\Psi_1\right]$$

Appendix B - Numerical Simulations

This appendix includes a description (B.1) of the procedures used for numerical simulations of system response (Eqns.12,19) and a list (B.2) of parameter values describing the simulations used for the figures in the text.

B.1

Numerical simulations of the single-degree (Eqn.19) and two-degree-of-freedom system (Eqn.12) were performed by explicit Runge-Kutta (RK) methods where the required order $O(h^m)$ was determined from a calculated truncation error of $O(h^{m+1})$ (Atkinson, 1989). A preliminary simulation with adaptive stepsize control was used to determine an approximate duration of transients and an initial configuration (Press et.al., 1989). Simulations were then conducted where error control was achieved via the passage of the response through the exact fixed equilibrium point and a truncation error was calculated via a RK-Fehlberg formulae (Morris, 1987). The truncation error was compared with results of numerical simulations of various nonlinear systems (Bert et al, 1988). The lengthy duration simulations of the chaotic system response ($N_P \approx 5{,}000$) were then repeated with high order RK simulation (Morris, 1987: RK-8).

Stability was found to be sensitive to the degree of nonlinearity (β) and the magnitude of the hydrodynamic drag force (δ). The limiting time steps ($h \propto T/2^n$, $T=2\pi/\omega$) varied (RK-4,5) from $h \approx T/2^6$ [$\beta \approx 1$, $\delta \approx 1$] to $h \approx T/2^7$ [$\beta=0$, $\delta \approx 1$] whereas simulation of a strongly nonlinear system [$\beta=0$, $\delta<1$] was unstable at $h \approx T/2^8$.

Consequently, simulation were conducted (RK-4,5,8) with $h=T/2^9$. Note that lengthy numerical integration of chaotic dynamical systems by implicit solvers (e.g. Newmark methods) will introduce hetroclinic tangles that will complicate the solution.

References:

Atkinson, K.E. (1989). An Introduction to Numerical Analysis. Wiley, New York.

Bert C.W. and Stricklin, J.D. (1988). Comparative evaluation of six different numerical integration methods for nonlinear dynamic systems. *J. Sound Vibrat.*, 127, 221-229.

Morris, A.H. (1987). NSWC Library of Mathematics Subroutines. NSWC.

Press, W.H., Flannery, B.P., Teukolsky, S.A. and Vetterling, W.T. (1989). Numerical Recipes. Cambridge University Press, Cambridge.

Reinhall, P.G., Caughey, T.K. and Storti, D.W. (1989). Order and chaos in a discrete duffing oscillator: implications on numerical integration. *ASME J. App. Mech.*, 56, 162-167.

B.2

The simulations depicted in the text describe response of a taut system ($\tau=\frac{1}{2}\sqrt{(1+\beta^2)}$):

a) single-degree-of-freedom system (Eqn.19) subject to a linearized excitation ($\kappa=0$):

$\alpha=4$ (Figs.12,20,26,31,33); $\alpha=40$ (Figs.13,16,17,18,19,25,)

$\beta=0$ (Figs.12.a,12b,17,18,20,25,26,31,33); $\beta=1$ (Figs.12c,16,19)

$\gamma^*=0.01$ (Figs.12,13b,16-20,25,26,31,33) $\gamma^*=0.05$ (Fig.13a)

$f_0=0$ (Figs.12,13b,16,18,-20,25b,26,31,33), $f_0=0.01$ (Figs.13a,17,25)

$\mu f_1=0.1$ (Figs.13a,17,25a,31), $\mu f_1=2$ (Figs.12,13b,16,18-20,25b,26,33)

b) single-degree-of-freedom system (Eqn.19) subject to nonlinear drag excitation ($\gamma=0.01$, $\kappa=0$, $\mu=1$, $f_0=0$):

$\alpha_1=0.1$ (Fig.32), $\alpha_1=0.25$ (Figs.8,10,11,22,24,27,28)

$\alpha_3=0.1$ (Figs.8,10,22), $\alpha_3=0.3$ (Figs.11,24,27), $\alpha_3=1$ (Figs.28,32)

$\delta=0.05$ (Figs.24,32), $\delta=0.1$ (Figs.8,10,11,27,28)

$f_1=0.1$ (Figs.8,22,32), $f_1=0.2$ (Figs.10,24,27,36), $f_1=0.3$ (Figs.11,28)

c) single-degree-of-freedom system (Eqn.19) subject to nonlinear drag and convective excitation:

$\alpha_1=1$, $\alpha_3=0$, $\gamma=0.01$, $\delta=0.1$, $\kappa=1$, $\mu=1$, $f_0=0$, $f_1=0.1$ (Figs.23,29,30,37,38)

d) two-degree-of-freedom system (Eqn.12) subject to nonlinear drag excitation ($\beta=0$, $\sigma=0$, $\gamma=0.01$, $\kappa=0$, $f_0=0$):

$\alpha=1$ (Figs.39,40,43a,b), $\alpha=10$ (Figs.41,42,43c)

$\delta=0.05$ (Figs.39,42,43c) $\delta=0.1$ (Figs.40,41,43a,b)

$\chi=0.1$ (Figs.40,43a), $\chi=0.2$ (Figs.39,41), $\chi=0.3$ (Figs.42,43c)

Appendix C - Nomenclature

$A_{i,n/m}$ - solution amplitudes

$A_{P1,3}$ - projected drag areas

a - wave amplitude

$a_{1,2,3,4}$ - coefficients in characteristic equation

B - beam of the body

B, $B^{U,L}$ - Bendixon functions

b - horizontal distance from body centroid to connecting mooring point

C - variable function

$C_{1,3,5}$ - structural damping coefficients

$C_{A1,3}$, $C_{D1,3}$ - hydrodynamic added mass and viscous drag coefficients

D - structural damping vector

D - draft of the body, variable function

$D_{1,2}$ - Hurwitz determinants

d - vertical distance from body centroid to connecting mooring point

E - variable function

$e_{j,(n/m)}$, $e_{j,(n/2m)}$ - variational amplitudes

F - exciting force vector [$\mathbf{F}=(F_1,F_3,F_5)^T$], potential vector [$\mathbf{F}(q)=(F_1(q),F_2(q))^T$]

$\mathbf{F_D}$, $\mathbf{F_M}$ - exciting drag and inertia force vectors ($\mathbf{F}=\mathbf{F_D}+\mathbf{F_M}$)

$F_{1,2}$, $F_{1,2}^{U,L}$ - variable functions

f_0, f_1, f_1', f_1^* - scaled current and wave forcing parameters

G - damping vector [$\mathbf{G}(q)=(G_1(q),G_2(q))^T$]

G, $G_{1,2}$, $G_{1,2}^{U,L}$, - variable functions

g - gravitational acceleration

$H_{1,2}$ - Hill's variational functions

H - Hamiltonian energy

H_0 - level set [$H_0=H(j_2,\phi_2)$]

h, h´ - water depth and scaled water depth (h´=h/d)

I - body inertia, degree of approximation

$I_{s,C}$ - integral functions of the drag force

i - index

J - nonlinear polar coordinate ("action" in averaged system) [$J=\sqrt{(u^2+v^2)}$]

$J_{\pm}$ - coordinate of homoclinic orbit

j - index

j - index of repeatability in resonance number

j_i, j'_i - J value of Hamiltonian and non Hamiltonian fixed points

K - elastic mooring force coefficient

k - wave number

L - length of the body

L - Liapunov function

$\mathcal{L}$ - Lagrangian function

l - index

l_0 - length of gap to be bridged by mooring line [$l_0=\sqrt{(d^2+b^2)}$]

$l_{1,2}$ - mooring line lengths

l_c - initial mooring line length ($l_c \leq l_0$)

M - body mass, exciting moment

M - Melnikov function

m - index of subharmonic

n - index of ultraharmonic

p_i - trace of derivative matrix at the fixed point location

Q' - generalized force

$\mathbf{q}$ - generalized coordinate vector [e.g. $\mathbf{q}=(J,\Phi)^T$]

q - generalized coordinate

$q^0_{\pm}$ - homoclinic orbit [$q^0_{\pm}(\theta)=(J^0_{\pm}(\theta),\Phi^0_{\pm}(\theta))$]

q_i - determinant of derivative matrix at the fixed point location

$\mathbf{R}$ - total restoring force vector [$\mathbf{R}=(R_1,R_3,R_5)^T$]

$\mathbf{R_B}$, $\mathbf{R_M}$ - buoyancy and mooring restoring force vectors ($\mathbf{R}=\mathbf{R_B}+\mathbf{R_M}$)

R - restoring force function

$R_{m/n,j,d}$ - resonance number

r - resonance ratio (r=n/m)

$\mathbf{S}$ - variable matrix

S_j - nonlinear set of equations

T - period of exciting wave ($T=2\pi/\omega$)

T - kinetic energy

t - time

$\mathbf{U}$ - particle velocity vector [$\mathbf{U}=(U_1,U_3)^T$]

U_0 - colinear current magnitude

U_1, U_3 - horizontal and vertical components of the particle velocity

U^* - velocity function ($U^*=U_1\sin X_5+U_3\cos X_5$)

$\mathbf{u}$ - scaled particle velocity vector [$\mathbf{u}=(u_1u_3)^T$]

u, u´ - velocity functions

u - van der Pol coordinate

V - total potential energy

V_M - mooring potential

$\forall$ - displaced volume

v - van der Pol Coordinate

W_0, W_{21}, W_{22} - coefficient function

$\mathbf{X}$ - displacement vector [$\mathbf{X}=(X_1,X_3,X_5)^T$]

X_1,X_3,X_5 - surge, heave and pitch

X_P - Poincaré displacement

$\mathbf{x}$ - scaled displacement vector [$\mathbf{x}=(x_1,x_3,x_5)^T$], $\mathbf{x}=\mathbf{X}/d$

x_0 - approximate displacement

$x_{c1,2,3}$ - value of fixed points

Y_P - Poincaré velocity

$\mathbf{y}$ - scaled velocity vector [$\mathbf{y}=(y_1,y_3,y_5)^T$, $\mathbf{y}=(1/d)d\mathbf{X}/dt$]

y_0 - approximate velocity

z´ - dummy variable

α, α_n, α_n' - scaled stiffness parameters

β - nonlinear geometric parameter

β^H_c, β^P_c, β^S_c - bifurcation values

Γ - variable function

γ, γ', γ^*, $\gamma_{1,3}$ - structural damping parameters

Δ - determinant

δ, δ^*, $\delta_{1,3}$ - hydrodynamic drag parameters

$\delta_{r,1}$, $\delta_{m,(2j+1)}$ - Kronecker delta functions

ϵ, ϵ_i - measure of smallness, perturbation coordinate $\epsilon(\theta)$

$\zeta_{0(n/m)}$, $\zeta_{Cj(n/m)}$, $\zeta_{Cj(n/m)}$ - Fourier coefficients

η - measure of smallness, perturbation coordinate $\eta(\theta)$

θ - scaled time ($\theta=\omega t$)

κ - scaled wave number ($\kappa=kd$)

Λ - variable function

λ - eigenvalue

μ, $\mu_{1,3}$ - buoyancy parameters

ν - measure of smallness in Liapunov function

$\xi_{Cj(n/m)}$, $\xi_{Sj(n/m)}$ - Fourier coefficients

ρ - water mass density

σ - buoyancy parameter

τ - pretension parameter

Φ - nonlinear polar coordinate ("angle" in averaged system) [$\Phi=\tan^{-1}(v/u)$]

$\Phi_{\pm}$ - coordinate of homoclinic orbit

ϕ_i, ϕ'_i - Φ value of Hamiltonian and non Hamiltonian fixed points

χ - wave amplitude parameter (χ=ka)

$\Psi_{i,(n/m)}$ - solution phases

$\psi_{j,(n/m)}$ - variational phases

Ω', Ω^* - detuning parameters [$\epsilon\Omega' = \omega^2 - (m/n)^2\alpha_1$], $\Omega^* = n\epsilon\Omega'/2m\omega$]

ω - wave frequency ($T = 2\pi/\omega$)

ω_n - natural frequency